Magma fertility related to Au - Cu mineralisation: Evaluating the potential for linked porphyry Cu – Au deposits at depths, North Queensland, Australia

Thesis submitted by

Helge Behnsen

August 2018

For the degree of Master of Philosophy in the
College of Science and Engineering,
James Cook University

Statement of Access

I, the undersigned author of this thesis, understand that James Cook University, will make this thesis available for use within the university library and allow access in other approved libraries after its submission. All users consulting this thesis will have to sign the following statement:

> *In consulting this thesis I agree not to copy or closely paraphrase it in whole or in part without the written consent of the author; and to make proper public written acknowledgment for any assistance which I have obtained from it.*

Beyond this, I do not wish to place any restrictions on access to this thesis.

Helge Behnsen

August, 2018

Declaration

I declare that this thesis is my own work and has not been submitted in any form for another degree or diploma at any university or other institute or tertiary education. Information derived from the published or unpublished work of others has been acknowledged in the text and a list of references is given

Every reasonable effort has been made to gain permission and acknowledge the owners of copyright material. I would be pleased to hear from any copyright owner who has been omitted or incorrectly acknowledged.

Helge Behnsen

August, 2018

Acknowledgments

First, I want to thank some of great the people I met along the way of my journey: Jelle, Sterling, Isaac, Jaime, Cass, Steph, Robbie, Chris, and many more – Thank you guys for many hours of fun, joy and stupidity, but also many serious conversations and interesting discussions.

My advisors Carl Spandler and Paul Dirks are gratefully acknowledged for providing necessary editorial assistance and general help, but especially being supportive and not giving up on me during a time of serious personal hardship, ultimately getting me to the point of submitting my work.

Thanks go to everyone involved in the GSQ-EGRU project 'Characterising and assessing the prospectivity and intrusion-related hydrothermal mineral systems in north-east Queensland': Vladimir Lisitsin (GSQ), Zhaoshan Chang, Paul Dirks, Carl Spandler, Bob Henderson, Arianne Ford, Yanbo Cheng, Isaac Corral, Fredrik Sahlström, Jaime Poblete, Peter Illig, Kairan Liu, Gavin Clarke, and Jan Marten Huizenga (all JCU/EGRU), are thanked for patiently listening to the same developing story over and over again during progressive research.

Evolution Mining Ltd and Basin Gold are greatly acknowledged for providing access to their mining operations and drill core samples used in Chapter 2, and Simon Beams (Terra Search) and Phillip Blevin (GSNSW) are thanked for providing their existing maps, data base, rock samples and thin sections of the Tuckers Igneous Complex used in Chapter 3.

Kevin Blake, Shane Askew and Yi Hu of the Advanced Analytical Centre (AAC), JCU, are thanked for assistance with mineral analyses.

JCU is acknowledged for providing a scholarship, which enabled me to work this project in the first place. GRS and the CSE at JCU are further thanked for providing financial support to attend the international Goldschmidt 2016 conference in Japan, and granting additional funding for analytical work.

Finally, I want to thank my family, for always being supportive no matter the outcome of this endeavour.

Statement of Contributions of Others

Nature of Assistance	Contributions	Names, Titles and Affiliations of Co-Contributors
Intellectual support	Proposal writing	Robert Henderson (JCU) Zhaoshan Chang (JCU) Carl Spandler (JCU) Paul Dirks (JCU) Vladimir Lisitsin (GSQ)
	Data analysis	Carl Spandler (JCU)
	Editorial assistance	Carl Spandler (JCU)
Financial support	Scholarship/Stipend	James Cook University Postgraduate Research Scholarship (JCUPRS)
	Research funding	Geological Survey of Queensland (GSQ) ($ 50,000) HDR Enhancement Scheme (JCU) ($ 2,600)
Data collection	Analytical assistance	Kevin Blake (JCU) Shane Askew (JCU) Yi Hu (JCU)
	Sample collection (Chapter 2)	Isaac Corral (JCU)
Other	Conference support	HDR Enhancement Scheme (JCU) ($ 1,700)
	Geological maps and reports of the TIC (Chapter 3)	Simon Beams (Terra Search)
	Rock samples and thin sections (Chapter 3)	Phillip Blevin (GSNSW) Simon Beams (Terra Search)

Abstract

Continental magmatic arcs host economically important porphyry ore deposit types for copper, gold, and molybdenum, and, if preserved, epithermal high- to intermediate-sulfidation gold and silver deposits. These deposits are genetically and/or spatially associated with magmatism, so understanding the link between magmatism and mineralisation is seen as a crucial endeavor to assist knowledge of mineralisation processes and strategies for regional-scale mineral exploration.

This thesis examines aspects of the mineralisation potential of continental arc magmatic rocks that are exposed as part of the Permo-Carboniferous Kennedy Igneous Association (KIA) from northeastern Queensland. This belt of upper crustal intermediate to felsic granitoids and associated volcanic rocks is recognised to host many economic ore deposits related to igneous activity. Using well-established analytical techniques to analyze whole-rock and mineral major- and trace element compositions combined with Sm-Nd isotopes, I investigate two different localities related by their occurrence in time and space, with the aim to better understand magma fertility, or more specifically the petrogenetic processes contributing to Permo-Carboniferous Cu-Au mineralisation in northeast Queensland. This work strives to improve the applicability of magma fertility concepts to confidently identify fertile igneous terranes potentially covering high grade Cu-Au deposits at depth.

The first location investigated lies to the south of Townsville at the northern edges of the Bowen Basin, where the early Permian Lizzie Creek Volcanic Group (LCV) hosts the Mount Carlton high-sulfidation epithermal Au-Cu deposit. Established whole-rock geochemical parameters, e.g. Sr/Y, V/Sc, used to distinguish fertile porphyry Cu-Au hosting intrusive rocks from barren intrusions, were tested on the “fertile” LCV succession, hosting the Mt. Carlton deposit and compared to contemporary “barren” volcanic rocks of the same group. The results reveal that the key control on generating the fertile LCV sequence was a high magmatic water content, reflected by early fractionation of amphibole at the source level, whereas the barren sequence was comparably dry, and formed by typical fractionation of plagioclase and clinopyroxene. This outcome has major implications for the applicability of whole rock geochemistry as a magma fertility indicator. The here presented results suggest that for volcanic rocks, which tend to be affected by hydrothermal alteration; a) Sr/Y is not a reliable fertility proxy and; b) Rare earth element ratios (e.g. La/Yb, Dy/Yb), which

are relatively resistant to alteration, can be used to reveal differences in magmatic evolution. This supports previous research on magma fertility, and provides strong evidence that fertile magmatic suites can be identified from volcanics sequences that evolved from basalt to rhyolite with a progressive increase in La/Yb, decreasing Dy/Yb, and consistent or slightly increasing V/Sc ratios, despite having experienced some degree of alteration.

The second location investigated in this thesis is the Tuckers Igneous Complex (TIC); a calc-alkaline, I-type igneous complex which intruded the Ravenswood Batholith between ~300-290 Ma and formed within the same convergent margin as the LCV. The TIC is part of the KIA and its relevance for this project lies within its close association with the major early Permian, breccia-hosted Mt. Leyshon Au deposit. The TIC contains a sequence of intrusive rocks from gabbro to felsic granodiorite, and hence offers the opportunity to investigate geochemical evolution, particularly volatile element evolution, of arc magmas at upper crustal levels. Here, I build on previous geochemical and petrographic data for the complex using newly acquired whole-rock geochemistry and in-situ mineral analyses of the major rock forming minerals plagioclase-clinopyroxene-orthopyroxene, and the halogen-bearing minerals apatite and biotite (and amphibole) to monitor and track volatile evolution (Cl and F). As volatile element behavior is recognised to have a fundamental control on magma fertility, this study, offers new insights into the fertility of this Permo-Carboniferous arc, which can be applied to other arc worldwide.

My new results show that the TIC formed through closed-system crystal fractionation from gabbro to mafic granodiorite varieties with only minor mixing and/or assimilation, and likely became an open system during cooling and crystallisation of the more felsic granodiorites. Based on apatite halogen contents, volatile saturation is suggested to have occurred at around ~63-65 wt.% bulk-rock SiO_2, up to which point estimated Cl melt contents steadily rise, and then suddenly drop from ~0.8 to 0.4 wt.%. This abrupt change likely relates to the exsolution of a Cl-rich volatile phase, and also marks important changes within the mineral assemblage from a dry Plag ± Px ± Fe-Ti oxide assemblage, towards a more hydrous and slightly more oxidised Plag ± Hbl ± Bt ± Mag assemblage. Fluorine enriches in the melt with fractionation, even once saturation in a volatile phase is reached, consistent with what is expected from experimental partitioning studies in the system apatite – melt – fluid. Local or temporal changes in the magma's fO_2 is indicated by a measurable increase in apatite S contents in evolved felsic granodiorite, as apatite preferentially

incorporates S as its oxidised species S^{6+}, which also coincides with the general observed changes in the rock forming mineral assemblages as described above. Indicated volatile exsolution, causing loss of significant proportions of Cl together with oxidising conditions at which the bulk of dissolved S may have been present and possibly degassed as $S^{4+}O_2$ (and causing the presence of low amounts of available S^{2-} to precipitate base metals) from the TIC magma may have caused mineralization within overlying, but now eroded rocks. A second possibility may be that the TIC was never able to produce mineralising fluids due to early segregation of sulfides, scavenging ore forming metals (e.g. Cu, Au, and Ag) prior to the crystallisation of TIC gabbro, and thereby stripping the TIC of its ore-forming potential early on. However, an exsolved Cl-rich fluid is very capable of transporting ore metals, therefore the role and true nature of such fluid(s) originating from the TIC can be subject of further investigations.

The here presented results help to understand Cu-Au fertility on a regional, magmatic arc terrane (both volcanic and intrusive) from initial lower crustal petrological processes to the surface, but also on a local scale; within confined individual igneous bodies, their respective mineral assemblages, and their potential role towards regionally present Cu-Au mineralisation. In particular the findings on volcanic rocks offer great potential as easily accessible first-order fertility assessment tool for magmatic-hydrothermal Cu-Au exploration worldwide.

Table of Contents

Contents of Digital Appendices

Chapter 2

Whole rock geochemistry and sample locations Chapter 2

Chapter 2_Appendix_WR Geochemistry

Chapter 3

Analytical conditions (EMPA and LA-ICP-MS)

Chapter 3_Appendix 3-I_Analytical conditions

Whole rock geochemistry and sample locations Chapter 3

Chapter 3Appendix 3-II_WR Geochemistry

Electron microprobe analyses of major rock-forming minerals

Chapter 3_Appendix 3-III_EMPA_Major rock-forming minerals

Apatite major and trace element analyses

Chapter 3_Appendix 3-IV_Apatite major and trace element analyses

Chlorine and fluorine melt estimates (formulations and justification)

Chapter 3_Appendix 3-V_Cl and F melt estimates

List of Figures

Chapter 1

Chapter 2

Chapter 3

Chapter 1

Introduction

1.1 Structure of this thesis

It is intended that the two major content chapters of this thesis will be published in internationally recognised Earth Science journals, and, as per prior agreement with the Geological Survey of Queensland (GSQ), the data presented in Chapter 2 will be made publically available after thesis submission and publication. The bulk of this thesis has been written as two independent papers (Chapters 2 and 3). At the time of submission, Chapter 2 is currently under review with Economic Geology, and the submission of the manuscript for Chapter 3 is undergoing final revisions. As one chapter is undergoing peer-review as part of the publication process, and the second chapter is close to journal submission, each chapter is presented in a format similar to a published manuscript. All sections are presented in the same written style with consistent use of specialist terms and geological unit names. Each chapter is presented as an individual body of work, geologically linked by their geotectonic setting in northeastern Australia, and their focus on understanding magma evolution in relation to metal fertility. Structuring of this thesis in this form inevitably leads to some repetition in the geological setting and analytical techniques. Therefore, I provide a very brief summary and overview of the large-scale geological setting as part of the introductory Chapter 1, but both Chapters 2 and 3 do contain their own individually tailored geological overview.

Reference lists are provided separately for the presented chapters. Although the overall idea and theme of this thesis addresses magma fertility, the methods, data, discussions and cited literature in Chapter 2 and 3 are of a very different nature. Therefore, I consider it easier for the reader to distinguish and follow the individually-cited literature in each chapter. Overall, the overlap in referenced material is minimal, and mainly due to their shared large-scale geotectonic setting.

1.2 Subject of this thesis

Hydrothermal porphyry and epithermal deposits associated directly or indirectly with subduction-related magmatism are the source of approximately 75% of the world's Cu supply as well as a major proportion of Mo, and Au (e.g. Sillitoe, 2010), which makes them the prime exploration target in active and ancient magmatic arc systems. These deposits generally occur as clusters or within age-related belts in arc or back-arc settings. It is now recognised that porphyry deposits commonly have a linked volcanic surface expression, present as either intensively altered lithocap that, under favourable circumstances, hosts high-sulfidation (HS) to intermediate-sulfidation (IS) epithermal mineralisation (e.g. Hedenquist et al., 1998; 2001; Sillitoe, 1999; 2010). However, the spatial relationships of linked porphyry-epithermal systems can be rather complex, and these systems may be vertically separated and/or horizontally offset by 100s to >1000s of metres. Active magmatic arcs are generally characterised by tectonic uplift, and hydrothermal ore deposits formed during those periods can be rapidly exhumed. Therefore, they are often assumed to have eroded away in regions where upper crustal granitoids of arc systems represent the major proportions of present day surface exposure (e.g. Sillitoe, 2010). However, progress in understanding of these connected magmatic-hydrothermal systems, and the future challenge to discover new economical grade ore deposits hidden under cover (e.g. Richards, 2016), has led to advancement in understanding of the processes and conditions that make arc magmas fertile, and thereby creating relatively fast, cheap, and easily applicable exploration tools to identify fertile igneous terranes.

Large magmatic-hydrothermal ore deposits are rare, generally because their formation requires the perfect interplay of consecutive and optimised execution of multiple steps, beginning with the generation of fertile magma, and ending with efficient hydrothermal metal transportation and ore precipitation (e.g. Richards, 2013). Understanding the processes forming fertile magmas capable of producing metal-rich, mineralising fluids is therefore mandatory when trying to develop and use Cu-Au magma fertility as mineral exploration tool.

1.2.1 Approaches to assessing Magma fertility

Two main approaches have been proposed in the literature to assess Cu-Au fertility and are referenced accordingly in the following paragraphs: i) whole rock geochemistry (e.g. element/element ratios), and ii) mineral major and trace element chemistry including volatile distribution and systematics within magmatic-hydrothermal systems. Naturally, these approaches are presented either individually, in combination or are complemented by additional analyses to offer a more comprehensive picture (e.g. age dating, isotope studies, fluid inclusion studies etc.).

Whole-rock geochemistry is easily accessible on a regional scale and has been used for nearly four decades to proxy the magmatic control on the formation of Cu ore productive compared to unproductive igneous suites (e.g. Baldwin and Pearce, 1982; Blevin et al., 1996; Tosdal and Richards, 2001; Richards, 2003; 2011; Rohrlach and Loucks, 2005; Richards and Kerrich, 2007; Schütte et al., 2010; Chiaradia et al., 2012; Richards et al., 2012; Loucks, 2014). The general consensus of all these studies is that proposed elements, element ratios and diagrams (e.g. Y vs. MnO, Fe_2O_3/FeO vs. Rb/Sr; La/Yb, Sr/Y, and V/Sc) used to discriminate fertile from barren suites reflect the presence of abundant magmatic H_2O and moderately oxidising conditions. In many cases, signatures like high La/Yb and Sr/Y are explained by early fractionation of amphibole (see references above) during stalling-mixing-replenishment of primitive mantle-derived basaltic melts in the lower crustal MASH zone (Hildreth and Moorbath, 1988) or hot zones (Annen et al., 2006); in the vast majority of cases, there is no definitive relationship to slab-melting, as has been proposed by other authors (e.g. Defant and Drummond, 1990). Therefore, the recognition of petrogenetic processes leading to, and reflecting increased magmatic H_2O contents on the basis of whole rock geochemistry, is a basic first step in establishing a fertile-barren distinction.

Magma fertility distinction based on magmatic and/or hydrothermal minerals is becoming an increasingly popular method largely owed to significant improvements in resolution and precision of existing, or implementation of new analytical techniques (e.g. EMPA, LA-ICP-MS, SIMS, µ-XANES). In general, the minerals of choice are used to recognize and monitor the same processes as whole rock geochemistry, which are mainly magmatic H_2O content and oxidation state.

Zones of increased Al_2O_3-contents in plagioclase crystals from porphyry intrusions have recently been suggested to reflect elevated magmatic H_2O contents at the time of crystallisation (Williamson et al., 2016), which is the only in-situ analytical concept proposed for a major rock-forming mineral. In general, accessory minerals are the preferred choice, as they are usually considered to be less affected by hydrothermal alteration. In this regard, the most commonly utilised accessory mineral is zircon, which is usually found in intermediate to felsic igneous rocks, and records aspects of the compositional evolution and conditions of the parental melt (e.g. Ballard et al., 2002; Dilles et al., 2015).

In recent years, apatite has been enjoying increasing popularity, and many studies employ apatite chemistry (e.g. trace element composition and distribution, luminescence) as an exploration tool to identify source rock types and fertile magmas (e.g. Belousova et al., 2002; Miles et al., 2014; Mao et al., 2016; Bouzari et al., 2016; Brugge et al., 2017). Apatite is ubiquitous in igneous rocks and ore-related hydrothermal assemblages and considerably resistant to alteration types associated with porphyry-epithermal mineralisation (e.g. Piccoli and Candela, 2002; Bouzari et al., 2016). Additional advantages of apatite are its relatively early crystallisation over a wide range and stages of magmatic evolution, and its capacity to host volatile elements (Cl, F, S), so apatite can track petrogenetic processes in its trace element inventory, and magmatic volatile evolution and distribution (e.g. Cl, F, and S) (e.g. Piccoli and Candela, 2002). Both, chlorine and sulfur are critical in transporting metals within a hydrous fluid or vapour phase to its place of precipitation as ore mineral(s) and hydrothermal alteration (e.g. Candela and Holland, 1984; Hedenquist and Lowenstern, 1994; Kouzmanov and Pokrovski, 2012; Pokrovski et al., 2015; Tattitch and Blundy, 2017; Lecumberri-Sanchez and Bodnar, 2018; Dolejš and Zajacz, 2018). In addition, the sulfur content of apatite is controlled by its crystal structure allowing S to be mainly incorporated as S^{6+} (Konecke et al., 2017), and has therefore been used to gain insights into the oxidation state and S content of porphyry-productive magmas at the time of apatite crystallisation (e.g. Richards, 2015; Chelle-Michou and Chiaradia, 2017). Thus, volatiles are undoubtedly important in and for hydrothermal ore-forming environments and their distribution and evolution - from parental magma formation to fluid exsolution and ore mineral precipitation – are additional key factors for Cu-Au fertility.

Nonetheless, remaining challenges for existing fertility concepts are numerous, and many magmas that are geochemically fertile, can still lack additional ingredients and/or steps necessary to form ore deposits of economic grade. Therefore, postulated concepts are constantly subject to refinement and improvement, all with the aim of more confidently distinguishing not only fertile from barren magmas, but also fertile ore forming suites from theoretically fertile magmas.

1.2.2 The Kennedy Igneous Province, NE Queensland

In northeast Queensland, Australia, are exposed large volumes of Permocarboniferous igneous rocks of the Kennedy Igneous Association (KIA) (e.g. Withnall and Henderson, 2012; Champion and Bultitude, 2013) (Figure 1-1). Coeval igneous rocks of similar character continue southwards, where for example the Lizzie Creek Volcanics Group forms the basal unit of the Bowen Basin (e.g. Malone et al., 1969). This Permocarboniferous assemblage of volcanic and granitoid rocks extending along eastern Queensland represents a Paleozoic continental magmatic arc which developed inboard of a convergent plate margin. In north Queensland, the KIA represents the last phase of this enduring episode of subduction-related magmatism lasting between 510 and ~260 Ma (Jell, 2013 and references therein).

The KIA allied with granitoids in the New England Orogen (NEO), hosts numerous magmatic-hydrothermal deposits typically associated with magmatic arc settings (e.g. Perkins and Kennedy, 1998; Sillitoe, 2010) including high-sulfidation (HS) epithermal deposits such as Mt. Carlton (Sahlström et al., 2018), intermediate-sulfidation (IS) deposits such as Ravenswood, Welcome, and the Scott lode in Pajingo (e.g. Morrison, 1988; Perkins and Kennedy, 1998), and large-scale porphyry diatreme ore bodies (e.g. Mt. Leyshon, Mt. Wright, Kidston, Red Dome) (e.g. Horton, 1978; Morrison, 1988; Kreuzer et al., 2007). Many additional small to medium sized hydrothermal deposits associated with Permocarboniferous igneous rocks have been discovered, but the potential for large-scale porphyry Cu deposits potentially linked to, but hidden underneath fertile igneous suites might have been underestimated.

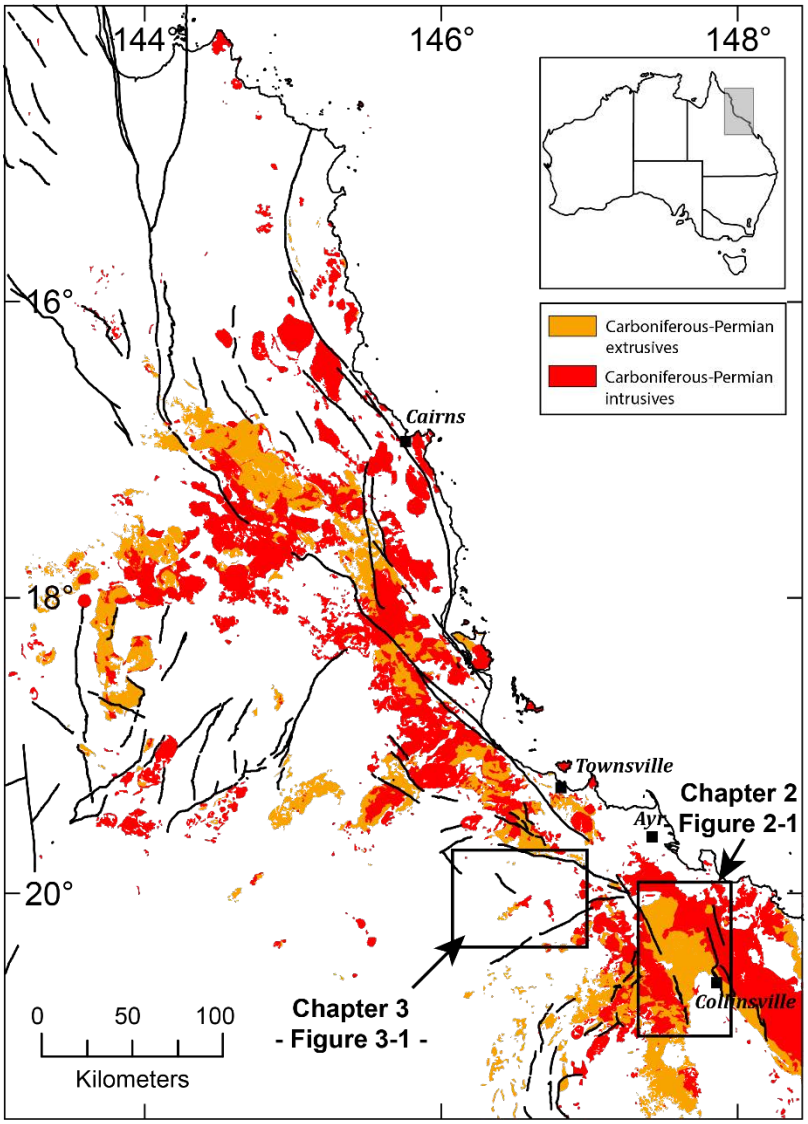

Figure 1-1 Distribution of Permocarboniferous igneous rocks in northeast Queensland (after Champion and Bultitude, 2013). Fields mark the study areas addressed in Chapter 2 and 3.

Compared to young magmatic arcs and related porphyry deposits of the Circum-Pacific region (e.g. Chile or the Philippines), the convergent margin related igneous rocks of north Queensland are relatively old and partially eroded, as large plutons comprise much of today's surface exposure. However, there are local indications of limited erosion/exhumation after the widespread Permocarboniferous mineralising event, such as the existence of HS and IS epithermal deposit at surface levels (e.g. the Mt. Carlton HS epithermal Au-Ag-Cu deposit) which is favourable for the preservation of subsurface porphyry Cu-Au-(Mo) deposits. With recent developments in the understanding of porphyry-epithermal systems (e.g. Sillitoe, 1999, 2010; Hedenquist et al., 1998, 2000, 2001), plus the necessity to explore for deposits undercover or at greater depths, the potential for buried major porphyry deposits needs to be re-evaluated.

This work seeks to offer new insights into the Cu-Au fertility of northeastern Australian Permocarboniferous igneous rocks, and presents a clear case as to the nature and applicability of whole rock and mineral geochemistry in relation to arc magmatism, but also its potential to serve as a mineral exploration tool. In this study, I primarily use well-established analytical techniques to analyze whole rock and mineral major- and trace element compositions (Chapter 2 and 3) complemented by whole rock Sm-Nd isotope compositions (Chapter 2 only), to investigate two different localities with the aim to better understand petrogenetic processes contributing to Permocarboniferous Cu-Au mineralisation in northeast Queensland. Further, I emphasize the complexities researchers, exploration geologists and mining companies will face when applying magma fertility concepts to unknown areas or an unfit data set to obtain the necessary geological conclusions, and therefore promote general caution in doing so. Overall, this work adds to the general understanding of arc magmatism, deepens our understanding of northeastern Australia's geological history, and improves the applicability of whole rock element ratios as a tool to aid future mineral exploration for these deposit types.

The two presented studies are subprojects within the large scale 'Characterising and assessing the prospectivity and intrusion-related hydrothermal mineral systems in north-east Queensland', funded and supported by the Geological Survey of Queensland (GSQ), the Economic Geology Research Center (EGRU) and industry partners (Evolution Mining Ltd., Terra Search, and Basin Gold), and therefore the work presented here also complements and lends petrogenetic background information to additional projects on the regional metallogeny of this area (Corral et al., in prep.) and localised epithermal Au-Ag-Cu mineralisation at the Mount Carlton deposit (Sahlström et al., 2018).

My work investigates different aspects of Cu-Au magma fertility within the Permocarboniferous convergent margin of northeastern Australia, and focusses on petrogenetic processes presumably occurring at different levels within the crust, with the goal to answer the questions: What processes are and/or were necessary at which petrogenetic stage of arc magmatism, to form contemporary, locally fertile magmas, and what causes most of the magmas to be barren with respect to economic grade mineralisation? The different chapters and investigated locations are linked in space and time by their geotectonic setting and outlines for the two papers are given below:

The first location investigated in Chapter 2, lies to the south of Townsville, in the northern edges of the Bowen Basin. There, the Lizzie Creek Volcanic Group (LCV) hosts the Mount Carlton high-sulfidation epithermal Au-Cu deposit which formed at ~280 Ma, during active back-arc extension, west of today's New England Orogen. The objective of Chapter 2 is to investigate and test the applicability of established whole-rock geochemical parameters, e.g. Sr/Y, V/Sc, used to distinguish plutonic, fertile porphyry Cu-Au hosting suites from barren intrusions, on a known locally "fertile" volcanic succession (LCV), hosting the Mt. Carlton deposit and compare these results to contemporary "barren" volcanic rocks of the same group. The overall aim is to answer the question: What first order magmatic controls are necessary to form locally fertile magmas? By doing so, I demonstrate that for volcanic rocks, which are generally highly altered, a) Sr/Y is not the most reliable fertility proxy and b) Rare Earth element ratios (e.g. La/Yb, Dy/Yb) which are less likely to be mobilised during alteration, can be used to reveal different magmatic evolution paths by recording the first order pre-requisite in ore deposit formation - the availability of sufficient magmatic H_2O. Based on my findings, we are capable to confidently extend plutonic Cu-Au fertility concepts to extrusive successions and differentiate between fertile-barren volcanic associations on a regional scale, even if rocks have been hydrothermally altered to certain degrees. The ability to make such distinctions is crucial for modern and future day mineral exploration, where one of the big challenges is and will be to identify fertile terranes that are potentially linked to buried high-grade ore deposits at depth.

Chapter 3 investigates the Tuckers Igneous Complex (TIC), a calc-alkaline, I-type igneous complex which intruded the Ravenswood Batholith at ~300 Ma. The TIC is part of the KIA and its relevance for this project lies within its close association and proximity to some major Permocarboniferous economic porphyry-style Au deposit (e.g. Mount Leyshon, Mount Wright). The TIC was investigated briefly in the early 1990's and the big remaining questions are: Why are there such prominent Au deposits nearby, but the TIC itself can be considered barren? This is similar to the questions addressed in Chapter 2, as in which magmatic processes dictate the fertility of individual locations. In order to answer these questions, I review and extend the previously proposed unpublished petrogenetic model using newly acquired extended whole rock geochemistry and in-situ mineral analyses of the halogen-bearing minerals apatite and biotite. Establishing the petrogenesis creates context for the minerals apatite and biotite which I use to investigate the volatile evolution (Cl, F and S) of the TIC with progressive magma evolution from gabbro to felsic granodiorites.

I utilize the findings from in-situ mineral analyses of apatite (and biotite) to compute magmatic halogen concentrations at the presumed time of apatite crystallisation using established partitioning models between apatite-melt-fluid. The behaviour of chlorine and sulfur are of particular interest, as they are crucial to transport and precipitate ore metals, and can therefore be used to answer the question why the TIC is apparently barren. With this study, I present the first halogen data set of Permocarboniferous granitoids in northeast Queensland, and my results are highly encouraging to further pursue this type of research with regards to magma fertility and ore-forming processes in north-eastern Australia. In addition, my data set adds to the general understanding of volatile behaviour during crystal fractionation processes in arc magmas, and further provides a comparable base line to systematically investigate and unravel halogen systematics in the Permocarboniferous igneous suites of northeastern Australia.

Subsequently, Chapter 4 contains a brief concluding summary of the two different approaches, the general implications of these results for magmatic fertility of northeastern Australian Permocarboniferous igneous rocks, and implications for the general applicability of whole rock magma fertility as mineral exploration tool, in particular with regards to volcanic terranes.

1.3 References

Annen, C., Blundy, J., & Sparks, R. (2005). The genesis of intermediate and silicic magmas in deep crustal hot zones. Journal of Petrology, 47(3), 505-539.

Baldwin, J., & Pearce, J. A. (1982). Discrimination of productive and non-productive porphyritic intrusions in the Chilean Andes. Economic Geology, 77(3), 664-674.

Ballard, J.R., Palin, M.J., and Campbell, I.H., 2002, Relative oxidation states of magmas inferred from Ce(IV)/Ce(III) in zircon: application to porphyry copper deposits of northern Chile: Contributions to Mineralogy and Petrology, v. 144, p. 347-364.

Belousova, E., Griffin, W., O'Reilly, S. Y., & Fisher, N. (2002). Apatite as an indicator mineral for mineral exploration: trace-element compositions and their relationship to host rock type. Journal of Geochemical Exploration, 76(1), 45-69.

Blevin, P. L., Chappell, B. W., & Allen, C. M. (1996). Intrusive metallogenic provinces in eastern Australia based on granite source and composition. Geological Society of America Special Papers, 315, 281-290. doi:10.1130/0-8137-2315-9.281

Bouzari, F., Hart, C. J., Bissig, T., & Barker, S. (2016). Hydrothermal alteration revealed by apatite luminescence and chemistry: a potential indicator mineral for exploring covered porphyry copper deposits. Economic Geology, 111(6), 1397-1410.

Brugge, E., Wilkinson, J. J., & Miles, A. (2017). Fingerprinting fertile porphyry magmas using apatite. Applied Earth Science, 126(2), 46-47. doi:10.1080/03717453.2017.1306236

Candela, P. A., & Holland, H. D. (1984). The partitioning of copper and molybdenum between silicate melts and aqueous fluids. Geochimica et Cosmochimica Acta, 48(2), 373-380.

Champion, D. C., & Bultitude, R. J. (2013). Chapter 6 - Kennedy Igneous Association. In P. A. Jell (Ed.), Geology of Queensland (pp. 473-514): Geological Survey of Queensland, Brisbane.

Chelle-Michou, C., & Chiaradia, M. (2017). Amphibole and apatite insights into the evolution and mass balance of Cl and S in magmas associated with porphyry copper deposits. Contributions to Mineralogy and Petrology, 172(11), 105. doi:10.1007/s00410-017-1417-2

Defant, M. J., & Drummond, M. S. (1990). Derivation of Some Modern Arc Magmas by Melting of Young Subducted Lithosphere. Nature, 347(6294), 662.

Dilles, J.H., Kent, A.J.R., Wooden, J.L., Tosdal, R.M., Koleszar, A., Lee, R.G., and Farmer, L.P., 2015, Zircon compositional evidence for sulfur-degassing from ore-forming arc magmas: Economic Geology, v. 110, p. 241-251.

Dolejš, D., & Zajacz, Z. (2018). Halogens in silicic magmas and their hydrothermal systems. In The Role of Halogens in Terrestrial and Extraterrestrial Geochemical Processes (pp. 431-543): Springer.

Hedenquist, J. W., Arribas, A., & Reynolds, T. J. (1998). Evolution of an intrusion-centered hydrothermal system; Far Southeast-Lepanto porphyry and epithermal Cu-Au deposits, Philippines. Economic Geology, 93(4), 373-404. doi:10.2113/gsecongeo.93.4.373

Hedenquist, J. W., Arribas, A., & Gonzalez-Urien, E. (2000). Exploration for epithermal gold deposits. Reviews in Economic Geology, 13, 245-277.

Hedenquist, J., Claveria, R., & Villafuerte, G. (2001). Types of sulfide-rich epithermal deposits, and their affiliation to porphyry systems: Lepanto-Victoria-Far Southeast deposits, Philippines, as examples. Paper presented at the ProExplo Congreso. Lima, Peru.

Hildreth, W., & Moorbath, S. (1988). Crustal contributions to arc magmatism in the Andes of central Chile. Contributions to Mineralogy and Petrology, 98(4), 455-489.

Jell, P. A. (2013). Geology of Queensland (P. A. Jell Ed.): Geological Survey of Queensland.

Konecke, B. A., Fiege, A., Simon, A. C., Parat, F., & Stechern, A. (2017). Co-variability of S6+, S4+, and S2− in apatite as a function of oxidation state: Implications for a new oxybarometer. American Mineralogist, 102(3), 548-557.

Kouzmanov, K., & Pokrovski, G. S. (2012). Hydrothermal controls on metal distribution in porphyry Cu (-Mo-Au) systems.

Lecumberri-Sanchez, P., & Bodnar, R. J. (2018). Halogen geochemistry of ore deposits: contributions towards understanding sources and processes. In The Role of Halogens in Terrestrial and Extraterrestrial Geochemical Processes (pp. 261-305): Springer.

Loucks, R. R. (2014). Distinctive composition of copper-ore-forming arc magmas. Australian Journal of Earth Sciences, 61(1), 5-16. doi:10.1080/08120099.2013.865676

Malone, E. J., Olgers, F., & Kirkegaard, A. G. (Cartographer). (1969). Geology of the Duaringa and St. Lawrence 1:250000 sheet areas, Queensland

Mao, M., Rukhlov, A. S., Rowins, S. M., Spence, J., & Coogan, L. A. (2016). Apatite Trace Element Compositions: A Robust New Tool for Mineral Exploration*. Economic Geology, 111(5), 1187-1222. doi:10.2113/econgeo.111.5.1187

Miles, A. J., Graham, C. M., Hawkesworth, C. J., Gillespie, M. R., Hinton, R. W., & Bromiley, G. D. (2014). Apatite: A new redox proxy for silicic magmas? Geochimica et Cosmochimica Acta, 132, 101-119. doi:https://doi.org/10.1016/j.gca.2014.01.040

Piccoli, P. M., & Candela, P. A. (2002). Apatite in Igneous Systems. Reviews in Mineralogy and Geochemistry, 48(1), 255-292. doi:10.2138/rmg.2002.48.6

Pokrovski, G. S., Kokh, M. A., Guillaume, D., Borisova, A. Y., Gisquet, P., Hazemann, J.-L., . . . Dubessy, J. (2015). Sulfur radical species form gold deposits on Earth. Proceedings of the National Academy of Sciences, 112(44), 13484-13489. doi:10.1073/pnas.1506378112

Richards, J. P. (2003). Tectono-Magmatic Precursors for Porphyry Cu-(Mo-Au) Deposit Formation. Economic Geology, 98(8), 1515-1533. doi:10.2113/gsecongeo.98.8.1515

Richards, J. P. (2011). High Sr/Y arc magmas and porphyry Cu ± Mo ± Au deposits: Just add water. Economic Geology, 106(7), 1075-1081.

Richards, J. P., Spell, T., Rameh, E., Razique, A., & Fletcher, T. (2012). High Sr/Y Magmas Reflect Arc Maturity, High Magmatic Water Content, and Porphyry Cu ± Mo ± Au Potential: Examples from the Tethyan Arcs of Central and Eastern Iran and Western Pakistan. Economic Geology, 107(2), 295-332. doi:10.2113/econgeo.107.2.295

Richards, J. P. (2013). Giant ore deposits formed by optimal alignments and combinations of geological processes. Nature Geoscience, 6, 911. doi:10.1038/ngeo1920

Richards, J. P. (2015). The oxidation state, and sulfur and Cu contents of arc magmas: implications for metallogeny. Lithos, 233, 27-45. doi:https://doi.org/10.1016/j.lithos.2014.12.011

Rohrlach, B. D., & Loucks, R. R. (2005). Multi-million-year cyclic ramp-up of volatiles in a lower crustal magma reservoir trapped below the Tampakan copper-gold deposit by Mio-Pliocene crustal compression in the southern Philippines. Super porphyry copper and gold deposits: A global perspective: Adelaide, PGC Publishing, 2, 369-407.

Sahlström, F., Dirks, P. H. G. M., Chang, Z., Arribas, A., Corral, I., Obiri-Yeboah, M., & Hall, C. (in press). The Paleozoic Mt Carlton Deposit, Bowen Basin, NE Australia: Shallow high-sulfidation epithermal Au-Ag-Cu mineralisation formed during rifting. Economic Geology.

Sillitoe, R. (1999). Styles of high-sulphidation gold, silver and copper mineralisation in porphyry and epithermal environments. Paper presented at the Pacrim'99 Congress, Bali, Indonesia, 1999, Proceedings: Parkville, Australasian Institute of Mining and Metallurgy.

Sillitoe, R. H. (2010). Porphyry copper systems. Economic Geology, 105(1), 3-41.

Tattitch, B. C., & Blundy, J. D. (2017). Cu-Mo partitioning between felsic melts and saline-aqueous fluids as a function of XNaCleq, fO2, and fS2. American Mineralogist, 102(10), 1987-2006.

Tosdal, R., & Richards, J. (2001). Magmatic and structural controls on the development of porphyry Cu ± Mo ± Au deposits. Reviews in Economic Geology, 14, 157-181.

Williamson, B. J., Herrington, R. J., & Morris, A. (2016). Porphyry copper enrichment linked to excess aluminium in plagioclase. Nature Geoscience, 9, 237. doi:10.1038/ngeo2651

Withnall, I. W., & Henderson, R. A. (2012). Accretion on the long-lived continental margin of northeastern Australia. Episodes-Newsmagazine of the International Union of Geological Sciences, 35(1), 166.

Chapter 2

Copper-gold fertility of arc volcanic rocks

-

A case study from the Early Permian Lizzie Creek Volcanic Group, NE Queensland, Australia

Abstract

The early Permian Lizzie Creek Volcanic Group (LCV) of the Bowen Basin, NE Queensland, Australia, has compositions that range from basalt through andesite to rhyolite and has geochemical signatures (e.g. LILE enrichment, Nb and Ta depletion) that are typical of arc lavas. In the Mount Carlton District (northern Bowen Basin) the LCV are host to epithermal and porphyry Cu-Au-Ag mineralisation, whereas further to the south (near Collinsville, ~50 km from Mount Carlton) these volcanic sequences are barren of magmatic-related mineralisation. Here, I assess the suitability of geochemical indicators of magma fertility (e.g., Sr/Y, La/Yb, V/Sc) for volcanic rocks through study of coeval volcanic sequences from two locations; 1) Mineralised LCV from the Mount Carlton District, and; 2) Unmineralised LCV from the Collinsville area.

The two volcanic suites share similar petrographic and major element geochemical characteristics, and both have undergone appreciable hydrothermal alteration during, or after, emplacement. Nevertheless, the two suites have distinct differences in concentrations of alteration-immobile trace elements (V, Sc, Zr, Ti, REE, and Y) and Nd isotopes that can be related to magmatic evolution processes. The unmineralised suite has relatively low Sr/Y, V/Sc and La/Yb, particularly in the high SiO_2 rocks, which is related to magma evolution dominated by fractionation of clinopyroxene, plagioclase and magnetite. By contrast, the mineralised suite retains relatively high V/Sc, but evolves high SiO2 rocks with depleted HREE and Y contents, and hence high La/Yb. These trends, together with distinct concave-up REE patterns, are interpreted to reflect magma evolution under high magmatic H_2O conditions leading to enhanced amphibole crystallisation and suppressed plagioclase and magnetite crystallisation. These rocks have somewhat elevated Sr/Y compared to the unmineralised suite, but are likely affected by hydrothermal mobility of Sr, so Sr/Y is not considered to be a reliable indicator of magmatic conditions.

The data support previous findings from other fertile volcanic arc terranes in the world and show that geochemical proxies such as V/Sc and La/Yb that are used to assess Cu-Au fertility of porphyry intrusions can also be applied to cogenetic volcanic sequences, provided a sufficient number of samples of a volcanic suite are used to assess elemental trends with fractionation. These geochemical tools may aid regional-scale exploration for Cu-Au mineralisation in convergent margin terranes, especially where epithermal and porphyry mineralisation may be buried beneath cogenetic volcanic successions.

2.1 Introduction

Given the increasing reliance on ore deposit discovery under cover, a major future challenge for porphyry Cu-Au exploration will be the ability to recognize fertile terranes covered by related but potentially barren volcanic successions (Loucks, 2014; Richards, 2016). Geochemical fingerprinting of magma fertility for mineralisation is seen to hold great promise in this endeavour, and has been applied to intrusive and volcanic rocks that are host to porphyry mineralisation (e.g., Richards et al., 2012; Loucks, 2014).

It is understood that the parental magmas to large Cu+Au porphyry deposits are necessarily water-rich (typically ≥4 wt.%), highly oxidised (often ≥NNO +2) and have undergone significant crystal fractionation of amphibole ± titanite (Burnham, 1979; Cline and Bodnar, 1991; Candela, 1992; Rohrlach and Loucks, 2005; Candela and Piccoli, 2005; Richards, 2003; Richards and Kerrich, 2007; Richards, 2011; Chiaradia et al., 2012; Richards et al., 2012; Loucks, 2014). High magmatic water contents greatly suppress plagioclase crystallisation, so that amphibole precedes plagioclase on the liquidus of andesitic melt (Hildreth and Moorbath, 1988). As these minerals have very different affinities for trace elements, the early crystallisation of hornblende relative to plagioclase is interpreted to result in observed high Sr/Y (>35) and absence of significant negative Eu anomalies (Eu/Eu* ~1) of fertile arc magmas (Lang and Titley, 1998; Richards et al., 2001; Rohrlach and Loucks, 2005; Richards and Kerrich, 2007; Richards, 2011; Loucks, 2014). Crystallisation of amphibole (± titanite) also fractionates high field strength elements (HFSE) and rare earth elements (REE) from differentiating arc magmas, with fertile arc magmas having distinct REE signatures with elevated La/Yb (>20), and relative depletion in middle rare earth elements (MREE; Kay and Mpodozis, 2001; Richards et al., 2001; Richards and Kerrich, 2007; Glazner et al. 2008; Bachmann and Bergantz, 2008; Richards et al., 2012). Redox sensitive proxies, such as whole-rock Fe_2O_3/FeO (Blevin et al., 1996), and V/Sc (Loucks, 2014) have also been used to infer relatively oxidising conditions of magmatism.

These geochemical and petrographic indicators of magma fertility have primarily been formulated for application to unaltered intrusive rocks by Loucks (2014), which are commonly not exposed in many geological terranes, including greenfields exploration areas that have potential for significant porphyry mineralisation at depth. Volcanic sequences that overly porphyry deposits may be extensively altered by hydrothermal fluids, and in some

cases are host to high- and intermediate-sulfidation epithermal deposits that are thought to have genetic links to porphyry systems (e.g., Hedenquist and Lowenstern 1994; Arribas, 1995; Hedenquist et al., 1998; Sillitoe, 2010). Therefore, development of magma fertility indicators that are insensitive to hydrothermal alteration, and can be applied to both the shallow (volcanic and epithermal level) and deeper (porphyry intrusive) environments of arc terranes would greatly assist regional exploration targeting of Cu-Au mineralisation.

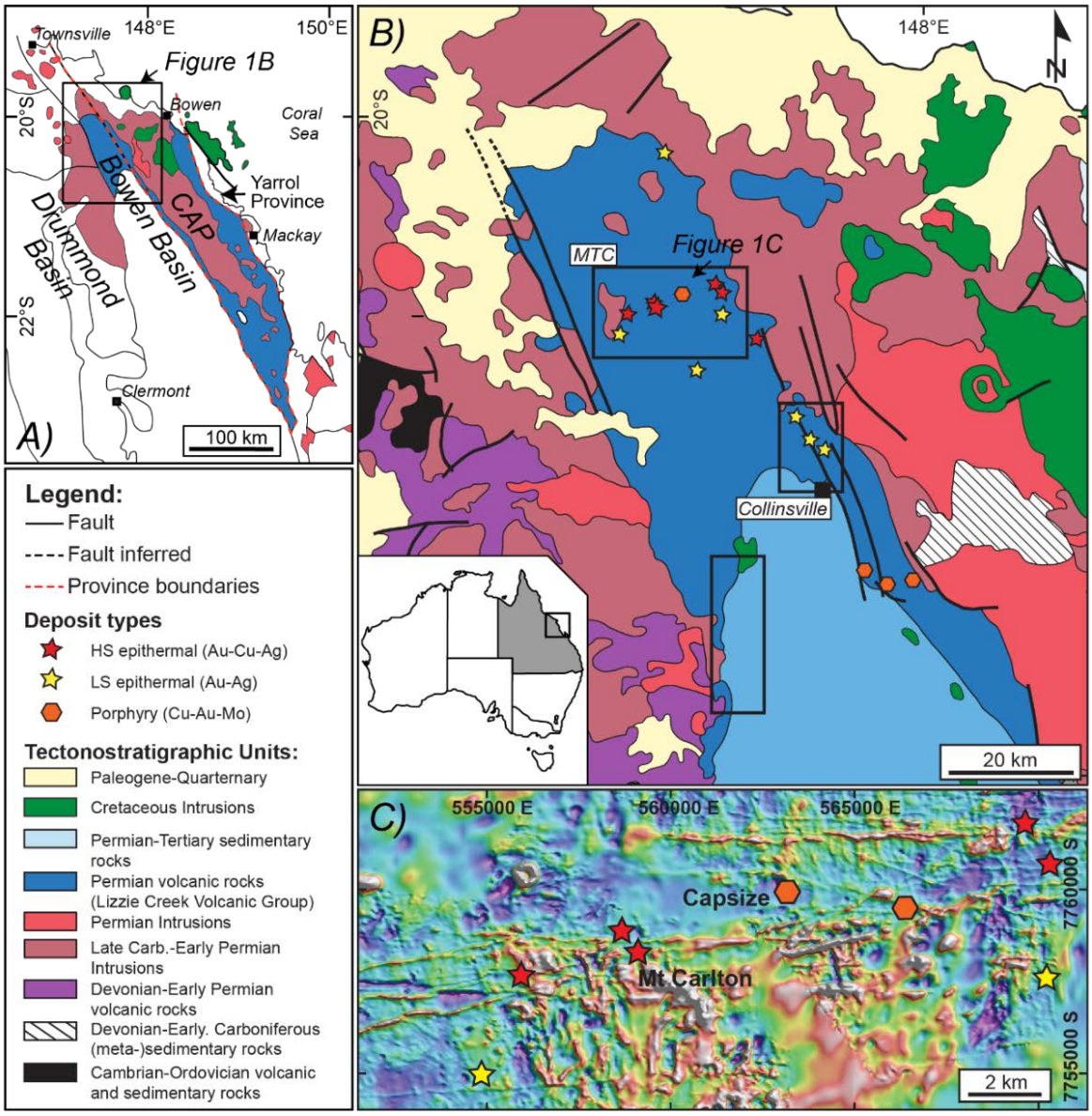

Figure 2-1: A: Geological provinces of the northern New England Orogen, (modified from Allen, 2000). Dashed red lines mark the boundaries between Bowen Basin, Connors-Auburn Province (CAP, Connors Arch) and Yarrol Province (see Donchak et al., 2013). B: Simplified geological map of the northern Bowen Basin including the major tectonostratigraphic units and mineral occurrences/deposits within the Lizzie Creek Volcanic Group (Map courtesy of Ian Withnall, 2015). Black squares refer to areas of rock sampling for this study. C: Magnetic anomaly map (reduced to pole) of the Mount Carlton District. Note, the distinct E-W and ENE-WSW trending structures (mafic dykes and faults) have clear spatial associations with most of the mineral deposits.

A practical indicator for magma fertility derived from previously established geochemical fertility indicators such as Sr/Y and La/Yb (e.g. Rohrlach and Loucks, 2005; Richards and Kerrich, 2007), is the presence of magmatic amphibole in arc magma (Richards et al., 2012). However, arc andesites commonly lack abundant hydrous phases (amphibole and/or biotite) in their mineral assemblage, despite having whole-rock geochemical characteristics that are indicative of amphibole fractionation (Davidson et al. 2007). Davidson et al. (2007) used the term 'cryptic' fractionation, and suggested that an amphibole ± clinopyroxene ± titanite cumulate/restite ('amphibole-sponge') should be present at low to mid crustal depth of arcs. This premise is confirmed by studies of hornblende-rich cumulate xenoliths found in amphibole-free arc lavas (Smith, 2014; Cooper et al., 2016) and by the preservation of hornblende-rich cumulate rocks formed from fractionating arc magmas (Larocque and Canil, 2010; Dessimoz et al., 2012). These cases suggest that neither mineralogical criteria, nor geochemical signatures susceptible to hydrothermal alteration of arc volcanic sequences are likely to be effective for assessing the prospectivity of underlying Cu+Au porphyry mineralisation.

In this chapter, I test the potential of applying existing whole-rock geochemical criteria of magma fertility to a package of Permian arc-related volcanic rocks known as the Lizzie Creek Volcanic Group (LCV), NE Queensland, Australia (Figure 2-1). I evaluate geochemical indicators of magmatic Cu-Au fertility in relation to magma compositions and evolution, which are viewed as first order controls on ore-genesis and porphyry system formation. The LCV is an excellent case example to study because it includes both Cu-Au mineralised sequences in the Mount Carlton district (Sahlström et al., 2017, 2018; Corral et al. in prep.), and unmineralised volcanic rocks in the Collinsville area some ~50 km south of Mount Carlton. This study examines a full suite of major and trace elements, as well as bulk rock Sm-Nd isotopes, but I place a focus on the use of immobile trace element ratios, such as REE and Y, that are little affected by the hydrothermal alteration and weathering that is near ubiquitous in exposed arc volcanic rocks. These findings aim to improve and extend existing Cu-Au fertility concepts from the intrusive environment to the commonly altered volcanic level, particularly in cases where causative intrusions and/or parental magmas to porphyry mineralisation are unexposed or unrecognised.

2.2 Regional Geology and Geodynamic Setting

The northern New England Orogen (NEO) of eastern Australia is a convergent margin accretionary complex formed due to westward dipping subduction from the late Devonian to early Permian (e.g. Allen, 2000; Glen, 2005). The tectonostratigraphic framework and geochronology of the northernmost NEO is summarised in Donchak et al. (2013), and comprises, from east to west, three major coast-parallel geological provinces: 1. The forearc Yarrol Province; 2. The arc-front Connors-Auburn Province, and; 3. The backarc-related Bowen Basin (Figure 2-1A). The Connors-Auburn Province (Connors Arch) includes the ~320 to 278 Ma Urannah Batholith, which extends to the west of the study area (Webb and McDougall, 1978; Allen et al., 1998; Cross et al., 2012).

During the Early Permian, eastward retreat of the subducting slab is suggested to have initiated continental extension in the back arc of the Connors Arch (Allen, 2000), and opening of the proto-Bowen Basin and syn-rift emplacement of the LCV Group in locally isolated NNW-trending graben and half-graben basins (Murray, 1990; Hutton et al., 1999; Korsch et al., 2009). This volcanic sequence is the subject of this paper and will be described in more detail below. The late Permian-Triassic (~265-235 Ma) Hunter-Bowen Orogeny (Donchak et al., 2013) terminated back-arc volcanism. Subsequent magmatic activity was limited to minor Triassic and Cretaceous plutonism and mafic dike emplacement in the northern NEO, and emplacement of the voluminous Whitsunday Volcanic Province along the coast during the early to mid Cretaceous (Allen, 2000; Bryan et al., 2000).

2.3 The Lizzie Creek Volcanic Group

The LCV (Figure 2-1B) represents a calc-alkaline basaltic to rhyolitic arc volcanic sequence encompassing both subvolcanic porphyritic dacite to rhyolite dome facies and extrusive rocks that are locally interbedded with terrestrial sediments (Malone et al., 1969; Hutton et al., 1991; Oversby et al., 1994; Sahlström et al., 2017, 2018). The volcanic sequence was unconformably deposited onto granitic rocks of the Urannah Batholith during the Early Permian (~288-275 Ma; Allen et al., 1998; Cross et al., 2012; Corral et al., 2016) and is locally intruded by rhyolitic porphyries (e.g., Capsize porphyry, see Corral et al., 2016).

The LCV is host to a range of Paleozoic magmatic-hydrothermal deposits and occurrences including porphyry Au-Cu, and high- and low-sulfidation epithermal Au-Ag-Cu mineralisation. Mineralisation is mainly concentrated in the Mount Carlton district located in the northernmost reaches of the Bowen Basin (Sahlström et al., 2018; Figure 2-1B). Mount Carlton preserves an early Permian near-surface high-sulfidation epithermal system hosted in massive porphyritic rhyodacite of the LCV, numerous low-sulfidation epithermal prospects, and the Capsize porphyry prospect (Corral et al., 2016). The most significant (and only currently producing) Au-Ag-Cu deposit in this region is the Mount Carlton high-sulfidation epithermal deposit which contains estimated resources (indicated + inferred) of ~1 Moz Au (Evolution Mining, as of December 2017). Mineralisation at Mount Carlton mainly occurs as structurally controlled lodes within silicic and advanced argillic alteration (Sahlström et al., 2018), and appears to be controlled by E-W and ENE-WSW trending structural lineaments (Figure 2-1C). $^{40}Ar/^{39}Ar$ ages of hypogene alunite from Mount Carlton range from ~284 to 277 Ma (Sahlström et al., 2018; Corral et al., in prep), which links the mineralising event to syn-volcanic deposition of the LCV and back-arc extension.

The oldest volcanic unit (~288 Ma) consists of andesite lavas and interbedded layers of monomict autoclastic breccia, unconformably deposited onto monzogranite of the Urannah Batholith. Overlying the lower andesite is a syn-mineralisation rhyolite to rhyodacite unit that includes massive quartz-feldspar porphyry, flow-banded lava and monomictic autoclastic breccias and interbedded sediments; this unit is host to the high-sulfidation mineralisation at Mount Carlton (Sahlström et al., 2018). Overlying, and partially mineralised, are massively bedded rhyodacite tuffs and rhyodacite lapilli tuffs (interbedded with lacustrine sediments and conglomerates), followed by a sequence of volcaniclastic dacites. These are in turn overlain by a unit of fragmental to agglomeritic andesite with minor andesite lava capped by terrestrial sediments including minor coal horizons. The youngest volcanic member (ca. 275 Ma; Corral et al., in prep) defines the topographic highs within the Mount Carlton district and consists of flow-banded rhyolite.

The LCV extend south of the Mount Carlton district to Collinsville and further south along the eastern and western flanks of the Bowen Basin (Figure 2-1B). In the Collinsville area there are no known occurrences of high-sulfidation epithermal or porphyry mineralisation of any significance.

There are low-sulfidation epithermal prospects ~9 km north of Collinsville (Crushed Creek prospects), but these are not considered to be related to a magmatic source (e.g. Hedenquist and Lowenstern, 1994; Hedenquist et al., 2000), and so are not of consequence for evaluating magma fertility. Likewise, small porphyry prospects to the south-east of Collinsville are thought to be of Cretaceous age, and hence post-date formation of the LCV (Horton, 1978). Rock exposures along the western flank of the Bowen Basin to the south of Collinsville consist of basaltic to basaltic andesite lavas, with minor rhyolite. The LCV in the area around Collinsville (eastern margin of the basin) consist predominately of basaltic andesitic to dacitic-rhyolitic lavas and ignimbrites (Hutton et al., 1991). SHRIMP U-Pb zircon dating of dacitic lava near Collinsville returned an age of ~283 Ma (Cross et al., 2012), which is similar to the mineralisation-hosting unit and mineralisation age (284-277 Ma) at Mount Carlton. Therefore, Permian volcanism across the northern Bowen Basin appears to be contemporaneous, despite the fact that direct links between volcanism and mineralisation are only seen within the Mount Carlton District. In other areas, rocks of this volcanic suite are not known to host mineralisation of Permian age.

2.4 Sampling and Analytical Techniques

For this study, 63 samples of the LCV were examined for petrographic and whole-rock geochemical analysis. This includes samples taken from drill cores, open pit operation and surface outcrops. Given the significant and unequivocal magmatic-related mineralisation in the Mount Carton District (MTC), I classify volcanic samples from Mount Carlton as a 'proximal' or Au-Cu 'fertile' suite. Samples well away from the Mount Carlton District were collected from outcrops in the Collinsville area (hereafter referred to as CV) including locations north and south-west of Collinsville (~40 km south, and ~75 km south-south west of the Mt. Carlton deposit, respectively; Figure 2-1B). These samples are classified as 'distal' to porphyry-epithermal-related Au-Cu mineralisation, or unmineralised.

Prior to geochemical analysis, all samples were screened for alteration intensity using SWIR (short wavelength infrared) spectroscopy. Samples deemed to be highly altered were not processed further. All other samples (37 from MTC, 26 from CV) were prepared by removing weathering crusts and avoiding secondary veinlets (commonly calcite) where possible.

The samples were analysed for 74 major and trace elements by Bureau Veritas Commodities Canada Ltd. (former ACME Laboratories Ltd), Vancouver, using the LF300, LF100 and AQ252 packages. Major element oxides and the majority of trace element composition were obtained by lithium metaborate/tetraborate fusion followed by a combination of inductively coupled plasma mass spectrometry (ICP-MS) for major element oxides and atomic emission spectrometry (ICP-ES) for trace element concentrations. For metal concentrations, 30 g of samples where dissolved in Aqua Regia (1:1:1 HNO_3:HCl:H_2O). This solution was then analysed by ICP-MS. Ferrous iron concentrations were determined separately by titration. Based on repeated analyses of standards and duplicates, the accuracy for major elements is typically within 5 relative %, and 10 relative % for minor and trace elements.

Back scattered electron (BSE) images and major element compositions of pyroxene and plagioclase were obtained in situ from polished thin sections at the Advanced Analytical Centre (AAC), James Cook University (JCU) using a Jeol JXA8200 Superprobe. The microprobe was operated using a 15 kV acceleration voltage, and a 20 nA beam current.

Spot sizes where usually ≤10 μm. Mineral compositions were quantified using well-characterised mineral standards, and matrix corrections are based on a routine ZAF method.

Samarium-Nd bulk rock isotope analyses of 12 samples were carried out by the University of Adelaide, using an Isotopx Phoenix thermal ionisation mass spectrometer (TIMS). Approximately 60-200 mg of rock powder was digested together with a $^{147}Sm+^{150}Nd$ mixed spike and Sm-Nd separation was obtained by two-step column chromatography. A first column pass through 2 ml AGW X8 200-400 mesh resin in Polyprep columns, was followed by a second column pass through 1 ml Leichrom 50-100 mesh Ln resin SPS in quartz glass columns, to separate Sm from Nd. Nd isotopic abundance measurements were carried out in multidynamic mode using at least 5 blocks of 20 cycles (100 ratios). Analyses were corrected for mass bias by normalising to $^{146}Nd/^{144}Nd = 0.7219$ (Wasserburg et al., 1981) using exponential mass fractionation correction. Samarium and Nd concentrations were corrected for 50 pg and 100 pg blanks, respectively. Samarium isotopic abundances were analysed in static mode using 5 blocks of 20 cycles (100 ratios). External reproducibility (2σ) for Nd isotope standard measurements (JNdi-1 standard; Tanaka et al., 2000) is 5 ppm for $^{143}Nd/^{144}Nd$.

2.5 Results

2.5.1 Petrography

Mount Carlton District: Basaltic andesites to andesites in the Mount Carlton District occur throughout the volcanic sequence and both pre-date and post-date mineralisation events (Corral et al., in prep). Pre-mineralisation, fine-grained plagioclase-pyroxene phyric andesite that forms the basal unit of the Mount Carlton sequence consists of sub- to euhedral plagioclase (0.2 to 2 mm) and clinopyroxene (0.1 to 0.4 mm) phenocrysts (~30-40% of the rock) and minor magnetite, in a fine-grained plagioclase (± pyroxene ± magnetite ± quartz) groundmass (Figure 2-2A). Accessory apatite occurs as inclusions within pyroxene, and patchy titanite and calcite has been observed as replacement products of pyroxene, feldspar and magnetite in some cases. Plagioclase phenocrysts are strongly affected by albitisation, giving them a reddish stained appearance in hand specimen and feldspar cores are commonly sericitised. Unaltered plagioclase domains range in composition from An_{48-73}, and both normal ($An_{core} > An_{rim}$) and reverse ($An_{core} < An_{rim}$) zonation has been observed. Clinopyroxene crystals (augite) occur as anhedral to euhedral phenocrysts together with magnetite, or as glomerocrysts. Some grains have resorption textures and chlorite rims formed by alteration. Fully chloritised grains (<5 % of mafics) after an unknown mafic precursor mineral can occasionally be found in these andesites. Amphibole of magnesio-hastingsite composition (following the classification of Leake et al., 1997) has only been found as a single xenocrystic resorbed grain in sample 0409_111.0 (Figure 2-2B).

Plagioclase-augite phyric porphyritic andesite flows (Figure 2-2C) characterize the intermediate post-mineralisation unit. These rocks are similar to the lower andesitic unit, except that they have a higher proportion of feldspar phenocrysts that extend to more sodic compositions (An_{35-65}), and coarser augite (Mg# 62 to 69) phenocrysts (0.5 to 5 mm). The groundmass feldspar and augite compositions range from An_{31} to An_{52}, and Mg# of 51 to 62, respectively.

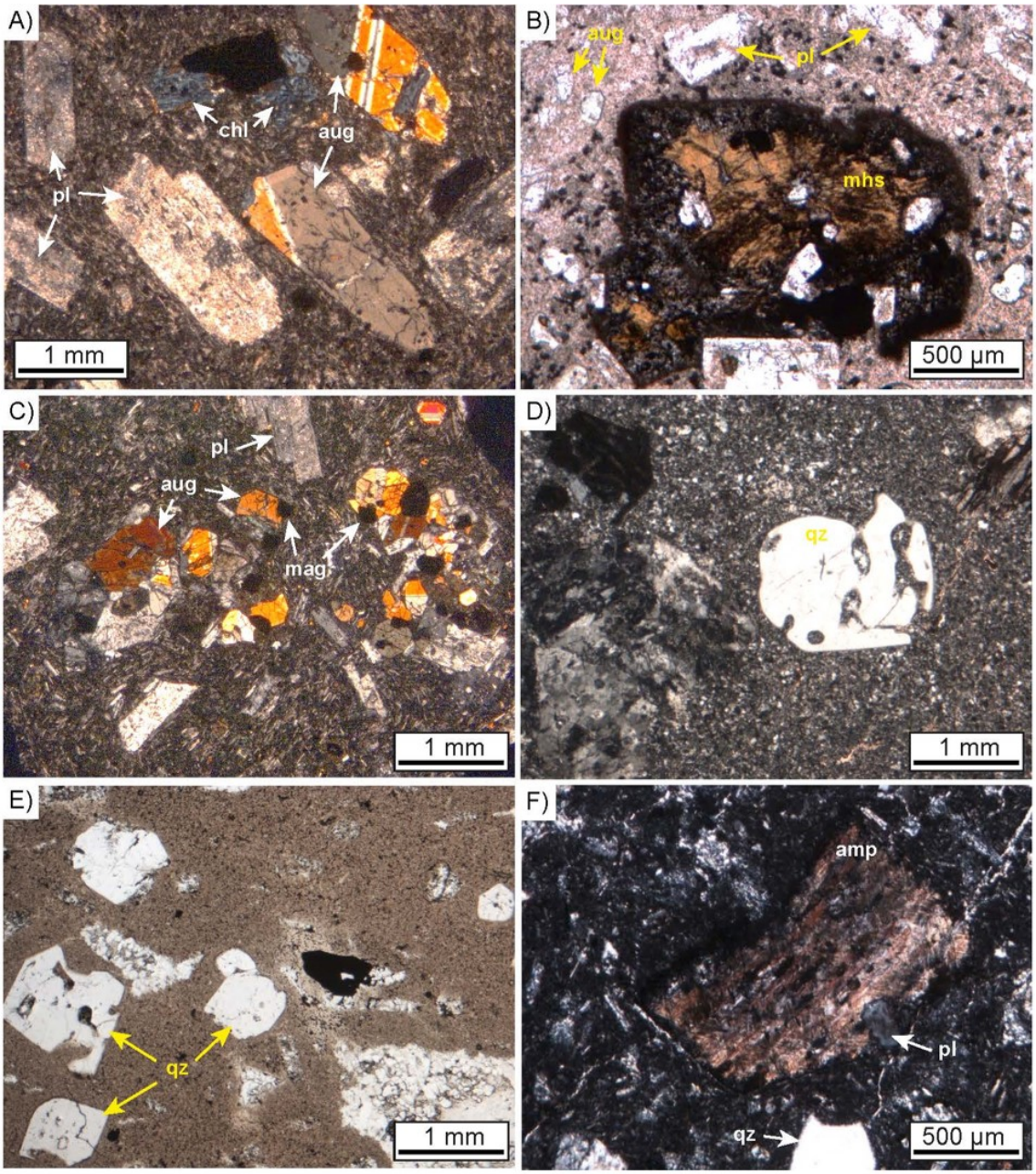

Figure 2-2 Photomicrographs of samples from the Mount Carlton District. A: Lower MTC andesite with partially altered augite and plagioclase phenocrysts. Chlorite (top centre of image) has replaced an unknown mafic precursor mineral. B: Partially resorbed magnesio-hastingsite xenocryst in an augite-plagioclase phyric andesite. C: Typical augite-plagioclase glomerocrysts within a porphyritic Upper MTC andesite lava. D: Embayed quartz phenocryst in feldspar-quartz phyric rhyodacite. E: Quartz-feldspar porphyritic rhyolite, with clay-altered matrix after glass. F: Amphibole xenocryst in a quartz-feldspar rhyodacite from the Capsize porphyry prospect. Mineral abbreviations after Whitney and Evans (2010).

Feldspar-quartz porphyritic dacite and rhyolite in the MTC are commonly auto-brecciated, with amoeboid-shaped clasts of the same rock type. In hand specimen, the dacitic samples contain reddish feldspar phenocrysts in a greyish-green groundmass with subordinate quartz. The rhyolites are distinguished by abundant quartz and feldspar phenocrysts in a reddish-brown matrix. Quartz phenocrysts in the dacites and rhyolites are angular to subrounded grains and commonly show embayment textures (Figure 2-2D). Primary plagioclase phenocrysts are An_{62-70}, although most grains have undergone pervasive albitisation (Ab >95) and sericitisation. Some dacite samples preserve secondary biotite ± apatite ± titanite wrapping around feldspar phenocrysts and Fe-oxide clusters that represent pseudomorphic replacement of phenocrysts of an unidentified mafic mineral(s), which likely were clinopyroxene and/or amphibole.

Collinsville area: Basalts and basaltic andesites around Collinsville occur as seriate porphyritic plagioclase-augite bearing lava flows, as evident from typical flow alignment of plagioclase laths, and locally abundant amygdoidal textures (Figure 2-3A-D). Plagioclase and augite (mostly plagioclase > augite) are the predominant phenocryst phases in a plagioclase-augite-magnetite (+ accessory apatite) groundmass and can occur as multiphase glomerocrysts. Basalts are usually phenocryst poor (less than ~5%), whereas basaltic andesites can contain up to 40% phenocrysts with variable plagioclase to clinopyroxene ratios.

Plagioclase in basalt ranges in composition from An_{68-84} with no observable difference between the phenocryst and groundmass phases. Plagioclase from representative basaltic andesites returned compositions of An_{41-78}, with phenocryst cores extending to more calcic compositions (An_{52-78}) compared to phenocryst rims (An_{48-57}) and groundmass plagioclase (An_{41-57}). Augite occurs in the basalts as skeletal grains and in basaltic andesites as partially resorbed phenocrysts commonly with chlorite rims (Figure 2-3B). Compositional zoning in augites is evident from BSE imaging (Figure 2-3C) and mainly expressed in basaltic samples by varying TiO_2 contents, with phenocryst cores generally having lower TiO_2 compared to rims. Augite phenocrysts in basaltic andesites commonly show normal core-rim zonation, with core compositions being slightly more magnesian (Mg# = 57-68) compared to rim compositions (Mg# = 49-68).

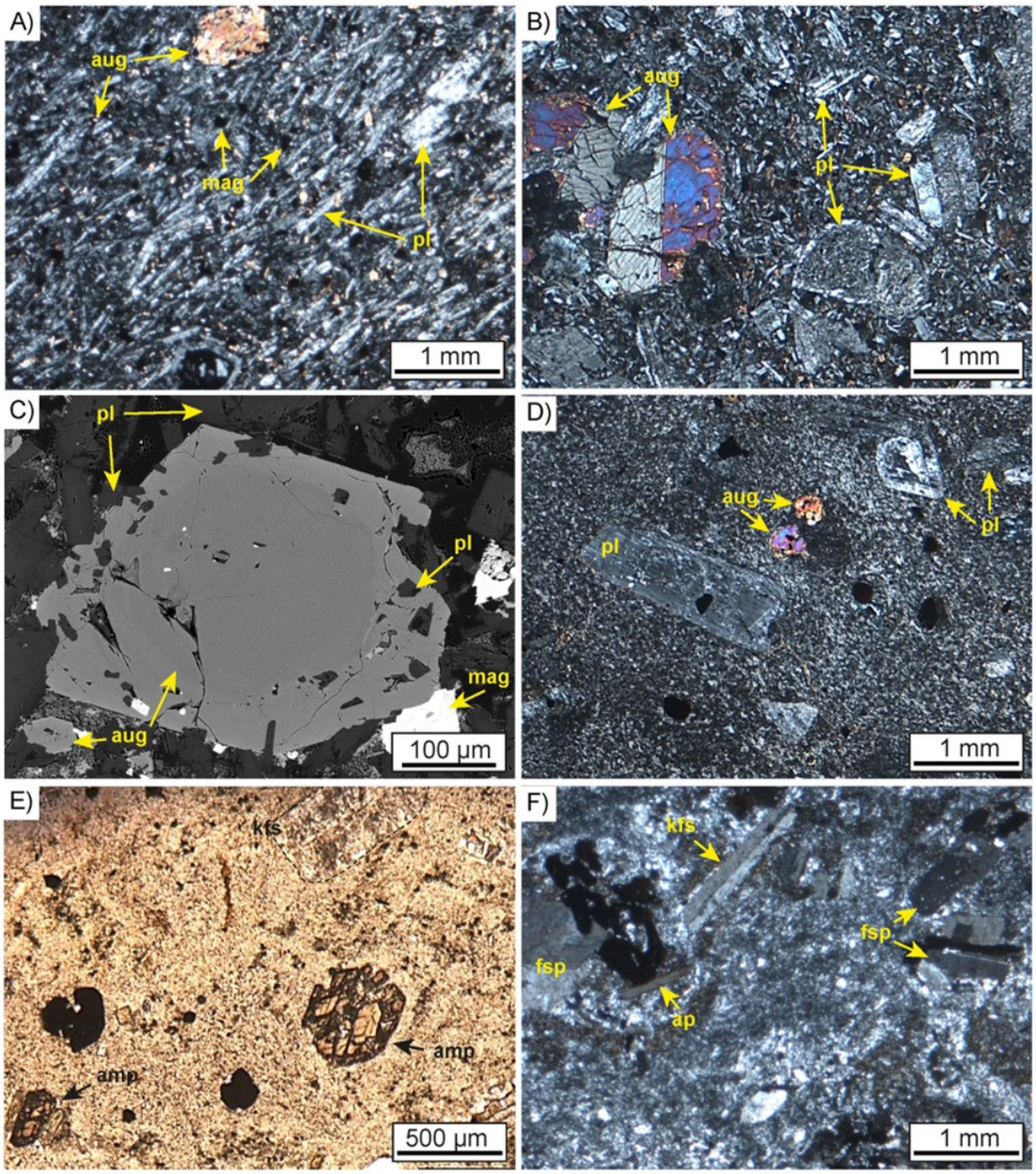

Figure 2-3 Microphotographs of samples from the Collinsville area. A: Augite-plagioclase phyric, basalt with flow alignment of matrix plagioclase. B: Phenocryst-rich plagioclase-augite phyric basaltic andesite. The cores of plagioclase phenocysts are partially sericitised, and augite phenocrysts typically have chloritic rims. C: Backscatter electron image of normally-zoned augite phenocryst. Prismatic plagioclase inclusions occur within the phenocryst rim. D-E: Dacite lava flow from Mount Touissant, Collinsville, featuring oscillatory-zoned plagioclase phenocrysts and anhedral microphenocrysts of augite in quartz-feldspar groundmass (D), and microphenocrysts of amphibole (E). F: Rhyolitic ignimbrite with K-feldspar phenocrysts and an unknown mafic phenocrysts now completed altered to Fe-oxides. Mineral abbreviations after Whitney and Evans (2010).

In the Collinsville area, felsic volcanic samples are dominantly feldspar-quartz porphyritic dacitic to rhyolitic lava flows and rhyolitic ignimbrites. The porphyritic dacites are crystal-rich (30 – 60% phenocrysts), with sodic and minor potassic feldspar phenocrysts (~15%; 0.5 – 1 mm; An_{35-46}) and low Ti-augite + amphibole phenocrysts (commonly resorbed and embayed rims; ~5%, usually <0.5 mm) in a medium- to fine-grained (<0.2 mm) feldspar-quartz groundmass (Figure 2-3E, F). Augite phenocrysts have similar core-rim zonation patterns and compositions (Mg# = ~61, TiO_2 = 0.2 – 0.84 wt.%) to those found in the basaltic andesite samples. Secondary opaque pseudomorphs after prismatic, subhedral mafic precursor minerals are common. Accessory minerals include magnetite, apatite and zircon. Dacitic and rhyolitic lava flows and ignimbrites of the Crushed Creek prospect (North of Collinsville; Corral et al., in prep) are flow-banded and contain up to 10 % K-feldspar and minor quartz phenocrysts.

2.5.2 Major element geochemistry

Results of major and trace element analyses are reported in the Supplementary data files. Regardless of the field location, all LCV samples form a volcanic sequence of calc-alkaline affinity, with variable total alkali contents ranging from intermediate to high values ($K_2O + Na_2O$ of ~3 to 9.5 wt.%). The SiO_2 content of the samples ranges from ~48 to 76 wt.% which gives a rock classification range from basalt to rhyolite (Figure 2-4A), although there is a compositional gap (Daly gap) between 59 – 63 wt.% SiO_2 for the MTC samples, and between 55 – 65 wt.% SiO_2 for the CV samples. Harker variation diagrams for major elements (Figure 2-5) show that both MTC and CV samples follow similar trends with increasing SiO_2 composition. MgO, FeO (as total FeO), Al_2O_3, CaO, TiO_2 and P_2O_5 decrease, and K_2O contents increase with increasing SiO_2. Sodium contents show scattered values across the SiO_2 range. The CV samples trend to higher overall TiO_2, and P_2O_5 and lower MgO compared to the MTC samples.

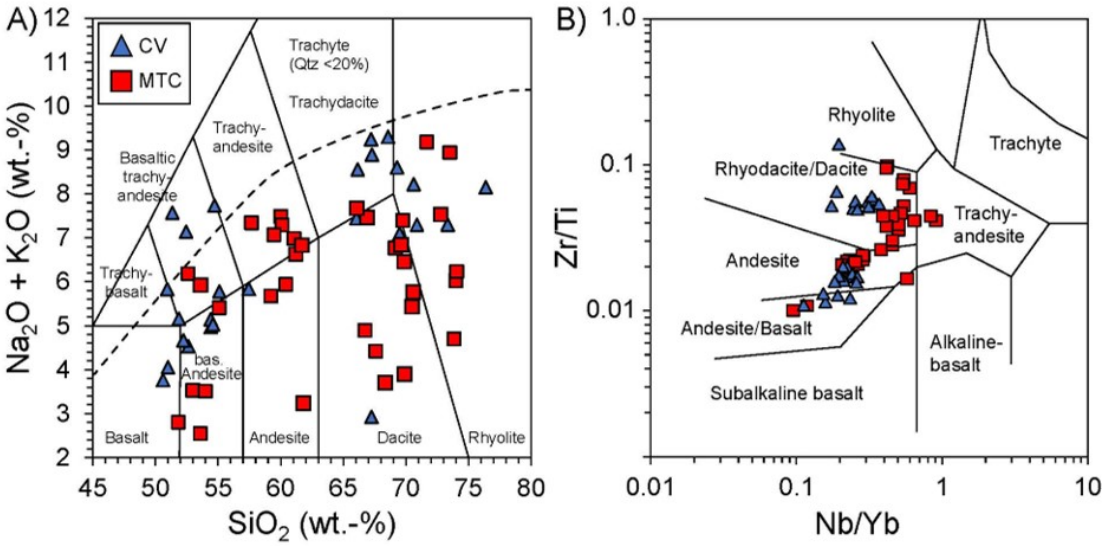

Figure 2-4 Total alkali versus silica (TAS; from Le Maitre et al., 1989) and Zr/Ti vs Nb/Yb (after Winchester and Floyd 1977) plots for volcanic rock classification. The dashed line on the TAS plot is the alkaline-subalkaline division of Irvine and Baranger (1971).

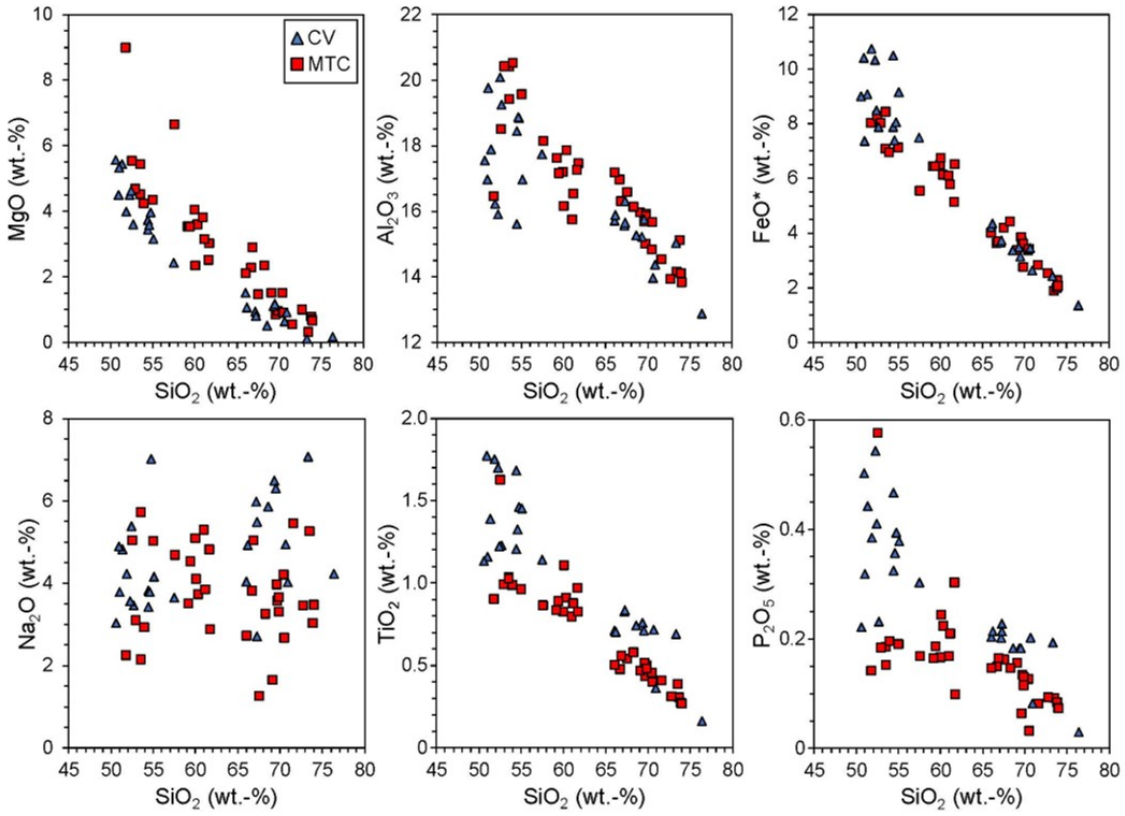

Figure 2-5 Harker diagrams of concentrations of selected major elements versus SiO_2 concentration (volatile-free basis).

Loss on ignition of the investigated samples are variable (LOI = 0.4 to 8 wt.%), with the MTC samples extending to higher LOI (4 to 8 wt.%) compared to the bulk of the CV samples (0.4 to 4 wt.%). Exemptions are CV samples collected close to the low-sulfidation epithermal Crushed Creek prospect (LOI = 4.5 to 8 wt.%). High LOI values are commonly linked to alteration and scatter in hydrothermally mobile elements (e.g. Na, K, Ca, Sr, Rb), but we have observed no systematic correlation between these elements and LOI (Figure 2-6).

Initial SWIR analyses of the here investigated samples did not show excessive alteration typically found in close periphery to high-sulfidation epithermal or porphyry deposits (e.g. samples did not contain alunite or indicated extensive silicification; for comparison of highly altered MTC samples (see Sahlström et al., 2018)). The application of the Advanced Argillic Alteration Index (AAAI) vs Ishikawa Alteration Index (AI) box plot (Figure 2-6; Large et al., 2001; Williams and Davidson, 2004) offers a quantitative method to evaluate bulk-rock chemical modification due to alteration in porphyry-epithermal environments. The Ishikawa Alteration Index (AI = molar $100*[K_2O+MgO]/[K_2O+MgO+Na_2O+CaO]$, Ishikawa et al., 1976) relatively reflects the

abundance of chlorite and sericite and depletion of CaO and Na_2O associated with feldspar destruction. An increase in AAAI represents strong SiO_2 enrichment and destruction of chlorite, carbonate and feldspar; these correspond to mineralogical changes observed from advanced argillic alteration zones of high-sulfidation epithermal systems (Hedenquist et al., 1998).

Almost all of the samples plot within, or close to, the unaltered box, as defined by Large et al. (2001). However, this does not mean that these samples are strictly unaltered, but rather not excessively altered compared to the highly altered MTC samples investigated by Sahlström et al. (2018) and Corral et al. (in prep.). Only two highly sericitised MTC samples (BB15_006, BB15_043) plot well outside of the unaltered field. These two samples are characterised by extreme K_2O (>10 wt.%) and Na_2O (<1 wt.%) compositions and were not considered further in my data analysis.

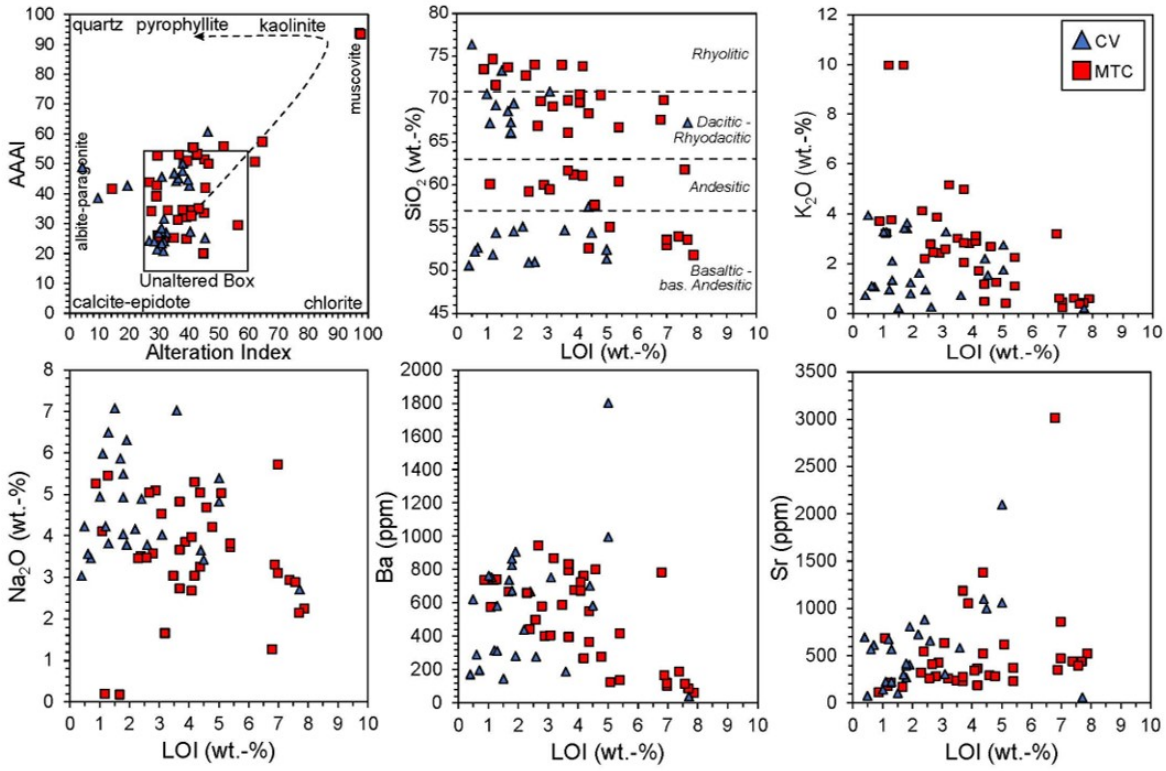

Figure 2-6 Alteration Box Plot (Williams and Davidson, 2004) and scatter plots of alteration sensitive elements against loss on ignition (LOI). Dashed arrow in the alteration box plot indicates the typical trend from least altered (propylitic) towards pyrophilite alteration zones. CV = Collinsville sample suite; MTC = Mount Carlton district sample suite.

2.5.3 Trace element geochemistry

Classification based on immobile trace element ratios Zr/Ti and Nb/Yb (Winchester and Floyd, 1977) indicate a rock-type range from basalt to rhyodacite for both the MTC and CV samples (Figure 2-4B); this classification is broadly consistent with the major element geochemistry and petrographic results for these samples.

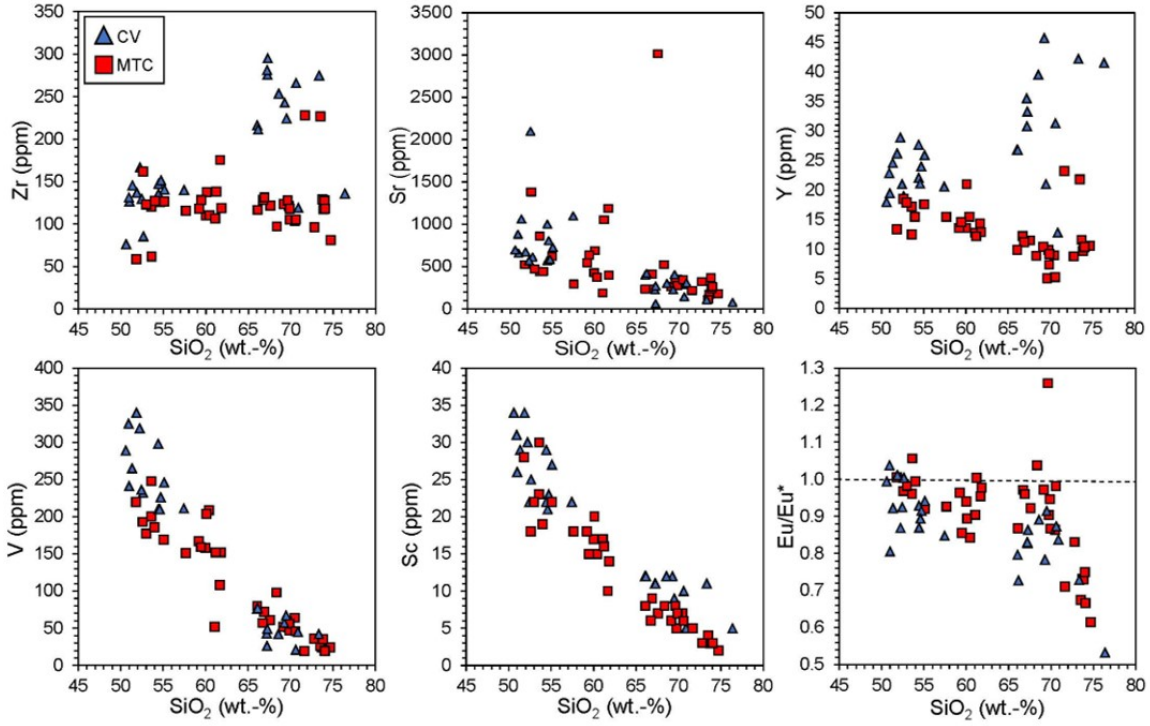

Figure 2-7 Scatterplots of concentrations of selected trace elements and Eu/Eu* versus SiO2 concentration.

Most incompatible trace elements (e.g., Sr, V, Sc) follow broadly defined decreasing trends with increasing SiO_2 contents in both sample suites (Figure 2-7). By contrast, some incompatible elements show contrasting trends with SiO_2 between the two suites. The MTC samples show progressive depletion in Y, MREE, HREE and Zr with increasing SiO_2, whereas the CV samples become enriched in these elements with increasing SiO_2. Sr/Y for MTC and CV suites cover a similar broad range between ~2 and 100 (with one outlier at ~ 261, resulting from Sr ~3000 ppm), although the CV samples tend to have lower Sr/Y compared to the MTC samples. The V/Sc ratios for most samples fall between 6 and 12, although the most evolved CV samples (65 to 76 wt.% SiO_2) have notably lower V/Sc (V/Sc = 2 – 9), compared to MTC (V/Sc = 4 – 12).

Trace elements plotted against primitive mantle values show that both sample suites feature relative incompatible element enrichment with positive Pb, Th and U anomalies and relative depletion in Nb and Ta (Figure 2-8); features that are characteristic of subduction zone magmas (Tatsumi and Eggins, 1995). Rare earth element distribution patterns for the MTC samples are slightly concave up (Figure 2-8) with strong to moderately fractionated LREE/HREE and MREE/HREE (La/Yb = 7 – 39, Dy/Yb = 1.5 – 2.3). La/Yb generally increases with SiO_2, while Dy/Yb remains relatively uniform in intermediate compositions (Dy/Yb = 1.6 – 2.25), and slightly decrease (Dy/Yb = 1.5 – 2) in the more evolved samples (>65 wt.% SiO_2).

MTC samples have M-HREE depleted REE patterns, except two samples of the upper flow-banded rhyolite, which post-date mineralisation in the region. MTC basaltic andesites to dacite (SiO_2 = 51 – 71 wt.%) show no significant Eu anomaly (Eu/Eu* = 0.8 – 1.05), whereas the more evolved rhyolites have slight negative Eu anomalies (Eu/Eu* = 0.61 – 0.75) (see also Figure 2-7).

REE diagrams for the mafic to intermediate CV samples are similar to the MTC samples, whereas the evolved CV samples do not show the distinct M-HREE depletion that characterize the MTC samples (Figure 2-8). Hence, La/Yb in the CV samples remains low (<20) and Dy/Yb ratios (~1.4 – 2.14) decrease slightly with increasing SiO_2. CV samples show no significant Eu anomalies (Eu/Eu* ~0.72 – 1.02) except for the most evolved rhyolite sample (BB15_031; Eu/Eu* ~0.53).

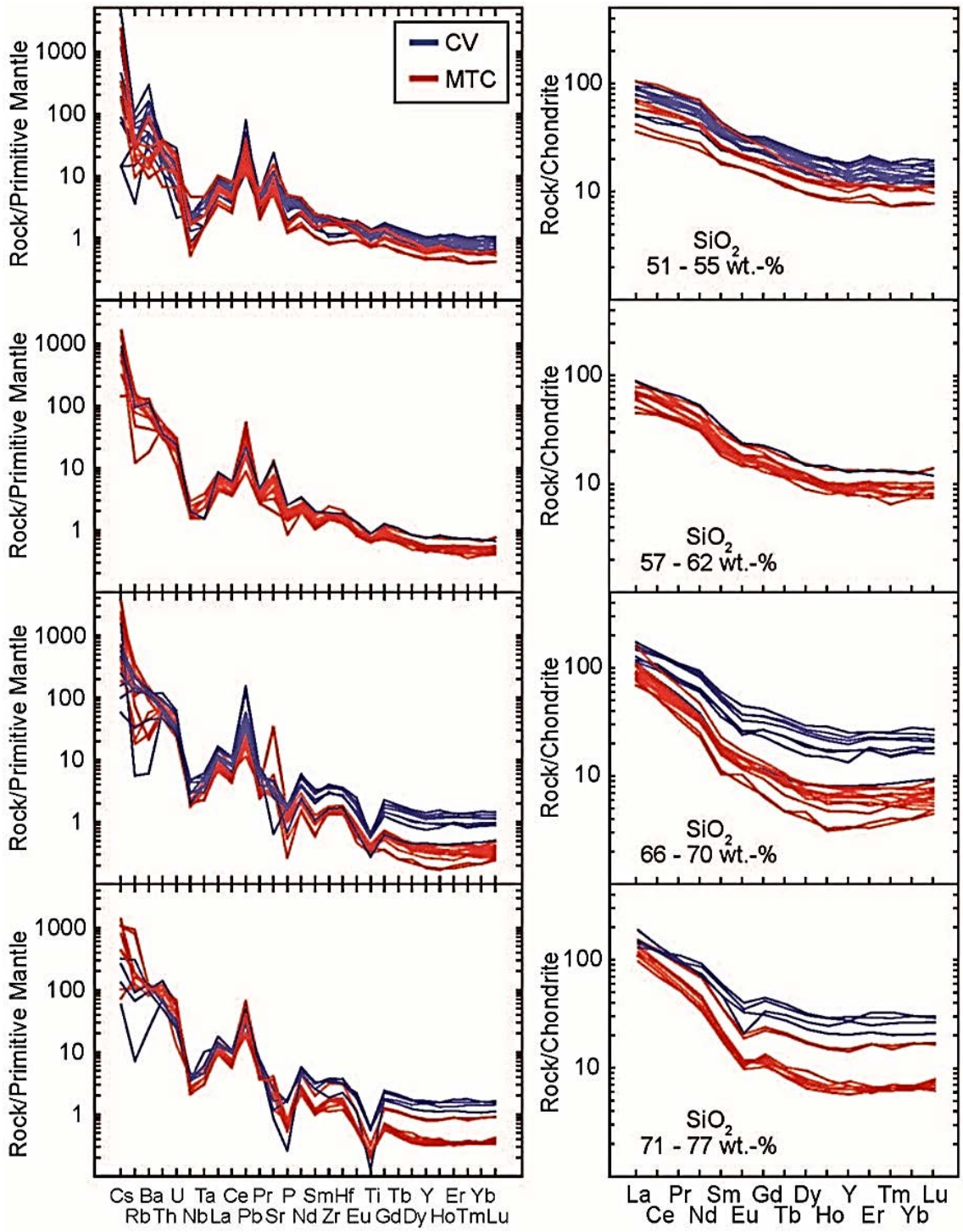

Figure 2-8 Primitive mantle-normalised trace element abundance and chondrite-normalised REY plots for the MTC and CV volcanic rocks. Normalising values are taken from Sun and McDonough (1989). The CV samples are generally more enriched in HFSE and REE+Y compared to MTC samples.

2.5.4 Sm-Nd isotope compositions

εNd values of 12 samples (6 MTC and 6 CV samples) covering the range of SiO_2 contents were calculated to an initial age of 280 Ma, which represents an appropriate approximation of the age of the LCV (Sahlström et al., 2018; Figure 2-9). Most of the analysed samples show a restricted compositional range within 1 epsilon unit of CHUR (εNd = +1 to -1), expect one basaltic CV sample that returned εNd = +3.16. The MTC samples have slightly negative εNd (-0.40 to -1.05), and CV samples have slightly positive εNd (0.14 to 3.16) values. Overall, all samples overlap with the range of values for plutonic basement rocks of the northern New England Orogen (εNd = -1.48 – +6.5; Figure 2-9; Champion, 2013 and references therein).

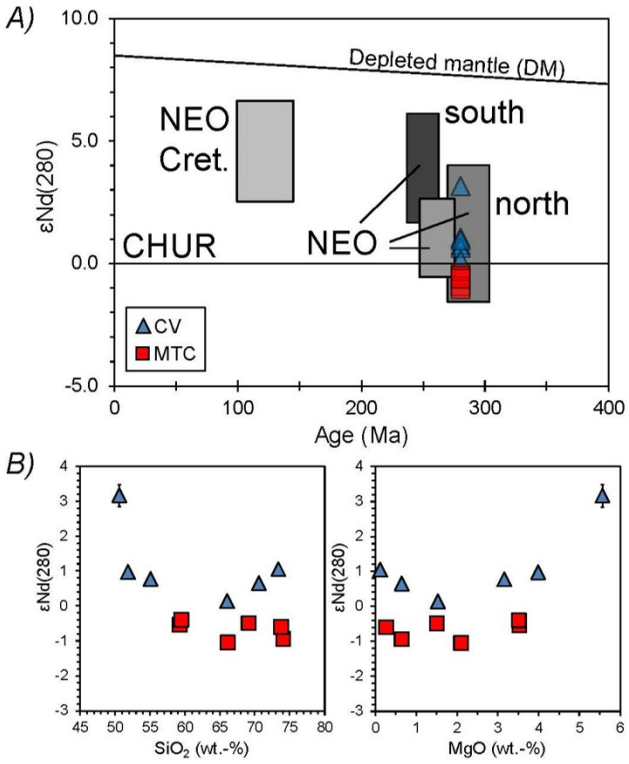

Figure 2-9 A: εNd versus time plot of analysed MTC and CV samples. εNd calculated to 280 Ma. The values fall well within the field reported for Permian northern New England Orogen (NEO) intrusions and minor volcanic rocks (NEO data from Champion (2013). Cret. = Cretaceous. Depleted mantle (DM) evolution curve from DePaolo (1981). B: εNd vs. SiO_2 and MgO. The lack of systematic isotopic variation across the compositional range indicates that contamination by older crust during magmatic evolution was insignificant.

2.6 Discussion

The Early to Mid Permian LCV as a whole represents a medium to high-K calc-alkaline volcanic sequence emplaced in a back-arc setting inboard of the northern New England Orogen (Sahlström et al., 2018). The distinctive geochemical signatures of my samples, with negative Nb and Ta anomalies, and enrichment in Pb, Th, U and LILE (Figure 2-8), are entirely consistent with a subduction-related origin (Tatsumi and Eggins, 1995). Although porphyry-epithermal mineralisation forms in arc settings, this arc signature of the volcanic rocks is not particularly useful as an indicator of fertility in itself, as magmatic arc rocks dominate convergent margin terranes. It would, nevertheless, be highly beneficial to distinguish magmatic arc suites further into those that are mineralisation fertile and those that are not. Hence, being able to distinguish between the contemporaneous 'fertile' MTC and supposedly 'infertile' CV volcanism within a volcanic sequence that is exposed across a large region, may be particularly beneficial for mineral exploration targeting. There are notable differences between the geochemical records of magmatic evolution of the two suites, which, when linked to causative petrogenetic processes, allow us to qualitatively test and improve the applicability of established geochemical proxies (e.g. Sr/Y, V/Sc, La/Yb; Richards and Kerrich, 2007; Loucks, 2014) as indicators of the fertile arc magma suites. Prior to this, evaluation of the potential influence of hydrothermal alteration on magmatic geochemical signatures, and discussion of the petrogenetic evolution of the volcanic sequences is warranted.

2.6.1 Hydrothermal alteration and effects on whole-rock geochemistry

My sample selection and preparation procedures were designed to minimize effects of hydrothermal alteration and/or weathering. Nevertheless, all of the samples have alteration mineral assemblages including secondary calcite and titanite, albitisation and sericitisation of plagioclase, and chlorite replacing mafic silicates. Hutton et al. (1991) also described quartz, prehnite, epidote, clinozoisite, albite and possibly chlorite as secondary minerals in the LCV from along the eastern flank of the Bowen Basin. The most commonly applied monitor of bulk rock geochemical alteration is the LOI value, as this increases with formation of hydrothermal alteration product phases, such as sericite, chlorite and calcite.

Although many samples do have elevated LOI (>3 wt.%), the majority of the samples falls within the unaltered field of the alteration box plot (Figure 2-6; Williams and Davidson, 2004). This does not mean that these samples (in particular MTC samples) did not experience any alteration as the petrography shows that e.g. feldspars are generally strongly albitised, mafic minerals were replaced by chlorite and/or Fe-Ti oxide and SWIR analyses showed the presence of clay minerals (mainly illite) in the ground mass. However, these samples are interpreted to not be exessively altered compared to mineralised MTC samples as demonstrated by Sahlström et al. (2018) and thus, are not considered to have experienced wholesale geochemical modification by high-grade hydrothermal alteration.

In general, alkali major elements (K, Na and Ca) and large ion lithophile elements (LILE: e.g. Ba, Cs, Rb, Sr) are regarded to be highly mobile during hydrothermal alteration and/or metamorphism. Here, these elements show variable degrees of scatter when plotted against SiO_2 (e.g., Figure 2-4; 2-5), which I assume is due to hydrothermal alteration, particularly the breakdown and alteration of magmatic plagioclase, pyroxene and glass to albite, sericite, and chlorite. Extreme Sr contents (> 1000 ppm) in some samples are attributed to the formation of secondary carbonate. Strontium in particular has been demonstrated to can be either lost or gained during hydrothermal alteration as shown during alteration and interaction of oceanic crust with seawater (e.g. Staudigel et al., 1981), and original Sr contents prior to any alteration would be difficult to determine. In these cases, ratios involving these elements (e.g. Rb/Sr or Sr/Y) should at least partially reflect alteration processes, rather than magmatic compositions and, hence, are of limited use for evaluating magma fertility. This necessitates the use of element ratios that are noticeably immobile during hydrothermal alteration and weathering processes to evaluate magma petrogenesis and for assessing magma fertility of volcanic arc terranes.

Previous work on REE and HFSE mobility in hydrothermal environments demonstrates that in general, these elements are not significantly affected by hydrothermal or metamorphic fluid-rock interaction (e.g., Bau, 1991; Hammerli et al., 2016), except in cases of very high fluid flux, or alteration by unusual highly solvent fluids (e.g., HF). Studies from high-sulfidation epithermal environments have demonstrated that REE remain immobile in rocks affected by propylitic to intermediate argillic alteration conditions (Arribas et al., 1995; Fulignati et al., 1999; Parsapoor et al., 2009). Only under extreme

alteration conditions of advanced argillic and silicic alteration do some HREE become mobilised.

Despite the petrographic and geochemical evidence for hydrothermal alteration of both the MTC and CV samples, there is no evidence to suggest that REE, HFSE and selected transition metal (V, Sc, Ti) contents have been modified during alteration. These elements tend to vary systematically with SiO_2 in accordance with expected magmatic fractionation trends (Figure 2-7 and Figure 2-8), and REE patterns are smooth and consistent within samples suites, and do not have anomalies that may be related to oxidative alteration (e.g., Ce anomalies). I conclude that REE and HFSE systematics "see through" the alteration that has affected the LCV, and hence are useful for evaluating magmatic petrogenesis and magma fertility.

2.6.2 Magmatic petrogenesis

The Lizzie Creek Volcanic Group including both, the CV and MTC sample suites have a compositional range from medium to high-K (minor) basalt to rhyolite, which is consistent with the continental back-arc setting and is typical for many porphyry-related arc rocks (Cooke et al., 2005, 2014; Sillitoe, 2010). Both suites also feature trace element patterns that are indicative of a subduction–related origin (Figure 2-8) and both suites share a similar igneous mineral assemblages dominated by calcic-plagioclase, augite and (Ti)-magnetite, with amphibole and/or biotite only occurring as accessory phases at more evolved dacitic compositions; these assemblages are also typical of arc volcanic sequences. The CV and MTC samples feature LREE-enriched REE patterns, but show no indication of accumulated plagioclase (i.e., as Al_2O_3 <22 wt.% and Eu/Eu* <1.3; Loucks, 2014).

Based on the geochemical trends (Figures 2-4; 2-5; 2-7; and 2-8) and mineral assemblages observed, I consider crystal fractionation to be the primary process that produced the observed compositional range across both magma suites; a premise supported by the similarity of Nd isotope compositions of each suite across the range of SiO_2 contents (Figure 2-9). One basaltic sample from Collinsville has a more primitive εNd value than other samples of that suite, indicating the least degree of crustal contamination compared to the other analysed samples with εNd value close to 0. Therefore, crustal contamination likely

affected the parental (high temperature) magmas of this suite to a negligible degree, and did also not play a major role during subsequent magmatic differentiation.

Despite their similarities, the CV and MTC suites are clearly distinguished by their HFSE and REE concentration trends, and differences in overall εNd values (Figure 2-7 - Figure 2-10). These differences are clearly evident from the REE plots that show two distinct patterns at elevated SiO_2 contents. The CV suite trends, particularly the incompatibility of Zr, Y and REE, and relative constancy of La/Yb (Figure 2-8 andFigure 2-10) are consistent with magma evolution dominated by fractionation of plagioclase, clinopyroxene, and magnetite, with a minor role for hydrous phases such as hornblende and biotite (e.g., Davidson et al., 2007). Sr/Y vs. Y as well as La/Yb vs. Yb trends for CV samples also conform with typical arc volcanic rock suites (Figure 2-10A; B).

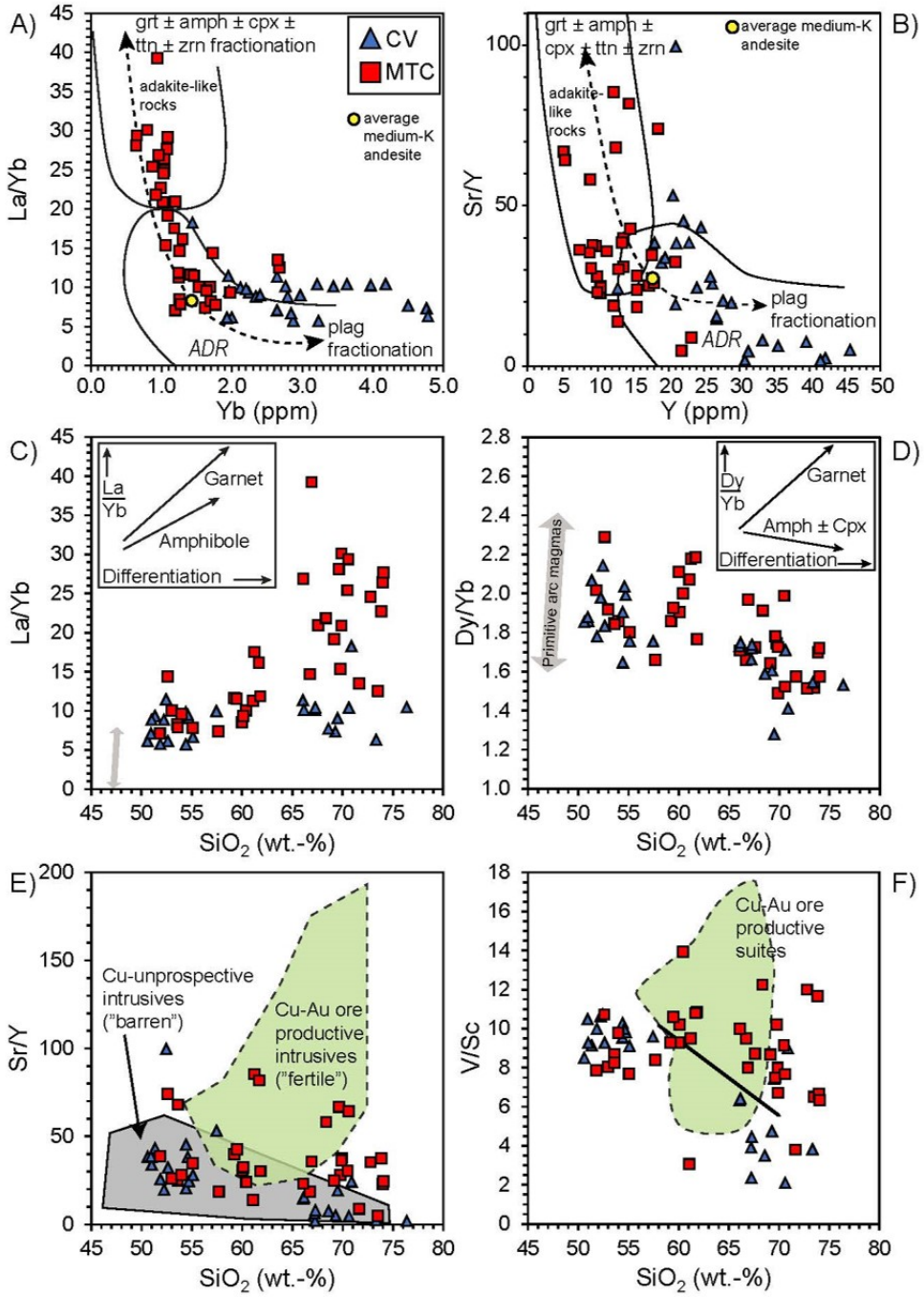

Figure 2-10 A: La/Yb versus Yb (after Castillo et al., 1999), and; B: Sr/Y versus Y (after Defant and Drummond, 1993), showing fields for adakite-like and island arc andesite-dacite-rhyolite (ADR) lavas, as defined by Richard and Kerrich (2007). Black arrows indicate differentiation paths resulting from crystal fractionation of various minerals from an average medium-K andesite (Richards and Kerrich, 2007). C-D: La/Yb and Dy/Yb vs. SiO_2 with schematic geochemical trends resulting from crystal fractionation of garnet or amphibole (from Davidson et al., 2007). Grey arrows indicate La/Yb and Dy/Yb ranges expected for primitive arc magmas before amphibole fractionation (Davidson et al., 2007). E: Sr/Y versus SiO_2 magma fertility scheme (from Loucks, 2014). Note, only a few sample of the MTC suite plot in the 'fertile' field. F: V/Sc versus SiO_2 magma fertility scheme (from Loucks, 2014). Dashed line ($y = 32.5 – 0.385$*wt.-% SiO_2) is defined as the general fertile-barren boundary by Loucks (2014). Note, most MTC sample with >60 wt.% SiO_2 fall into the 'fertile' field.

V/Sc ratios drop from ~8 to 11 in CV basaltic andesite to ~ 2 to 9 in more evolved volcanic rocks; a feature that has been linked to the onset of magnetite crystallisation and

shift in the oxidation state of the melt (i.e., the 'magnetite-crisis' of Jenner et al., 2010). This would also be consistent with the drop in FeO, TiO_2 and P_2O_5 across this transition (Figure 2-5), as magnetite and apatite are often observed to crystallize in tandem (Jenner et al., 2010).

The mineralisation fertile MTC samples are distinguished from the CV samples by their combined trends of increasing La/Yb and decreasing Dy/Yb ratios with progressive fractionation (increasing SiO_2), and their distinctly concave-up, M-HREE depleted REE patterns (Figure 2-7 and Figure 2-8). These features of the MTC suite are consistent with magma evolution controlled by amphibole fractionation, rather than garnet or clinopyroxene alone (Davidson et al., 2007; see also Cline and Bodnar, 1991; Lang and Titley, 1998; Richards et al., 2001; Richards and Kerrich, 2007; Richards, 2011, Loucks, 2014). The distinctive concave–up REE patterns are also a close match to modelled melt compositions after fractionation of amphibole (Cooper et al., 2016).

High water content (≥4 wt.%) in the parental magmas is required for amphibole saturation (e.g. Burnham, 1979; Naney, 1983; Ridolfi et al., 2010). Moreover, high magmatic water content (> 6 wt.%) is a prerequisite for fertile magmas (e.g. Chiaradia and Caricchi, 2017), and has been shown to suppress plagioclase and titanomagnetite fractionation in favour of amphibole (Burnham, 1979; Hildreth and Moorbath, 1988; Candeal, 1992; Loucks, 2014). Similar relative shifts in the stability of crystallising phases can be achieved by fractionation at high pressure (>1GPa; Ulmer, 1989; Kägi et al., 2005), but extensive fractionation at such high pressures seems unlikely given that the MTC suite (and LCV) were emplaced during a period of extension and crustal thinning (Allen, 2000; Sahlström et al., 2018). The suppression of plagioclase fractionation in intermediate to more felsic MTC rocks is indicated by the lack of Sr and Eu depletion (i.e., weak Eu anomalies) and the lack of extensive titanomagnetite fractionation in andesites is in agreement with relatively constant V/Sc content, as titanomagnetite should deplete V, but not Sc (Loucks, 2014).

The MTC samples follow trends in Sr/Y and La/Yb ratios similar to those of adakite-like rocks (Figure 2-10A, B). Adakites were long regarded as "slab melts" (e.g., Defant and Drummond, 1990), but it has since been shown that 'adakite-like' signatures can be produced in derivative magmas of amphibole (± garnet ± clinopyroxene ± titanite) fractionation from primitive hydrous, arc magmas (Moore and Carmichael, 1998; Müntener et al., 2001; Richards and Kerrich, 2007; Loucks, 2014).

Hydrous magma reservoirs could be generated by stalling/underplating of primitive mantle-derived basaltic melts in the deep MASH zone (Hildreth and Moorbath, 1988) or more locally confined 'hot zones' (Annen et al., 2006), where replenishment-mixing cycles subsequently increase the dissolved H_2O content in magmas (Hildreth and Moorbath, 1988; Rohrlach and Loucks, 2005).

The important role of amphibole fractionation in the MTC suite appears to contradict petrographic observations that amphibole is generally lacking or only present in accessory amounts (<5%) in these rocks. Evidence for amphibole crystallisation is indicated by resorbed amphibole xenocrysts in MTC andesite (sample 0409_111.0) and dacite units (e.g. sample 1118_31.0). Nevertheless, a dearth of amphibole as phenocysts or matrix components is a common feature of arc volcanic rocks that have undergone amphibole fractionation (Davidson et al., 2007; Larocque and Canil, 2010; Smith, 2014; Cooper et al., 2016). This lack of petrographic evidence for amphibole (i.e., cryptic amphibole fractionation; Davidson et al., 2007) may be due to very efficient removal of cumulus amphibole crystallised from the melt within the crust, or because amphibole formed through reaction between cumulate clinopyroxene and hydrous melt to make secondary magmatic amphibole (Larocque and Canil, 2010; Smith, 2014; Cooper et al., 2016).

Both, MTC and CV samples have moderately radiogenic εNd(t) compositions close to CHUR, with CV samples having slightly more positive values (εNd(t) = +0.14 to +3.16), than MTC samples (εNd(t) = -0.4 to -1.05). Parental magmas for both suites are interpreted to be primarily mantle derived, with the less radiogenic MTC samples undergoing a higher degree of assimilation of older (Ordovician to Carboniferous; Baker et al., 1993) basement than the CV suite.

Both the MTC and CV suites belong to the same general LCV sequences; they were deposited contemporaneously in relatively close proximity (within 40 to 70 km), and overall share similar petrographic and geochemical characteristics. The observed differences in εNd and geochemical variation with fractionation are likely related to conditions of magma storage and evolution within the crust, with the primary difference due to the relatively 'wet' versus 'dry' magma evolution conditions for MTC and CV suites, respectively. A comprehensive account of structural controls on magma evolution within the crust is beyond the scope of the present work, although I note that magmatism and mineralisation in the

Mount Carlton district is broadly controlled by E-W to ENE-WSW trending crustal structures, as revealed by surface mapping and airborne magnetic surveys (Figure 2-1C).

Magma plumbing along these structures may have provided conditions for enhanced crustal assimilation (relative to the CV suite to the south), and extensive deep magma replenishment and fractionation to produce hydrous derivative magmas (e.g. Hildreth and Moorbath, 1988; Rohrlach and Loucks, 2005; Loucks, 2014). This distinctive magmatic evolution for the MTC suite may also be linked to mineralisation potential, as discussed below.

2.6.3 Magma fertility

Comparison of the geochemistry of the fertile MTC and infertile CV sample sets allows us to investigate and to extend the applicability of existing whole-rock Cu-Au fertility parameters derived from porphyry intrusions (e.g., Loucks, 2014) to related volcanic successions. Mineralised Cu-Au porphyry intrusions are recognised to have high Sr/Y and V/Sc contents (Figure 2-10E, F) due to extensive and early amphibole fractionation relative to plagioclase and magnetite (Burnham, 1979; Hildreth and Moorbath, 1988; Candeal, 1992; Rohrlach and Loucks, 2005; Richards and Kerrich, 2007; Richards et al., 2011; Richards et al., 2012; Loucks, 2014). The CV samples tend to have low Sr/Y and low V/Sc at high SiO_2, which conforms to a classification of being infertile for mineralisation. The marked decrease in V/Sc with fractionation could be attributed to magnetite fractionation depleting the melt in V, which may also trigger redox-controlled sulfide saturation, which would then deplete the magma of chalcophile elements (including Cu and Au) and render the magma suite unproductive for mineralisation (Jenner et al., 2010). The MTC samples show somewhat elevated Sr/Y and V/Sc compared to CV samples, and do extend into the “ore productive” fields of Loucks (2014), and there is some scatter in the datasets. A complication to using the Sr/Y proxy for volcanic rocks is that Sr is mobilised under conditions of hydrothermal alteration and, can for example be gained (formation of secondary carbonate) or lost (e.g. breakdown of calcic plagioclase) (e.g. Staudigel et al., 1981). Some degree of alteration is ubiquitous in the analysed LCV samples, and widespread in arc volcanic rocks generally (Hastie et al., 2007). Mobility of Sr relative to Y can explain the variable Sr/Y ratios observed, and indicates that this proxy is not necessarily reliable for discriminating volcanic

sequences for mineralisation potential. Neither V nor Sc is expected to be affected by hydrothermal alteration, and the MTC samples do not follow the V/Sc depletion trend with fractionation as seen in the CV samples. This points to a lack of significant magnetite fractionation in the MTC samples, possibly due to the buffering effect that amphibole fractionation has on melt FeO content and fO_2 (Loucks, 2014). Nevertheless, I do note that there is significant scatter in V/Sc in the MTC suite, which may reflect heterogeneity caused by the dynamic volcanic processes (e.g., entrainment of volcaniclastic clasts or crystals, etc.). This scatter demonstrates that assessment of magma fertility will be highly unreliable if based on a single sample, or a small number of samples from a volcanic suite.

The REE can be employed as alternative geochemical proxy for magma fertility of arc volcanic rocks, as they are not affected by hydrothermal alteration or weathering in any great extent, and they are sensitive to the conditions of magma evolution due to fractional crystallisation. The REE signatures (e.g., increasing La/Yb, but not Dy/Yb, with increasing SiO_2) of the MTC suite are a manifestation of amphibole fractionation, which is argued to reflect high magmatic water content that is crucial for producing fertile magmas (Richards et al., 2012; Loucks 2014). Therefore, REE systematics of arc rocks are a powerful tool to assess fertility of rock suites associated with porphyry and high-sulfidation epithermal Cu-Au mineralisation and confirm earlier works in this field (e.g. Baldwin and Pearce, 1982; Richards et al., 2001; Richards and Kerrich, 2007, Schütte et al., 2010). However, emphasis is put on the requirement for analysis of sufficient samples to cover a broad compositional range (i.e., <55 wt.% SiO_2 to >70 wt.% SiO_2), so that magma evolution trends can be assessed. In general, such geochemical proxies for mineralisation should ideally be interpreted with other mineralisation indicators, such as structural preconditioning of the crust (e.g., crustal lineaments; Figure 2-1C; Sillitoe, 2010), and evidence of appropriate hydrothermal alteration halos (e.g., Chang et al., 2011).

2.7 Conclusions

The geochemical and petrographic data for two suites of volcanic rocks from the early Permian LCV of northern Australia are used to assess cryptic fractionation processes involved in generating the volcanic rock suites, and to assess the use of geochemical proxies as indicators of magma fertility for porphyry-epithermal Cu+Au mineralisation. I find that:

- Generation of the "fertile" LCV rocks associated with porphyry and high-sulfidation epithermal Au-Cu-Ag mineralisation in the Mount Carlton district involved fractionation of amphibole (± clinopyroxene) from hydrous parental arc magmas. Contemporary, mineralisation "infertile" volcanic rocks from the Collinsville region formed via crystal fractionation dominated by clinopyroxene, plagioclase ± magnetite from less hydrous parental magmas.
- Application of this dataset to magma fertility indicators developed for magmatic arc rocks indicates that Sr/Y may be of limited use for volcanic rocks, due to potential for Sr mobility with alteration. Only geochemical indicators for mineralisation that are insensitive to hydrothermal alteration should be used for evaluating magma fertility in volcanic arc sequences that invariably have experienced some hydrothermal alteration.
- Alteration-immobile REE and V/Sc can be used as magma fertility indicators for volcanic rocks, provided sufficient samples are used to confidently assess compositional heterogeneity/complexity, and to evaluate REE trends with magma evolution (i.e., over a range of bulk-rock SiO_2 contents). Depletion of M-HREE and Y or increasing La/Yb with increasing SiO_2 are regarded to be useful indicators of potential for associated porphyry and high sulfidation epithermal deposits.
- These geochemical proxies for magma fertility could be applied to exploration in areas where Cu+Au mineralisation may be buried beneath cogenetic volcanic successions. Most effective exploration targeting can be achieved by using these geochemical proxies of magma fertility together with other geological/geophysical datasets to delineate crustal structures/trends that may focus mineralisation, and to recognize alteration systems that are implicitly linked with mineralisation.

2.8 References

Allen, C. M., Williams, I. S., Stephens, C. J., and Fielding, C. R., 1998, Granite genesis and basin formation in an extensional setting: The magmatic history of the Northernmost New England Orogen: Australian Journal of Earth Sciences, v. 45, p. 875-888.

Allen, C. M., 2000, Evolution of a post-batholith dike swarm in central coastal Queensland, Australia: arc-front to backarc?: Lithos, v. 51, p. 331-349.

Annen, C., Blundy, J., and Sparks, R., 2005, The genesis of intermediate and silicic magmas in deep crustal hot zones: Journal of Petrology, v. 47, p. 505-539.

Arribas, A, 1995, Characteristics of high-sulfidation epithermal deposits, and their relation to magmatic fluid: Mineralogical Association of Canada Short Course, v. 23, p. 419-454.

Arribas, A., Cunningham, C. G., Rytuba, J. J., Rye, R. O., Kelly, W. C., Podwysocki, M. H., H., M. E., and Tosdal, R. M., 1995, Geology, geochronology, fluid inclusions, and isotope geochemistry of the Rodalquilar gold alunite deposit, Spain: Economic Geology, v. 90, p. 795-822.

Bachmann, O., and Bergantz, G. W., 2008, Rhyolites and their source mushes across tectonic settings: Journal of Petrology, v. 49, p. 2277-2285.

Baker, J. C., Fielding, C. R., De Caritat, P., and Wilkinson, M. M., 1993, Permian evolution of sandstone composition in a complex-back-arc extensional to foreland basin: The Bowen Basin, Eastern Australia: Journal of Sedimentary Petrology, v. 63, p. 881-893.

Baldwin, J., & Pearce, J. A. (1982). Discrimination of productive and nonproductive porphyritic intrusions in the Chilean Andes. Economic Geology, 77(3), 664-674.

Bau, M., 1991, Rare-earth element mobility during hydrothermal and metamorphic fluid-rock interaction and the significance of the oxidation state of europium: Chemical Geology, v. 93, p. 219-230.

Blevin, P. L., Chappell, B. W., and Allen, C. M., 1996, Intrusive metallogenic provinces in eastern Australia based on granite source and composition: Geological Society of America Special Papers, v. 315, p. 281-290.

Bryan, S. E., Ewart, A., Stephens, C. J., Parianos, J., and Downes, P. J., 2000, The Whitsunday Volcanic Province, Central Queensland, Australia: lithological and stratigraphic investigations of a silicic-dominated large igneous province: Journal of Volcanology and Geothermal Research, v. 99, p. 55-78.

Burnham, C. W. (1979). Magmas and hydrothermal fluids. In H. L. Barnes (Ed.), Geochemistry of Hydrothermal Ore Deposits (2 ed., pp. 71-136). New York: John Wiley and Sons.

Candela, P. A. (1992). Controls on ore metal ratios in granite-related ore systems: an experimental and computational approach. Earth and Environmental Science Transactions of The Royal Society of Edinburgh, 83(1-2), 317-326.

Candela, P., and Piccoli, P., 2005, Magmatic processes in the development of porphyry-type ore systems: Economic Geology, v. 100, p. 25-37.

Castillo, P. R., Janney, P. E., and Solidum, R. U., 1999, Petrology and geochemistry of Camiguin Island, southern Philippines: insights to the source of adakites and other lavas in a complex arc setting: Contributions to Mineralogy and Petrology, v. 134, p. 33-51.

Champion, D. C., 2013, Neodymium depleted mantle model age map of Australia: explanatory notes and user guide: Record 2013/44: Geoscience Australia, Canberra. http://dx.doi.org/10.11636/Record.2013.044.

Chang, Z. S., Hedenquist, J. W., White, N. C., Cooke, D. R., Roach, M., Deyell, C. L., Garcia, J., Gemmell, J. B., McKnight, S., and Cuison, A. L., 2011, Exploration Tools for Linked Porphyry and Epithermal Deposits: Example from the Mankayan Intrusion-Centered Cu-Au District, Luzon, Philippines, Economic Geology, v. 106, p. 1365-1398.

Chiaradia, M., Ulianov, A., Kouzmanov, K., and Beate, B., 2012, Why large porphyry Cu deposits like high Sr/Y magmas?: Scientific Reports, v. 2, p. 685.

Chiaradia, M., & Caricchi, L. (2017). Stochastic modelling of deep magmatic controls on porphyry copper deposit endowment. Scientific Reports, 7, 44523.

Cline, J. S., and Bodnar, R. J., 1991, Can economic porphyry copper mineralisation be generated by a typical calc-alkaline melt?: Journal of Geophysical Research: Solid Earth, v. 96, p. 8113-8126.

Cooke, D. R., Hollings, P., and Walshe, J. L., 2005, Giant Porphyry Deposits: Characteristics, Distribution, and Tectonic Controls: Economic Geology, v. 100, p. 801-818.

Cooke, D., Hollings, P., Wilkinson, J., and Tosdal, R., 2014, Geochemistry of Porphyry Deposits, in Holland, H., and Turekian, K., eds., Treatise on Geochemistry, 13: Oxford, Elsevier, p. 357-381.

Cooper, G. F., Davidson, J. P., and Blundy, J. D., 2016, Plutonic xenoliths from Martinique, Lesser Antilles: evidence for open system processes and reactive melt flow in island arc crust: Contributions to Mineralogy and Petrology, v. 171, p. 87.

Corral, I., Chang, Z., Behnsen, H., Sahlström, F., Spandler, C., Pocock, M., and Hewitt, D., 2016, The Capsize porphyry prospect, NE Queensland, Australia: A Paleozoic linked porphyry-lithocap system, Goldschmidt 2016: Yokohama.

Corral, I., Chang, Z., Dirks, P.H.G.M, Spandler, C., Henderson, R.A., Sahlström, F., and Hall, C., in prep., Age and Geodynamic Setting of Epithermal, Mesothermal and Porphyry Mineralisation in the Northern New England Orogen and the Northern Bowen Basin (NE Queensland, Australia), Economic Geology

Cross, A. J., Bultitude, R. J., and Purdy, D. J., 2012, Summary of results for the joint GSQ-GA geochronology project: Ayr, Bowen, Eulo, Mount Coolon, Proserpine and Warwick 1:250000 sheet areas, record no. 2012/19, Geological Survey of Queensland, Brisbane.

Davidson, J., Turner, S., Handley, H., Macpherson, C., and Dosseto, A., 2007, Amphibole “sponge” in arc crust?: Geology, v. 35, p. 787-790.

Defant, M. J., and Drummond, M. S., 1990, Derivation of Some Modern Arc Magmas by Melting of Young Subducted Lithosphere: Nature, v. 347, p. 662-665.

Defant, M. J., and Drummond, M. S., 1993, Mount St. Helens: Potential example of the partial melting of the subducted lithosphere in a volcanic arc: Geology, v. 21, p. 547-550.

DePaolo, D. J., 1981, Trace element and isotopic effects of combined wallrock assimilation and fractional crystallisation: Earth and planetary Science Letters, v. 53, p. 189-202.

Dessimoz, M., Müntener, O., and Ulmer, P., 2012, A case for hornblende dominated fractionation of arc magmas: the Chelan Complex (Washington Cascades): Contributions to Mineralogy and Petrology, v. 163, p. 567-589.

Donchak, P. J. T., Purdy, D. J., Withnall, I. W., Blake, P. R., and Jell, P. A., 2013, Chapter 5: New England Orogen, in Jell, P. A., ed., Geology of Queensland, Geological Survey of Queensland, p. 305-407.

Fulignati, P., Gioncada, A., and Sbrana, A., 1999, Rare-earth element (REE) behaviour in the alteration facies of the active magmatic–hydrothermal system of Vulcano (Aeolian Islands, Italy): Journal of Volcanology and Geothermal Research, v. 88, p. 325-342.

Glazner, A. F., Coleman, D. S., and Bartley, J. M., 2008, The tenuous connection between high-silica rhyolites and granodiorite plutons: Geology, v. 36, p. 183-186.

Glen, R., 2005, The Tasmanides of eastern Australia, Geological Society of London Special Publication, v. 246, p. 23.

Hammerli, J., Spandler, C., and Oliver, N. H. S., 2016, Element redistribution and mobility during upper crustal metamorphism of metasedimentary rocks: an example from the eastern Mount Lofty Ranges, South Australia: Contributions to Mineralogy and Petrology, v. 171, p. 36.

Hastie, A. R., Kerr, A. C., Pearce, J. A., and Mitchell, S. F., 2007, Classification of altered volcanic island arc rocks using immobile trace elements: Development of the Th-Co discrimination diagram: Journal of Petrology, v. 48, p. 2341-2357.

Hedenquist, J. W., and Lowenstern, J. B., 1994, The role of magmas in the formation of hydrothermal ore deposits: Nature, v. 370, p. 519-527.

Hedenquist, J. W., Arribas, A., and Reynolds, T. J., 1998, Evolution of an intrusion-centered hydrothermal system; Far Southeast-Lepanto porphyry and epithermal Cu-Au deposits, Philippines: Economic Geology, v. 93, p. 373-404.

Hedenquist, J. W., Arribas, A., and Gonzalez-Urien, E., 2000, Exploration for epithermal gold deposits: Reviews in Economic Geology, v. 13, p. 245-277.

Hildreth, W., and Moorbath, S., 1988, Crustal contributions to arc magmatism in the Andes of central Chile: Contributions to mineralogy and petrology, v. 98, p. 455-489.

Horton, D. J., 1978, Porphyry-type copper-molybdenum mineralisation belts in eastern Queensland, Australia: Economic Geology, v. 73, p. 904-921.

Hutton, L. J., Grimes, K. G., Law, S. R., and McLennon, T. P. T., 1991, Geology of the Mount Coolon 1:250,000 Sheet Area, Department of Resource Industries, Queensland, Record 1991/19.

Hutton, L., Withnall, I., Rienks, I., Bultitude, R.J., Hayward, M., von Gnielinski, F., Fordham, B., Simpson, G. 1999, A preliminary Carboniferous to Permian magmatic framework for the Auburn and Connors Arches, central Queensland: In: P. Flood ed., Proceedings of the 1999 New England Orogen conference, Armidale, p. 223-232.

Irvine, T., and Baragar, W., 1971, A guide to the chemical classification of the common volcanic rocks: Canadian Journal of Earth Sciences, v. 8, p. 523-548.

Ishikawa, Y., Sawaguchi, T., Iwaya, S., and Horiuchi, M., 1976, Delineation of Prospecting Targets for Kuroko Deposits Based on Modes of Volcanism of Underlying Dacite and Alteration Haloes: Mining Geology, v. 26, p. 105-117.

Jenner, F. E., O'Neill, H. S. T. C., Arculus, R. J., and Mavrogenes, J. A., 2010, The Magnetite Crisis in the Evolution of Arc-related Magmas and the Initial Concentration of Au, Ag and Cu: Journal of Petrology, v. 51, p. 2445-2464.

Kägi, R., Müntener, O., Ulmer, P. and Ottoline, L., 2005, Piston-cylinder experiments on H2O undersaturated Fe-bearing systems: An experimental setup approaching fO2 conditions of natural calcalkaline magmas: American Mineralogist, v. 90, p. 708–717.

Kay, S. M., and Mpodozis, C., 2001, Central Andean ore deposits linked to evolving shallow subduction systems and thickening crust: GSA Today, v. 11, p. 4-9.

Korsch, R., Totterdell, J., Cathro, D., Nicoll, M., 2009, Early Permian east Australian rift system. Australian Journal of Earth Sciences, v. 56, p. 381-400.

Lang, J. R.,, and Titley, S. R. (1998). Isotopic and geochemical characteristics of Laramide magmatic systems in Arizona and implications for the genesis of porphyry copper deposits. Economic Geology, 93(2), 138-170.

Large, R. R., Gemmell, J. B., Paulick, H., and Huston, D. L., 2001, The alteration box plot: A simple approach to understanding the relationship between alteration mineralogy and lithogeochemistry associated with volcanic-hosted massive sulfide deposits: Economic Geology, v. 96, p. 957-971.

Larocque, J., and Canil, D., 2010, The role of amphibole in the evolution of arc magmas and crust: the case from the Jurassic Bonanza arc section, Vancouver Island, Canada: Contributions to Mineralogy and Petrology, v. 159, p. 475-492.

Le Maitre, R.W., Bateman, P., Dudek, A., Keller, J., Lemeyre, J., Le Bas, M.J., Sabine, P.A., Schmid, R., Sorensen, H., Streckeisen, A., Wooley, A.R., and Zanettin, B., 1989, A classification of igneous rocks and glossary of terms: Oxford, Blackwell Science.

Leake, B. E., Woolley, A. R., Arps, C. E., Birch, W. D., Gilbert, M. C., Grice, J. D., Hawthorne, F. C., Kato, A., Kisch, H. J., and Krivovichev, V. G., 1997, Report. Nomenclature of amphiboles: report of the subcommittee on amphiboles of the international mineralogical association commission on new minerals and mineral names: Mineralogical Magazine, v. 61, p. 295-321.

Loucks, R. R., 2014, Distinctive composition of copper-ore-forming arc magmas: Australian Journal of Earth Sciences, v. 61, p. 5-16.

Malone, E. J., Olgers, F., and Kirkegaard, A. G., 1969, Geology of the Duaringa and St. Lawrence 1:250000 sheet areas, Queensland, report no. 121, Bureau of Mineral Resources, Australia, Canberra.

Moore, G., and Carmichael, I. S. E., 1998, The hydrous phase equilibria (to 3 kbar) of an andesite and basaltic andesite from western Mexico: constraints on water content and conditions of phenocryst growth: Contributions to Mineralogy and Petrology, v. 130, p. 304-319.

Müntener, O., Kelemen, P. B., and Grove, T. L., 2001, The role of H2O during crystallisation of primitive arc magmas under uppermost mantle conditions and genesis of igneous pyroxenites: an experimental study: Contributions to Mineralogy and Petrology, v. 141, p. 643-658.

Murray, C., 1990, Tectonic evolution and metallogenesis of the Bowen Basin: Beeston JW (compiler) Bowen Basin Symposium 1990 Proceedings. Brisbane, GSA (Queensland Division), 1990, p. 201-212.

Naney, M. (1983). Phase equilibria of rock-forming ferromagnesian silicates in granitic systems. American Journal of Science, 283(10), 993-1033.

Oversby, S., MacKenzie, B. E., McPhie, J. L. S. R. and Wyborn, D., 1994, The geology of Palaeozoic volcanic and associated rocks in the Burdekin Falls Dam-Conway area, northeast Queensland. Australian Geological Survey Organisation Record 94/21.

Parsapoor, A., Khalili, M., and Mackizadeh, M. A., 2009, The behaviour of trace and rare earth elements (REE) during hydrothermal alteration in the Rangan area (Central Iran): Journal of Asian Earth Sciences, v. 34, p. 123-134.

Richards, J. P., Boyce, A. J., & Pringle, M. S. (2001). Geologic evolution of the Escondida area, northern Chile: A model for spatial and temporal localization of porphyry Cu mineralization. Economic Geology, 96(2), 271-305.

Richards, J. P. (2003). Tectono-Magmatic Precursors for Porphyry Cu-(Mo-Au) Deposit Formation. Economic Geology, 98(8), 1515-1533. doi:10.2113/gsecongeo.98.8.1515

Richards, J. P., and Kerrich, R., 2007, Special paper: adakite-like rocks: their diverse origins and questionable role in metallogenesis: Economic Geology, v. 102, p. 537-576.

Richards, J. P., 2011, High Sr/Y arc magmas and porphyry Cu ± Mo ± Au deposits: Just add water: Economic Geology, v. 106, p. 1075-1081.

Richards, J. P., Spell, T., Rameh, E., Razique, A., and Fletcher, T., 2012, High Sr/Y Magmas Reflect Arc Maturity, High Magmatic Water Content, and Porphyry Cu ± Mo ± Au Potential: Examples from the Tethyan Arcs of Central and Eastern Iran and Western Pakistan: Economic Geology, v. 107, p. 295-332.

Richards, J., 2016, Clues to hidden copper deposits: Nature Geoscience, v. 9, p. 195.

Ridolfi, F., Renzulli, A., and Puerini, M., 2010, Stability and chemical equilibrium of amphibole in calc-alkaline magmas: an overview, new thermobarometric formulations and application to subduction-related volcanoes: Contributions to Mineralogy and Petrology, v. 160, p. 45-66.

Rohrlach, B. D., and Loucks, R. R., 2005, Multi-million-year cyclic ramp-up of volatiles in a lower crustal magma reservoir trapped below the Tampakan copper-gold deposit by Mio-Pliocene crustal compression in the southern Philippines: Super porphyry copper and gold deposits: A global perspective: Adelaide, PGC Publishing, v. 2, p. 369-407.

Sahlström, F., Blake, K., Corral, I., and Chang, Z., 2017, Hyperspectral cathodoluminescence study of indium-bearing sphalerite from the Mt Carlton high-sulphidation epithermal deposit, Queensland, Australia: European Journal of Mineralogy, V. 29, p. 985-993.

Sahlström, F., Dirks, P. H. G. M., Chang, Z., Arribas, A., Corral, I., Obiri-Yeboah, M., and Hall, C., in press, The Paleozoic Mt Carlton Deposit, Bowen Basin, NE Australia: Shallow high-sulfidation epithermal Au-Ag-Cu mineralisation formed during rifting: Economic Geology.

Schütte, P., Chiaradia, M., & Beate, B. (2010). Petrogenetic evolution of arc magmatism associated with late Oligocene to late Miocene porphyry-related ore deposits in Ecuador. Economic Geology, 105(7), 1243-1270.

Sillitoe, R. H., 2010, Porphyry copper systems: Economic Geology, v. 105, p. 3-41.

Smith, D. J., 2014, Clinopyroxene precursors to amphibole sponge in arc crust: Nature Communications, v. 5, p. 4329.

Staudigel, H., Hart, S. R., & Richardson, S. H. (1981). Alteration of the oceanic crust: processes and timing. Earth and Planetary Science Letters, 52(2), 311-327.

Sun, S.S., and McDonough, W. F., 1989, Chemical and isotopic systematics of oceanic basalts: implications for mantle composition and processes: Geological Society, London, Special Publications, v. 42, p. 313-345.

Chapter 3

Behaviour and evolution of Cl, F and S during magmatic differentiation; insights from apatite and biotite from the Tuckers Igneous Complex, northern Queensland

Abstract

Volatiles (Cl, F, H, and S) are recognised to influence not only physicochemical attributes of evolving magmas, but also are particularly crucial for the transport and deposition of ore metals via fluids exsolved from magmas. Therefore, understanding volatile behaviour during magmatic evolution may aid in understanding the distribution and fertility of magmas, and thereby help mineral exploration. Here, I examine halogen and S contents of apatite to evaluate the concentration and evolution of volatiles in the magmas that formed the Permocarboniferous Tuckers Igneous Complex (TIC) of northern Queensland, Australia. The TIC represents a typical calc-alkaline, moderately oxidised gabbro to granodiorite complex that formed by crystal fractionation, and hence represents an ideal sample suite to investigate volatile evolution during magma differentiation in the upper continental crust.

Earliest apatite in TIC gabbro is Cl-rich and evolves towards F-rich compositions with progressive magma evolution to granodiorite; but TIC gabbro also contains texturally different apatite that indicates selective hydrothermal Cl metasomatism. TIC apatites are generally S-poor, but there is a measurable increase in sulfur concentrations of apatites analysed from the most evolved felsic granodiorite. This is interpreted to relate to a change in oxygen fugacity, causing an increasing proportion of S to be present as S^{6+} compared to S^{2-} or S^{4+}. This likely favoured S degassing rather than precipitation of magmatic sulfide. Increasing S contents of apatite coincides with a substantial drop in calculated Cl melt compositions at the time of apatite crystallisation from ~0.7 – 0.8 wt.% in gabbro to quartz monzodiorite to ~0.4 wt.% in granodiorite. This, together with additional petrological observations confirms that the TIC formed by fractional crystallisation from an initially fluid undersaturated parental melt similar in composition to TIC gabbro. Progressive closed-system crystal fractionation caused volatile built-up to ~65 wt.% SiO_2 after which conditions are reached that caused; (i) crystallisation of amphibole and biotite, and; (ii) Cl-F trends indicative for fluid exsolution and/or degassing, likely at low crustal pressures (<2 kbar). Reaction of these, or similar, Cl rich fluids is invoked to explain Cl-rich apatite that forms texturally late in the gabbro unit. These insights into volatile evolution of arc magmas help our understanding of halogen and S behaviour during magmatic differentiation, volatile build-up, and fluid saturation, which affects metal transport in magmatic-hydrothermal environments, and volatile release to the surface (via volcanism).

3.1 Introduction

Volatiles (e.g. H_2O, halogens, S and CO_2) play an essential role in many magmatic and hydrothermal processes, where they exert important controls on the physical properties of magmas and are critical to the transport of metals (e.g. Au, Cu) in melts and hydrothermal fluids (Harlov and Aranovich, 2018). These volatiles may also have significant environmental impact due to their release during volcanic eruptions (e.g. Aiuppa et al., 2009; Pyle and Mather, 2009).

It is well established that halogens and S are critical elements in ore forming fluids owing to their capability to form ligands with ore metals (e.g. Au, Ag, base metals) and other cations (e.g. H+, alkali elements), allowing transport of metals to the site of ore precipitation and associated hydrothermal alteration (e.g. Candela and Holland, 1984; Kouzmanov and Pokrovski, 2012; Pokrovski et al., 2015; Tattitch and Blundy, 2017; Lecumberri-Sanchez and Bodnar, 2018; Dolejš and Zajacz, 2018). Therefore, unravelling the behaviour of Cl and S in magmatic and magmatic/hydrothermal systems using halogen-bearing minerals is of great interest for understanding magma fertility and the potential for ore deposit formation (e.g. Munoz, 1984; Webster and Botcharnikov, 2011; Chambefort et al., 2013; Richards, 2015; Zhang et al., 2016; Chelle-Michou and Chiaradia, 2017).

The study of the volatile inventories of magmatic rocks is often hindered by the fact that such rocks have: (a) lost a significant amount of their volatile budget by degassing and/or fluid exsolution, and/or; (b) have undergone post-magmatic changes that can modify the primary volatile concentration. Volatile–bearing igneous minerals like apatite, biotite and amphibole may be effective recorders of the volatile evolution of the magmas from which they crystallised, provided careful evaluation of the timing of crystallisation of these phase(s) is undertaken, and the partitioning of volatiles between various mineral phases, melt and fluid is well constrained (see Harlov and Aranovich, 2018 , and references therein).

Apatite is generally the mineral of choice when investigating volatile evolution in igneous rocks, owed to its presence in a large range of rock types ranging from peridotite to highly alkaline silicic rocks to carbonatites (e.g. Piccoli and Candela, 2002; Webster and Piccoli, 2015 and references therein). Apatite can incorporate significant amounts of halogens and S, with fluorapatite being the most common apatite in magmatic rocks (e.g. Webster and Piccoli, 2015, and references therein).

Chlorine-rich varieties (≥ 4 wt.%) have been reported from metasomatised rocks and also from layered intrusions (e.g. Harlov, 2015 and references therein). Apatite commonly occurs as an early magmatic phase compared to biotite or amphibole, both of which are only stabilised under hydrous magmatic conditions (≥4 wt.%, e.g. Ridolfi and Renzulli, 2010). Apatite therefore offers a snapshot into the early volatile compositions of magmas and has been used to investigate and estimate the Cl, F and S budget of magmas and their source region (e.g. Piccoli and Candela, 1994; Peng et al., 1997; Webster et al., 2009; Parat et al., 2002; 2011; Zhang et al., 2012; Chelle-Michou and Chiaradia, 2017). In addition, apatite is a major host of rare earth elements (REE), Sr, U and Th, and therefore can be used as a sensitive recorder of the trace element chemistry of magmatic systems (e.g. Sha and Chappell, 1999; Belousova, 2002), and was more recently suggested to be a good discriminant between Cu-Au fertile and barren granitoids, and therefore a potential indicator mineral for porphyry copper exploration (e.g. Bouzari et al., 2016; Mao et al., 2016; Brugge et al., 2017; Duan and Jiang, 2018).

In this study, I investigate the content and distribution of Cl, F and S in apatite and other hydrous igneous minerals from a mafic – intermediate - felsic plutonic complex known as the Tuckers Igneous Complex (TIC) of North Queensland, Australia. I first demonstrate that the suite of igneous rocks of the complex formed primarily via crystal fractionation, as was suggested previously (Beams, 1994; Blevin and Morrison, 1997; Murgulov et al., 2008). I then evaluate halogen and S contents in apatite and biotite from the range of intrusive rock-types across the complex. With the knowledge of textural relations (e.g. relative timing of apatite crystallisation) I investigate (1) the general halogen distribution in apatite and biotite over the course of magma evolution and/or late-magmatic conditions (e.g. halogen control by crystal fractionation and/or halogen re-equilibration), (2) estimate Cl and S melt compositions based on apatite analyses. These data can be used to further our understanding of the behaviour of halogen and S during fractional crystallisation of arc magmas in continental settings, since halogens offer a window into volatile build-up, distribution and fluid and/or vapour exsolution and therefore into the mineralisation potential of an evolving magma.

3.2 Geological setting

The Tuckers Igneous Complex (TIC) is located ~30 km east of Charters Towers, and stands out as a prominent geomorphological feature along the Bruce Highway within the Paleozoic Charters Towers Province (CTP; Withnall and Henderson, 2012; Fergusson and Henderson, 2013) of northeastern Queensland, Australia (Figure 3-1A). The CTP (formerly Cape River Province; Withnall and Hutton, 1997) is one of the major gold-bearing provinces of eastern Australia, hosting the Charters Towers goldfield, including the Charters Towers vein-hosted gold deposit, which produced >6.6. Moz of gold (at an average grade of 34 g/t Au) (e.g. Morrison, 1988; Perkins and Kennedy, 1998; Kreuzer et al., 2007). It comprises Late Cambrian to Early Ordovician metamorphic rocks and subordinate mafic volcanic rocks, and forms part of the Thomson Orogen of the Tasman Orogenic Zone of Eastern Australia. The internal structure of the CTP is poorly understood. It has a complex tectonic history with crustal growth dominated by subduction, lateral accretion and extensional tectonics that extends over 300 myr from the Late Cambrian to Permian (Fergusson et al., 2007a, b; Fergusson and Henderson, 2013).

Late Cambrian gabbros and Ordovician and Siluro-Devonian granite and granodiorite intrusions (e.g. Hutton et al., 1994) make up the bulk of the Ravenswood Batholith. During the Permo-Carboniferous, felsic granitoids and associated volcanic rocks of the Kennedy Igneous Association (KIA; Bain and Draper, 1997; Mackenzie and Wellman, 1997; Champion and Bultitude, 2013) were emplaced within, and along, prominent lineaments and structural corridors and junctions within the Ravenswood Batholith (Figure 3-1B). KIA rocks within the CTP predominantly comprise Permocarboniferous mafic to intermediate I-type granitoids and subvolcanic to extrusive, intermediate to felsic porphyry complexes emplaced during westward dipping subduction between ~310 – 280 Ma (e.g. Champion and Bultitude, 2013).

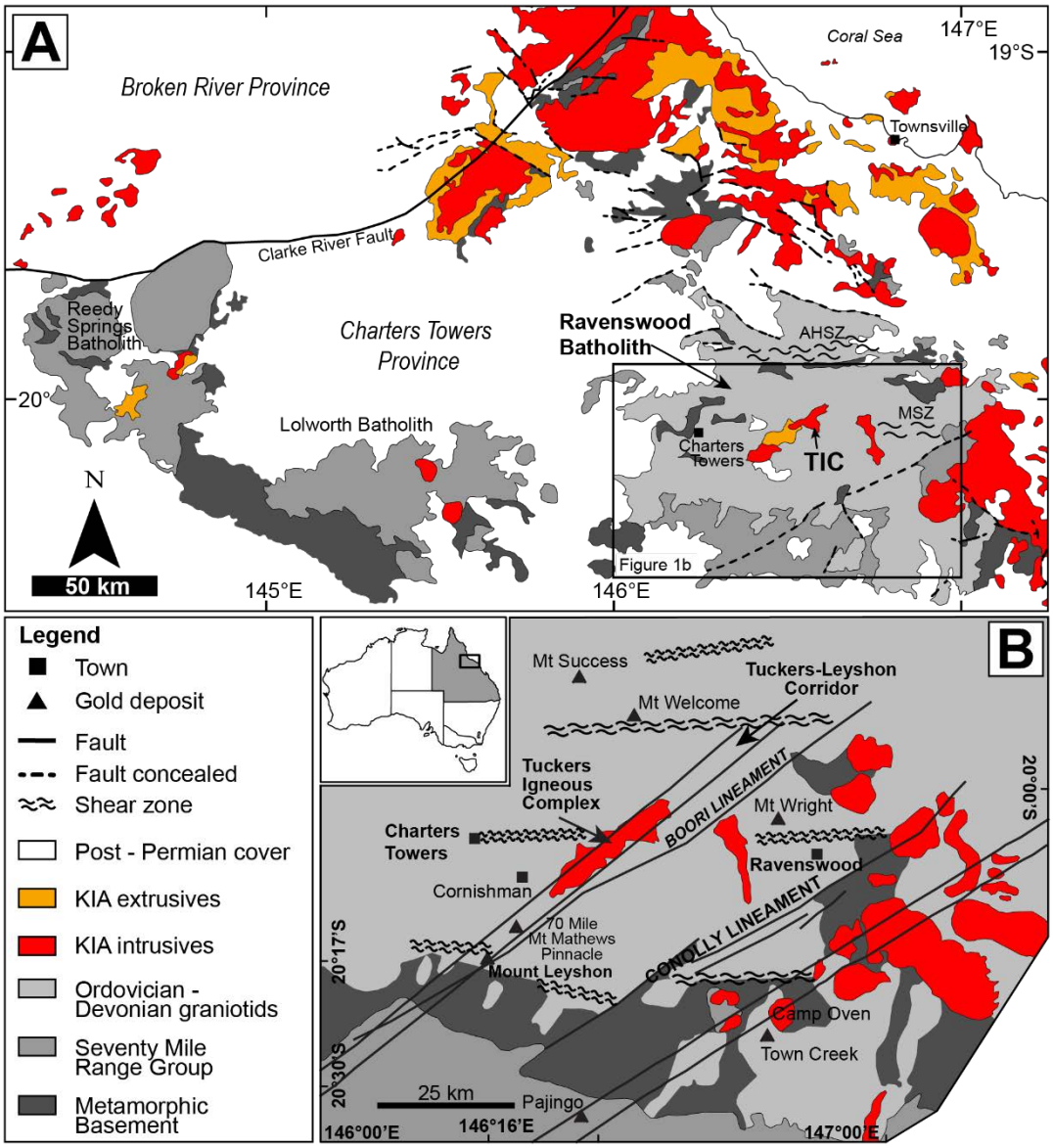

Figure 3-1 A) Generalised map of the Charters Towers Province (CTP) showing the Proterozoic metamorphic basement, the Late Cambrian to early Ordovician Seventy Mile Range Group, Ordovician – Devonian granitoids and the distribution of the Permocarboniferous KIA units (AHZ = Alex Hill Shear Zone; MSZ = Mosgardies Shear Zone) (after Fergusson and Henderson, 2013). B) Simplified map of the Ravenswood Batholith with focus on the positon of the Tuckers Igneous Complex (TIC), noteworthy gold deposits and structural corridors (after Hutton et al., 1994).

The TIC (Figure 3-2) is a polyphase nested complex with rock compositions spanning from gabbro to granodiorite (including minor late granite and aplite). The TIC forms an elongated body in outcrop plan, with a north-east oriented axis of 13.5 km and a south-east oriented axis of 5 km. A small outlier occurs to the south-east of the main complex. Emplacement of the complex into Siluro-Devonian and Ordovician granodiorites and Permo-carboniferous andesites of the Ravenswood Batholith occurred at ca. 300 Ma

(Murgulov et al., 2008) during late stages of westward dipping subduction spanning from the early Carboniferous to early Permian.

The geochemical and petrological features of the TIC have been briefly investigated and described by Beams (1994, unpublished data), Blevin and Morrison (1997), Clark and Lackie (2003) and Murgulov et al. (2008).

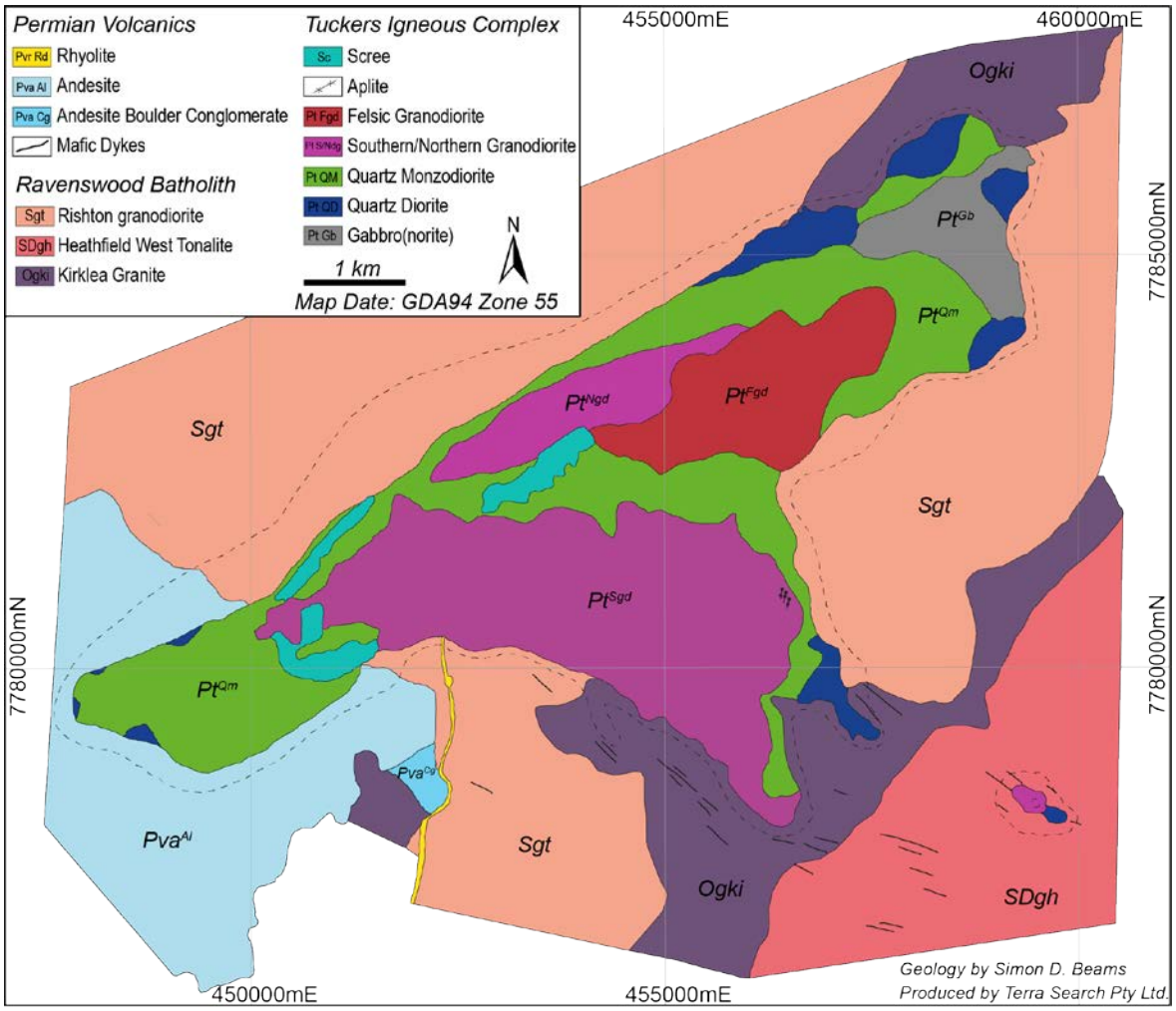

Figure 3-2 Geological map of the Tuckers Igneous Complex (TIC) and surrounding country rock of the Ravenswood Batholith (Terra Search Pty Ltd., 2016).

Mapping by Beams (1994, unpublished data) revealed that the complex consists of multiple intrusive stages, each internally zoned and intruding and stoping out earlier magmatic phases. The earliest intrusive stage comprises high-temperature gabbro and quartz diorite, followed by the intrusion of quartz monzodiorite and subsequent intrusions of granodiorite, which form the major surface exposure at present. Silica-rich aplite and biotite microgranite later intruded the granodiorite as minor bodies and dykes. Uranium-Pb age

dating of zircons by Murgulov et al. (2008) indicate that the major intrusive phases are all of similar age (within analytical error of ~10 myr).

The compositional trend from gabbro to granodiorite and late aplite together with very minor variations in the εHf compositions in the TIC has led to the conclusion that more evolved granodiorite and aplite were derived by crystal fractionation and minor assimilation (AFC) processes of a parent similar to the early gabbro to quartz diorite composition (Beams, 1994, unpublished; Blevin and Morrison, 1997; Murgulov et al., 2008). However, to date these interpretations were based on relatively limited whole rock elemental and isotopic analyses, and field observations where contact relationships between rock units are unclear in many cases.

The TIC is largely deficient of Cu-Au-Ag mineralisation (only minor mineralisation at the Mountain Maid prospect has been reported from miarolitic aplites). However, a genetic relationship based on similar rock types and ages between the TIC and the nearby Early Permian breccia-hosted porphyry-style Mount Leyshon Au-deposit (MLIC; e.g. Paull et al., 1990; Figure 3-2B) has been the subject of prior research (e.g. Morrison and Blevin, 2001; Murgulov et al., 2008). Blevin and Morrison, (2001) suggested that the magmas of the MLIC represent felsic-end-member magmas derived by fractional crystallisation of mafic to intermediate magmas similar to those of the TIC. This premise is supported by Lu-Hf isotope analysis of zircon from both the TIC and MLIC by Murgulov et al. (2008), who concluded that juvenile magmas were involved at the early stages in the formation of both complexes, and felsic magmas were derived by fractional crystallisation from the early mafic to intermediate rocks. However, the paleomagnetic study by Clark and Lackie (2003) suggests that the observed magnetic anomalies from the MLIC derive from hydrothermal alteration (secondary biotite and magnetite) and not from a mafic body beneath the MLIC.

3.3 Analytical techniques

Whole-rock major and trace elements (n = 74) were analysed by Bureau Veritas Commodities Canada Ltd. (former ACME Laboratories Ltd), Vancouver, using a combination of fusion and solution ICP-MS for major, and ICP-ES for trace element concentrations (LF300, LF100 and AQ252 packages and procedures). Ferrous iron concentrations were determined separately by titration. Repeated analyses of well-characterised CRM's and duplicates returned accuracies typically within 5% for major, and 10% for trace elements.

Apatite grains were investigated for zonation patterns with cathodoluminescence (CL) and EDS mapping using a Hitachi SU5000 scanning electron microscope run at 15 kV and 30 nA beam current. Major element concentrations of minerals were analysed in situ on epoxy-mounted polished rock chips and polished thin sections with a JEOL JXA8200 Superprobe at the Advanced Analytical Centre (AAC), James Cook University (JCU). For silicates the JEOL JXA8200 was run with a 15 kV accelerating voltage, 20 nA beam current and 1 – 10 µm spot size. The instrument was calibrated using well-characterised mineral standards, and run conditions, standards, typical errors and detection limits are given in appendix 3-I.

Apatite was analysed for major element compositions, Cl, F and S compositions in a separate session under similar conditions as silicates (15 kV and 20 nA beam current), using a 10 µm defocused beam, and limits of detection for halogens are typically ~300 ppm Cl, ~900 ppm F, and ~200 ppm S. Fluorine (and to minor extents Cl, Ca and P) behaves highly time-dependent when exposed to an electron beam, which can lead to a statistical overestimation of fluorine concentrations (in counts per second (cps)) (Stormer et al., 1993). One possibility to avoid such overestimation is to monitor individual spot analyses for time dependent cps increases in real time. However, in this study the time dependency was not monitored separately and, based on the consistency of analysed grains within samples, F migration is considered as negligible. However, apatite analyses with F > 3.77 wt.% (the stoichiometric maximum for F in apatite) were discarded. Halogen migration has been demonstrated to be the strongest when analysed parallel to the c-axis of apatite crystals and thus, optimal results are obtained when apatite grains are oriented with their c-axis perpendicular to the electron beam (Stormer et al., 1993; Goldoff et al., 2012; Stock et al., 2015). Therefore, analyses parallel to the c-axis of apatite grains were mainly avoided.

However, some grains analysed in this orientation (as determined by crystal habit) returned F-rich cores (~3.5 wt.%) and F-poor rims (<1 wt.%), but this 'zonation' could not be confirmed by EDS chlorine distribution mapping.

Apatite formulae were calculated on the basis of 16 cations and normalised to 25 anions following Deer et al. (2013). Rare earth elements and e.g. Sr and Mn were not analysed during EMPA sessions, but were determined by laser ablation ICP-MS (see below) and generally account for the discrepancies between presented cation totals and the ideal sum of 16. OH was calculated by difference, assuming that the halogen site (F-Cl-OH = 1) is completely filled and other volatiles are negligible (Piccoli and Candela, 2002).

Trace element concentrations of apatite were determined by LA-ICP-MS using a Geolas Pro 193nm ArF excimer laser system coupled with a Thermo Scientific iCAP™ RQ ICP-MS at the AAC, James Cook University. Ablation was conducted in a custom-built large volume cell (Fricker et al., 2011) using high-purity He as the carrier gas, which was subsequently mixed with Ar prior to introduction into the ICP-MS. Analyses were made in situ on the same polished rock chips and apatite grains (and spots where possible) of which major element compositions were obtained prior by EMPA. This process ensures the coupling of apatite major and trace element analyses and an accurate ^{43}Ca value could be used to normalise the LA-ICP-MS data. Spot sizes of 44 µm for standards, and 24 – 32 µm for spot analyses were used at a laser repetition rate of 10 Hz and a pulse energy of ~62 mJ. NIST SRM 612 and NIST SRM 610 were used for calibration and to monitor instrumental drift. NIST SRM 610 was also used as external bracketing standard and secondary standard to evaluate accuracy using the standard reference values of Spandler et al. (2011). Individual analyses consist of approximately 30 seconds of gas background followed by 30 seconds of signal collected during mineral ablation. Analysis of the NIST SRM 612 and 610 reference glass was conducted at the beginning, end and within every ~3 hrs of analytical sessions. Data reduction was performed using the SILLS (Signal Integration for Laboratory Laser Systems) software (Guillong et al., 2008).

3.4 Petrography

Here, I present a brief description of the major rock types (gabbro to granodiorite) forming the TIC (Figure 3-2). Detailed petrographic studies where produced in tandem with geological mapping by Beams (1994), and are complemented by more recent petrographic observations utilising microscale backscattered electron (BSE) and cathodoluminesce (CL) imaging. The descriptions focus on the four main intrusive rock types: (1) gabbro, (2) quartz diorite, (3) quartz monzodiorite and (4) granodiorite. I did not examine the biotite microgranite and quartz-albite-K-feldspar aplites but illustrate their general genetic relationship within the TIC based on whole-rock geochemistry; these rock-types are volumetrically minor and presumably represent extremely fractionated liquids. In general, with regards to Fe-Mg silicates and Fe-Ti oxide distribution, TIC lithologies successively developed from a 2-pyroxene + magnetite-ilmenite assemblage in gabbro and quartz diorite, to a pyroxene + biotite/amphibole + magnetite-ilmenite assemblage in quartz monzodiorite and more mafic granodiorite, followed by a hydrous, amphibole-biotite dominated, magnetite-only assemblage in more felsic granodiorites.

1.2.2 Gabbro (GB)

Black, coarse-grained gabbro crops out in the northeastern end of the TIC. The gabbro consists of abundant plagioclase laths (≤4 mm) and anhedral, resorbed orthopyroxene grains, subhedral poikilitic clinopyroxene, with abundant granular magnetite and large apatite grains (up to 0.5 mm) (Figure 3-3A; B). In thin-section, plagioclase laths exhibit a general orientation indicating some degree of a layered texture, with Fe-Mg silicates and Fe-Ti oxides occurring interstitially. This texture is consistent with a cumulate character of this lithology. Magnetite occurs along the grain boundaries of both pyroxene types, is anhedral and occurs together with ilmenite. BSE imaging reveals fine exsolution lamellae (possibly hematite) in ilmenite. Fresh biotite, as described by Beams (1994, unpublished) was not observed in the gabbro during this study, but abundant patches of chlorite and secondary amphibole replaced either primary hornblende, pyroxene or possibly biotite.

TIC gabbro contains three different types of apatite (Type I – III) (Figure 3-3C). Type I (early apatite) is the least abundant and is found as equant to subequant microlites (mostly <50 µm) in fractures of early magmatic resorbed orthopyroxene and as inclusions in augite. Type II apatite occurs as fully enclosed subequant inclusions (<100 µm) in magnetite-ilmenite, and Type III apatite is present as large (up to ~500 µm), subhedral, and commonly rounded grains and is predominantly associated with secondary amphibole ± chlorite. Apatite grains intergrown with magnetite-ilmenite, but exposed to the secondary amphibole-chlorite assemblage also show Type III characteristics (e.g. unregular, rounded grain boundaries along contacts). The petrographic differences between Types I – III besides their association with different minerals within the rock are mainly in size and abundance with Type I << Type II < Type III. The major difference however, is neither evident from petrographic observations in thin section, nor BSE imaging (higher and more optic resolution), but becomes evident using cathodoluminescence (CL) imaging and is clearly reflected in their differing geochemistry. These differences, together with textural relations are addressed and further explored in more detail as part of the discussion.

3.4.1 Quartz-Diorite (QD)

Dark medium-grained quartz diorite occurs as a series of small outcrops along the margin of the TIC. In thin section (Figure 3-3C; D), the diorite consists of plagioclase intergrown with orthopyroxene, clinopyroxene and interstitial amphibole, biotite and quartz. Plagioclase occurs dominantly as subhedral to euhedral normally-zoned laths, but multiple-zoned megacrystic plagioclase (~1 cm) is also present. Plagioclase megacryst rims are intergrown with pyroxenes. Orthopyroxene grains are usually resorbed and were observed as inclusions and exsolution lamellae in clinopyroxene. Abundant accessory magnetite grains are intergrown with or enclosed by mafic minerals. Small magnetite inclusions can be found in poikilitic clinopyroxene. Accessory subhedral apatite generally grows interstitial to plagioclase and pyroxene, but also occurs together with late amphibole and biotite. Orthopyroxene and clinopyroxene (only along grain boundaries) are variably converted to or overgrown by amphibole, biotite and chlorite.

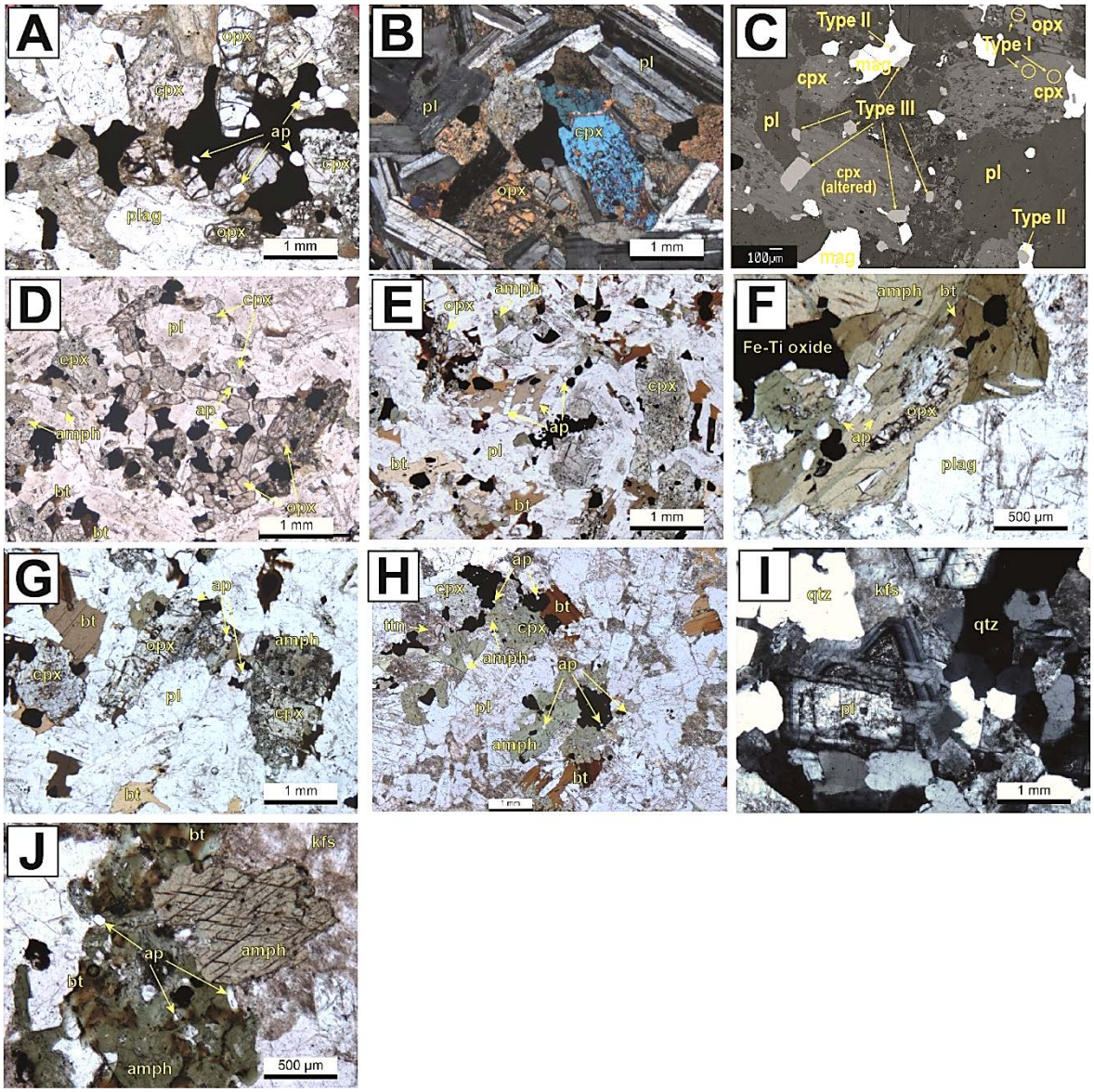

Figure 3-3 Examplary TIC petrography of typical mineral assemblages and relationships. (A) – (B) TIC gabbro, with resorbed orthopyroxene (opx) and clinopyroxene (cpx) crystals interstitial to plagioclase (pl) and large apatite grains (ap). (C) Representative backscatter electron (BSE) image of different types of apatite (Type I – III) present in TIC gabbro. Note the prominent differences in size and modal abundance where Type I << Type II < Type III. (D) and (E) Typical mineral assemblage of TIC quartz diorite. Note the difference between "clear" biotite (bt) (presumably magmatic) and cloudy biotite (late biotite, commonly found associated with Fe-Ti oxides or secondary green amphibole (amph)). Yellowish-green grains are uralitic pyroxenes, replaced by dark green amphibole. (F) - (G) Quartz Monzodiorite. The mineral assemblage and textural relations between minerals are similar to quartz diorite (e.g. late and/or secondary amphibole after pyroxene) but interstitial alkali feldspar (interstitial patchy dark phase) becomes increasingly abundant. (H) More mafic variety of granodiorite. Note the absence of opx and presence of late (?) euhedral titanite (ttn). Clinopyroxene is strongly hydrated or has been replaced by secondary amphibole. (I) and (J) showing general relationships in the most evolved granodiorite (sample TIC17-07), quartz - sodic plagioclase – alkali feldspar (kfs) assemblage (I) and primary hornblende with biotite/chlorite (brown cloudy phase) replacing earlier (?) hornblende (dark green - yellowish green) with enclosed apatite crystals.

3.4.2 Quartz Monzodiorite (QMD)

Quartz monzodiorite occurs as semi-continuous zone at the outer margin of the TIC, and as a continuous screen separating the major granodiorite bodies in the center of the complex. QMD varies from coarse, equigranular to slightly porphyritic textures, and consists primarily of feldspars, quartz, pyroxene and biotite. Large, well-formed, normal zoned plagioclase laths form the framework grains together with grains of orthopyroxene, large uralitic augite, large biotite flakes, granular magnetite and minor primary magmatic hornblende (Figure 3-3E - F). Beams (1994) further noted the presence of intergrowth textures of alternating lamellae of cpx and opx (interpreted to result from exsolution of pigeonitic pyroxene during cooling). Quartz and K-feldspar are interstitial to plagioclase, with the former minerals often intergrown with a granophyric texture. Magnetite commonly occurs in equilibrium with ilmenite. Accessory sub- to euhedral apatite grains occur with magnetite but also as small inclusions in plagioclase and biotite and occasional zircon and titanite grains can be found. Pyroxenes are extensively altered to secondary amphibole + magnetite and chlorite.

3.4.3 Granodiorite (GD/FGD)

Volumetrically, granodiorite makes up the main proportion of the surficial exposure of the TIC. During mapping of the TIC, Beams (1994) differentiated three types of granodiorite: the ‘Northern Granodiorite’, ‘Southern Granodiorite’ and ‘Felsic Granodiorite’.

Northern and Southern Granodiorite both comprise a grey speckled coarse-grained biotite hornblende, clinopyroxene granodiorite (Figure 3G). This rock is lacking in orthopyroxene and has framework (rather than interstitial) grains of quartz and K-feldspar, and so is considered to be more felsic in nature than the QMD. Clinopyroxene is occasionally present as relict grains within amphibole. Modal abundances of K-feldspar and quartz are variable, and in places K-feldspar forms large enveloping grains in a typical monzonitic fabric.

Accessory phases generally include magnetite, apatite and zircon. Secondary titanite can be found forming at the expense of biotite. Beams (1994) noted that virtually all mafic minerals (with the exception of a few clinopyroxene cores) within the 'Southern Granodiorite' are hydrated to amphibole and biotite.

The 'Felsic Granodiorite' is a grey to pinkish, speckled coarse-grained biotite hornblende granodiorite (Figure 3-3H; I). While generally similar in modal mineral composition to the other granodiorite phase(s), K-feldspar in the Felsic Granodiorite is more prominently developed as coarse interstitial grains. Beams (1994) interpreted the 'Felsic Granodiorite' to have intruded the 'Northern Granodiorite' and 'Quartz Monzodiorite', but noted that contact relations are not entirely clear.

3.5 Results

3.5.1 Whole-rock major and trace element chemistry

Samples analysed in this study are metaluminous, volcanic arc granitoids ranging from gabbro, quartz diorite and quartz monzodiorite to high-K granodiorite and aplite (48 – 77 wt.% SiO_2). TIC rocks are considered fresh and loss on ignition (LOI) over the range of all samples is <1 wt.%, with no systematic correlations of e.g. mobile elements such as Na, K or Ba (not shown). The general major and selected trace element behaviours are illustrated in Figure 3-4. Across the sample suite MgO ranges from 6.6 to 0.1 wt.%, CaO from 10 to 0.5 wt.% and $Na_2O + K_2O$ from 3 to 8.5 wt.%. P_2O_5 slightly increases from gabbro to quartz diorite (0.35 to 0.38 wt.%) and then continuously decreases to 0.01 wt.% with evolving SiO_2 contents. TIC rocks define typical fractionation trends with decreasing MgO, FeO, CaO and increasing total alkalis with increasing SiO_2. P_2O_2 and TiO_2 show a minor fractionation peak at ~53 wt.% SiO_2, indicating saturation in apatite and a Ti-bearing phase. Trace elements mirror the very regular behaviour shown by in major elements, increasing or decreasing in value with increasing SiO_2 depending on their respective compatibility. Some noteworthy changes in trace element behaviour are, for example, the change from increasing to decreasing values in Zr presumably as a result of the onset of zircon crystallisation and bulk rock F at ~65 wt.% SiO_2. Barium continuously increases up to felsic granodiorite composition (~70 wt.% SiO_2) and only shows decreased values in the late-stage aplites.

With respect to trace element abundance patterns, the TIC display typical subduction related trace element patterns with enrichment in LILE and depletion in Nb and Ta (not shown) (Tatsumi and Eggins, 1995). Chondrite-normalised REE patterns show strong enrichment of LREE over HREE (Figure 3-5). Increasing SiO_2 content correlates with continuous REE enrichment (e.g. $(La/Yb)_N$ ~9.3 in gabbro to ~13.5 in granodiorite), and increasingly negative Europium anomaly values ($Eu/Eu^* = 1.23 – 0.58$).

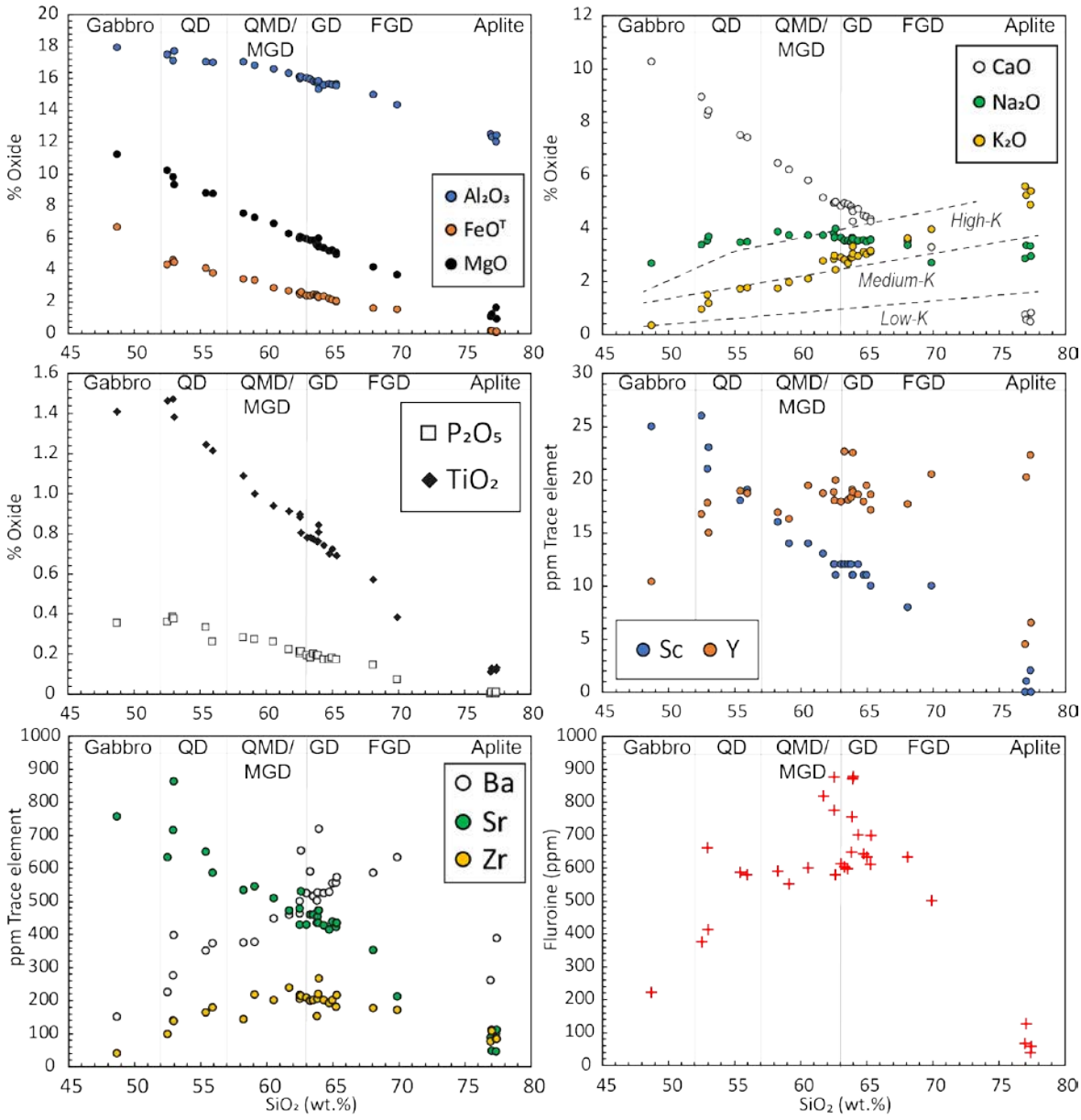

Figure 3-4 Harker diagrams illustrating the general trends of major and selected trace elements of the TIC (QD = Quartz Diorite; QMD/MGD = Quartz Monzodiorite to mafic Granodiorite; GD = Granodiorite; FGD = Felsic Granodiorite). Fields for Low-, Medium- and High-K igneous rocks after Peccerillo and Taylor (1976). Note (1) the remarkable consistency of increasing and decreasing element trends over the range of bulk rock SiO_2 compositions, and (2) changing trends of e.g. Zr and F at ~65 wt.% SiO_2.

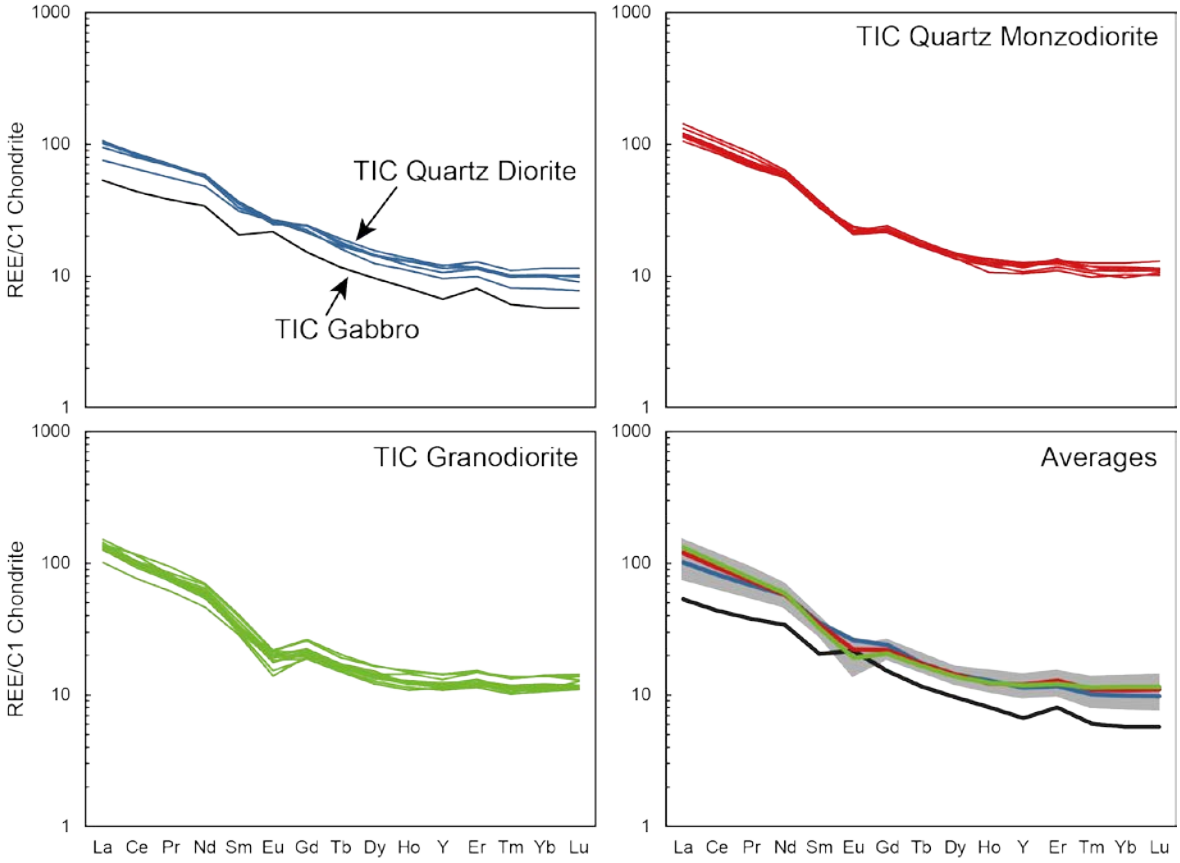

Figure 3-5 Chondrite-normalised REE patterns of TIC gabbro to granodiorite with normalising values after McDonough and Sun (1995). The grey field represents the range of TIC quartz diorite to granodiorite). Note the increasing REE compositions and correlating decreasing europium anomalies.

3.5.2 Mineral major and trace element chemistry

3.5.3 Feldspar

Plagioclase is the modally dominant phase in all studied samples, and develops from anorthite-rich compositions in gabbro (An_{70-54}) to more sodic compositions in quartz diorite (An_{50-30}), quartz monzodiorite (An_{60-17}) and granodiorite (An_{45-21}) (Figure 3-6A). Quartz monzodiorite (sample TIC17-03) records the largest range of plagioclase compositions, with plagioclase cores being similar to plagioclase rim compositions found in gabbro and plagioclase core compositions found in quartz diorite. Plagioclase rim zones in quartz monzodiorite and granodiorite are commonly oligoclase with $<An_{30}$, and low values might indicate small degrees of albitisation. In the majority of cases, plagioclase grains are normally zoned, with $An_{core} > An_{rim}$, but oscillatory zonation is commonly observed in some grains throughout quartz monzodiorite and granodiorite. Some interstitial K-feldspar was analysed in samples TIC17-03 and TKR-26 and is sanidine with Or_{77-90} and Or_{85-96}, respectively.

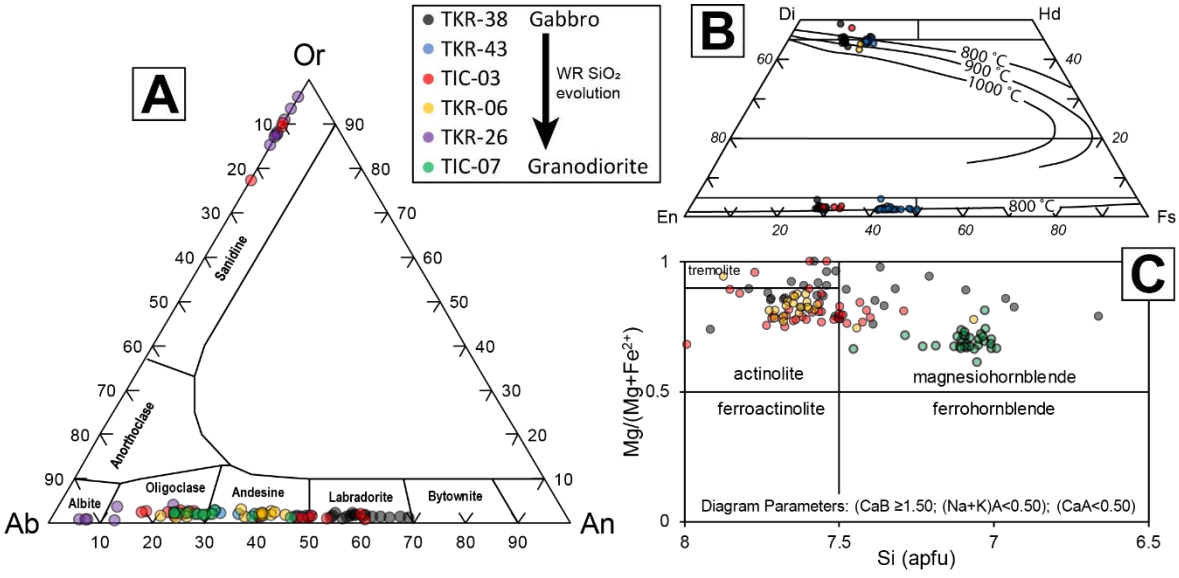

Figure 3-6 A) Feldspar ternary, B) pyroxene ternary (after Morimoto, 1988 and isotherms after Lindsley, 1983), and C) amphibole (after Leake et al., 1997) classification diagrams for TIC samples.

3.5.4 Pyroxene

Pyroxene is present in gabbro to mafic granodiorite varieties, but is absent in the more felsic granodiorites (e.g. samples TKR-26, TIC17-07). Gabbro, quartz diorite and quartz monzodiorite contain both, orthopyroxene (opx) and clinopyroxene (cpx) with opx ≈ cpx in gabbro, and opx modal abundances generally decreasing with evolving bulk-rock SiO_2 content, until opx is only minimally present as strongly resorbed grains in the quartz monzodiorite (Figure 3-3A-F). More mafic varieties of granodiorite rarely contain relics of strongly uralitic clinopyroxene, which is commonly replaced by secondary amphibole and/or chlorite. Compositions of TIC pyroxenes are presented in Figure 3-6B.

Orthopyroxene compositions of TIC rocks range in composition from Mg# 72 - 49 and En_{70-52}. Orthopyroxene in gabbro is most magnesian (Mg# 72 - 69 and En_{70-68}), followed by the monzodiorite sample (TIC17-03) opx (Mg# 70 - 66 and En_{68-64}), and opx from the quartz diorite (Mg# 58 - 49 and En_{56-52}).

Clinopyroxene, where present is Ca-rich, Al- and Ti-poor augite to diopside with Mg# 82 - 68. Clinopyroxene from quartz diorite to granodiorite has slightly lower Mg# (70 - 67) compared to gabbro (Mg# 81 - 77). There is no observable compositional difference between core and rim spot analyses. Al_2O_3 compositions are relatively low and with significant scatter but comparable in between samples with 0.3 - 1.4 wt.% in gabbro, 0.4 - 2.1 wt.% in quartz diorite and 0.2 – 1.9 wt.% in quartz monzodiorite. All pyroxene roughly fall between the 800 and 900 °C isotherms, which is considered the equilibration (cooling) temperature (Lindsley, 1983).

3.5.5 Amphibole

Amphibole where present is generally strongly altered and predominantly present as secondary amphibole after pyroxene, so limited quantitative analysis was conducted for this study. Amphibole formulae were calculated on the basis of 24 anions (O, Cl, OH, and F) using the Excel spread sheet of Locock (2014). According to the classification of Leake et al. (1997) (Figure 3-6C) amphiboles analysed in gabbro, monzodiorite and granodiorite sample TKR-06 predominantly classify as actinolite to tremolite, with only a few analyses returning magnesio-hornblende compositions. Ferric anthophyllite was further identified in TIC gabbro replacing an unknown mafic precursor mineral. Felsic granodiorite sample TIC17-07 contains primary magmatic amphibole which classifies as ferric magnesio-hornblende, with only limited outliers close to actinolite composition.

Total aluminium (atoms per formula unit) scatters from 1.2 to 0.08 in gabbro and 0.56 to 0.11 in quartz monzodiorite. The two analysed granodiorites have Al_{tot} 0.97 to 0.3 (TKR-06) and Al_{tot} 1.1 to 0.63 in the more evolved sample TIC17-07. Chlorine compositions are highly variable and range from <0.1 to 0.46 wt.% (<0.01 to 0.11 a.p.f.u) across the different lithologies. Significant concentrations were obtained from monzodiorite sample TIC17-03 (0.03 – 0.46 wt.%; but >80 % fall within the range of 0.1 – 0.18 wt.%) and granodiorite sample TKR-06 (0.08 – 0.15 wt.%), which are both slightly lower compared to sample TIC17-07 (0.12 – 0.21 wt.%).

3.5.6 Biotite

The biotite compositions and halogen systematics are listed in the electronic appendix 3-III, and are shown inFigure 3-7. TIC biotite is characterised by relatively high MgO (11.7 – 16.6 wt.%) and low Al2O3 (11.4 – 13.7 wt.%) concentrations, with Mg# ranging from 50 to 70, total Al a.p.f.u. of 2.1 – 2.4 (mostly), and Ti a.p.f.u of 0.45 – 0.6 (mostly). Biotite compositional range in the nomenclature diagram of Rieder et al., (1998) is shown in Figure 3-7B.

Biotite from the quartz diorite (TKR-43) has the lowest Mg# (50 – 55). Quartz monzodiorite biotite (TIC17-03), interpreted to be the next intrusive phase after quartz diorite and gabbro, shows a bimodal distribution characterised by in-grain variations in total Al and Mg#, with higher total Al (~2.1 – 2.16) corresponding to lower Mg# (60 – 65) compared to total Al ~ 2 and Mg# 62 – 66). Biotites from granodiorite samples TKR-06 (Mg# 58 – 64) and TIC17-07 (Mg# 51 – 60) have compositions that are intermediate to biotite of quartz diorite and monzodiorite, which are likely the result of co-crystallising hornblende. Biotite from sample TIC17-07 shows systematically lower Ti (0.3 – 0.4 p.f.u.), whereas biotites of granodiorite sample TKR-26 have generally higher MgO (15.1 – 17.1 wt.%) and lower FeO (12.3 – 16.4 wt.%) compared to other samples.

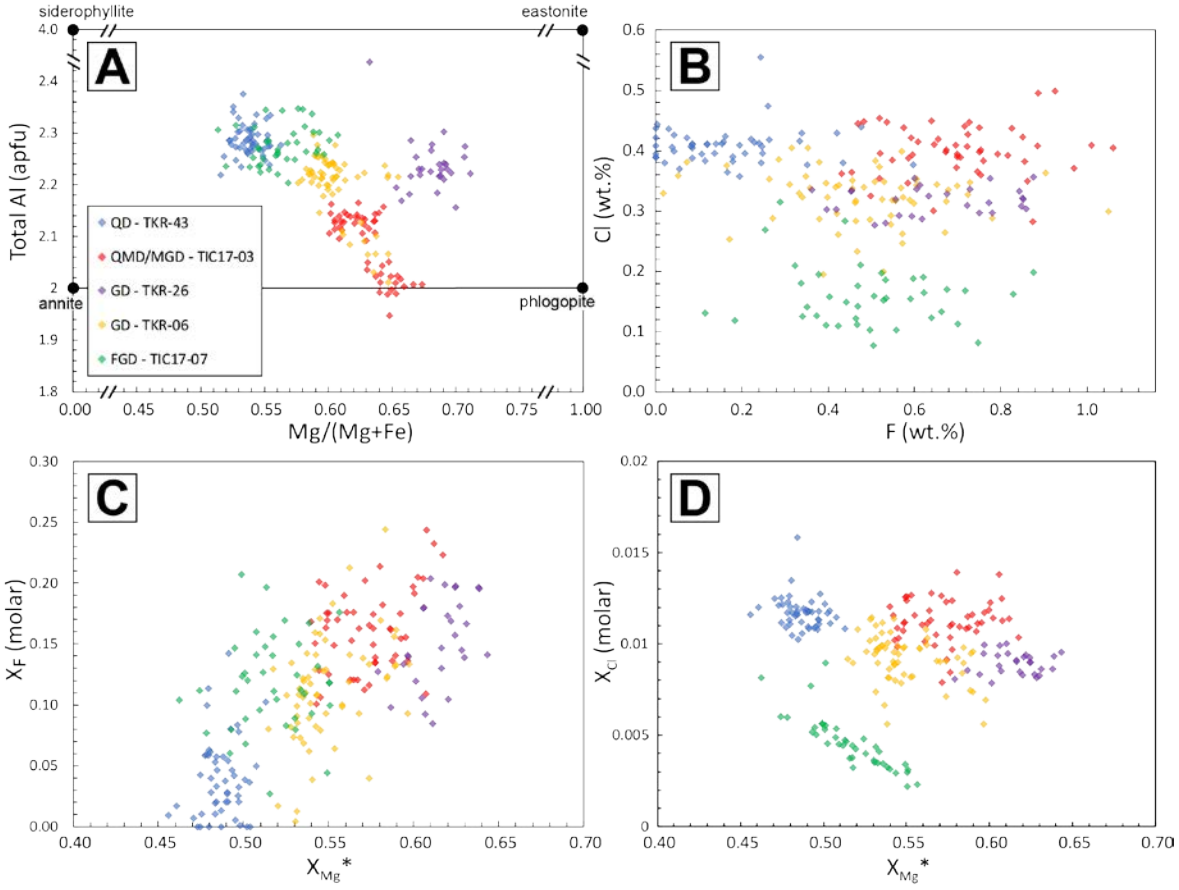

Figure 3-7 TIC biotite compositions and halogen systematics. A) Biotite compositional quadrilateral after Rieder et al. (1998).

Chlorine and fluorine contents of TIC biotites range from 0.1 to 0.5 wt.% and 0.01 to 1.06 wt.%, respectively (Figure 3-7B-D), and are generally consistent within individual samples. The Cl and F contents tend to vary systematically with the SiO_2 content of the host rock, from low F – high Cl biotite in quartz diorite (F/Cl = 0.1 – 1.6), to high F – lower Cl biotite in quartz monzodiorite (F/Cl = 1.1 – 3.1). Biotites from the granodiorite samples cover a large range of F/Cl ratios (0.1 – 9.2), but are relatively consistent within single samples.

As illustrated in Figure 3-7C and D, molar proportions of F and Cl (calculated based on a.p.f.u. as e.g. $X_F = [F/(Cl + F + OH)]$), increase or decrease with increasing X_{Mg}* (with X_{Mg}* = $Mg/[(Mg+Fe+Mn+Ti+Al^{VI})]$). This observation is consistent with the Mg-Cl (or Fe-F) avoidance rule for biotite (e.g. Munoz, 1984; Leger et al., 1996), where Cl is incorporated into biotite in favour of F by substitution of Mg by Fe and some other octahedral cations (Al, Ti, and Mn). The significantly difference in the slope of X_{Cl} vs X_{Mg}* in sample TIC17-07 compared to other samples might be related to differences in the respective Ti concentration (Leger et al., 1996) (Figure 7D).

3.5.7 Apatite

Apatite compositions and formula calculations are provided in appendix 3-IV, and general trace element and halogen systematics are illustrated in Figure 3-8.

Trace elements contents of apatite show minor to significant differences between the different TIC lithologies, but are fairly homogeneous within individual samples. Trace element compositions generally conform with a granitoid origin (Belousova et al., 2002; Figure 3-8A). In general, no significant differences were observed between cores and rim compositions with regards to trace element distribution besides the observation that TIC apatite is minimally more enriched in REE in core regions of crystals compared to rims (not shown). Most notable differences in trace element contents are recorded in apatite from TIC gabbro (sample TKR-38) when compared to more evolved samples. Some apatites from gabbro are characterised by significantly higher Sr (560 – 1390 ppm), lower Y (240 – 560 ppm) and lower TREE (0.3 – 0.5 wt.%) compositions, compared to apatite from other lithologies (Figure 3-8B); these apatites also have higher Sr and lower TREE, Y, Th and U in analysed rims compared to cores (not shown) and the cause for these differences will be addressed in detail later. Chondrite-normalised REE patterns show subsequent enrichment of REE and increasingly negative Europium anomalies (Eu/Eu* 0.5 – 0.07) correlate with increasing bulk rock silica compositions (Figure 3-8C).

Halogen contents in apatite from the TIC are illustrated in Figure 3-8D and E. TIC apatites show a general trend of decreasing Cl and coupled increasing F compositions with increasing bulk rock silica content: However, the three petrographically-defined apatite types in the TIC gabbro have quite distinct halogen geochemistry. Type I (early apatite) is characterised by elevated Cl (1.93 – 2.78 wt.%) contents with lower F (1.01 – 1.41 wt.%) and a relatively constant molar proportion of OH (~40%). Type II apatite is significantly more F-rich (2.7 – 3.3 wt.%) and Cl-poor (0.51 – 0.84 wt.%) compared to Type I apatite and similar to apatite compositions found in quartz monzodiorite (sample TIC17-03). Type III apatite is characterised by high Cl (3.7 to 6.1 wt.%) and low F (0.06 – 1.01 wt.%) compositions and largely falls along a Cl-OH exchange line. Quartz diorite apatite is compositionally homogenous with ~20% molar OH, but lower Cl (1.3 – 2.02 wt.%) and higher F (1.78 – 2.34 wt.%) compared to Type I apatite in TIC gabbro.

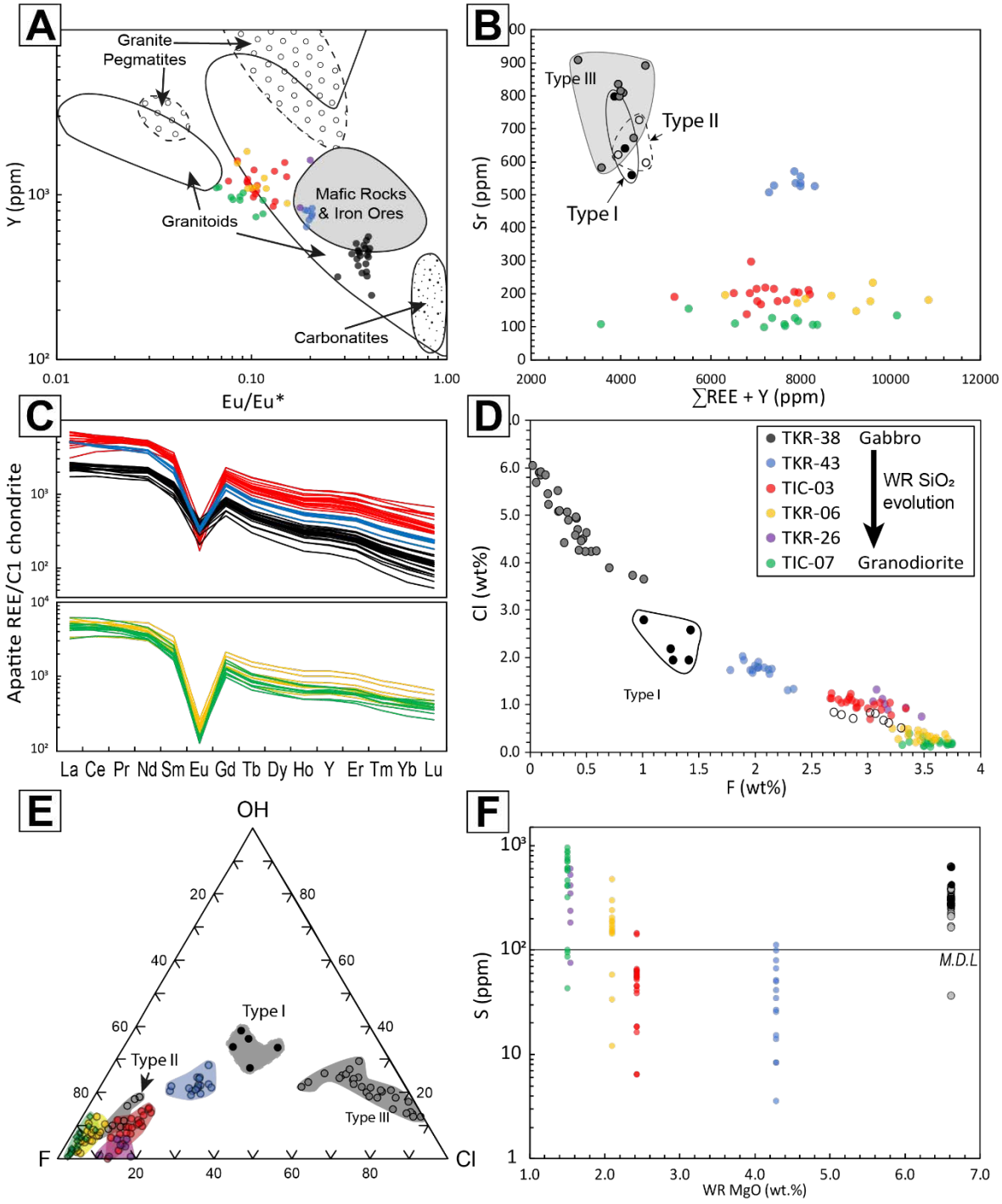

Figure 3-8 General trace element and Cl, F and S behaviours as analysed in TIC apatite. A) Y vs. Eu/Eu* apatite provenance diagram of Belousova et al. (2002). B) – F) show general compositional characteristics. E) Ternary apatite classification diagram based on the molar proportions of Cl – F – OH, calculated after Piccoli and Candela (2002). F) Note that most S contents are below or very close to the limit of detection (M.D.L.), and the plotted data are mainly indicative.

Quartz monzodiorite to granodiorite apatite form a F-rich group (fluorapatite molar proportion > 80%). Monzodiorite apatite compositionally bridges the gap between diorite and granodiorite with 0.18 to 1.23 wt.% Cl and 2.7 to 3.3 wt.% F. Granodiorite apatite is F-rich (3.2 – 3.75 wt.%) with invariably low Cl (0.1 – 0.49 wt.%) and decreasing molar OH (~ 15 – 1%), and fall on a F-OH exchange line. Apatite of granodiorite sample TKR-26 is comparable in composition to Quartz Monzodiorite apatite.

Most analyses of sulfur in apatite are close to or below the limit of detection (≤100 ppm S), with only few analyses returning values of >0.01 wt.% SO_3 (i.e. ~0.01 S p.f.u.). Results are illustrated in Figure 3-8F and plotted as S (ppm) against whole-rock MgO as a measure of magma evolution. Sulfur contents above the limit of detection were found in TIC gabbro (S = ~160 – 400 ppm, with two outliers of ~600 ppm), and the granodiorite samples with ~140 – 400 ppm (sample TKR-06), ~180 – 609 ppm (sample TKR-06) and ~320 – 960 ppm (~0.03 S p.f.u; sample TIC17-07). As shown in Figure 3-8F, sulfur contents of apatites measured in quartz diorite and quartz monzodiorite are below the limit of detection, but increase from mafic granodiorite (sample TKR-06) towards felsic granodiorites TKR-26 and TIC17-07.

3.6 Discussion

Apatite is an ubiquitous but minor phase in a large range of magmatic rocks. It is the main repository for bulk rock P, and in addition, can be an important carrier of halogens, sulphate, carbonate, Sr, REE and other trace elements (e.g. Piccoli and Candela, 2002; Webster and Piccoli, 2015 and references therein). Apatite can be found at various stages of a rock's crystallisation history, which is owed to the fact that local P saturation and apatite crystallisation can occur along grain boundaries of crystallising major rock-forming minerals (e.g. plagioclase, pyroxene or Fe-Ti oxides), even before a melt reaches its theoretical P saturation and the ability to crystallize apatite at a given temperature. Once a magma is saturated in P, apatite crystallisation commonly occurs over a relatively restricted temperature interval within 60 – 100 °C below the apatite saturation temperature (AST) (Harrison and Watson, 1984; Piccoli and Candela, 2002). Further, volatile contents of apatite are generally found to be a function of melt composition and temperature, and only to a lesser extent pressure (e.g. Piccoli and Candela, 2002). Therefore, the relative timing (e.g. petrographic relationships) and a relative constraint of the temperature (internal or external) at which apatite crystallised are important factors when estimating halogen compositions in an evolving magmatic system (e.g. Mathez and Webster, 2005; Webster et al., 2009; Doherty et al., 2014, McCubbin et al., 2015; Webster and Piccoli, 2015; and summaries in Dolejš and Zajacz, 2018 and Webster et al., 2018). Additional challenges to obtain reasonable estimates may occur due to presence of other halogen-bearing minerals (e.g. amphibole and biotite) and exsolution and/or reaction with a fluid and/or vapour phase(s), questions which have long been investigated by various researchers (e.g. Zhu and Sverjensky, 1991; 1992; Icenhower and London, 1997; Coulson et al., 2001; Zhang et al., 2012; Teiber et al., 2015; Wang et al., 2016).

Apatite is abundantly present as a magmatic phase in the TIC lithologies and can therefore be used to unravel some aspects of halogen evolution with respect to magma evolution. Thus, I; (1) discuss the general petrogenesis of the TIC; (2) discuss apatite textures and petrographic relations, and thereby developing a framework of relative timing of apatite within single samples; (3) provide estimates of Cl, F and S melt compositions based on apatite analyses, and; (4) investigate possible relationships of Cl and F distribution between apatite and biotite. In combination these observations will help to understand volatile distribution in continental arc intrusions. In addition, the presented data set can be used as a

base line to systematically investigate halogen systematics, and thus fertility of igneous suites of north-eastern Australia, and elsewhere in the world.

3.6.1 Petrogenesis of the TIC

The TIC has previously been the subject of petrographic and whole-rock geochemistry studies (Beams, 1994; Blevin and Morrison, 1997), zircon U-Pb dating and Lu-Hf isotope analysis (Murgulov et al., 2008). Here I combine results of these previous studies with additional insights based on newly acquired geochemical data to evaluate the petrogenesis of the TIC.

Based on geological mapping, petrographic descriptions and whole-rock geochemistry, Beams (1994) and Blevin and Morrison (1997) proposed that the TIC formed as a calc-alkaline, subduction-related, I-type igneous complex, with various rock units derived by continuous fractional crystallisation of two pyroxenes + plagioclase + Fe-Ti oxide ± apatite, with late hornblende, biotite, quartz and K-feldspar. The parental magma was proposed to be similar in composition to the TIC gabbro/qtz diorite. Early intrusive phases produced a pyroxene hornfels aureole in the surrounding country rock, suggesting that the intruding TIC magmas were relatively hot (Beams, 1994).

The remarkably smooth bulk rock geochemical trends of decreasing compatible elements (CaO, MgO, FeO) concentrations and increasing incompatible element contents (REE, Zr, Ba, K) with increasing SiO_2 (Figure 3-4 and Figure 3-5) are entirely consistent with magma evolution via fractional crystallisation. The TIC gabbro represents the most mafic lithology and forms the most primitive end-member composition in Harker diagrams (Figure 3-4). However, low MgO concentrations of ~6 wt.% and an Mg# of 51 indicate that this rock had already undergone a significant degree of fractionation and/or hybridisation from a more primitive basaltic melt. Petrographic observations suggest that TIC gabbro is a cumulate rock, characterised by oriented large plagioclase laths (~70-80 vol.%) with interstitial orthopyroxene and clinopyroxene, (Ti-)-magnetite – ilmenite solid solutions and abundant apatite. Excessive accumulation of plagioclase is further supported by high Al_2O_3 and the significant positive Eu/Eu* of 1.2 for this rock.

Relative constraints on the redox conditions of the TIC magmas, can be obtained using the empirically and theoretically derived granitoid redox assessment of Blevin (2004) (Figure 3-9). This approach is justified since I do not observe extensive oxidation of magnetite (e.g. crystallization of secondary hematite or goethite along magnetite rims) in thin sections. In addition, LOI's of TIC rocks are generally <1 wt.% indicating little to no alteration and further, Fe^{2+} compositions were individually measured by titration method (see Analytical methods), therefore I can calculate reliable log(Fe_2O_3/FeO) ratios. As illustrated inFigure 3-9, the TIC suite falls along the 'moderately' to 'strongly oxidised' boundary, indicating a broadly constant fO_2 with differentiation.

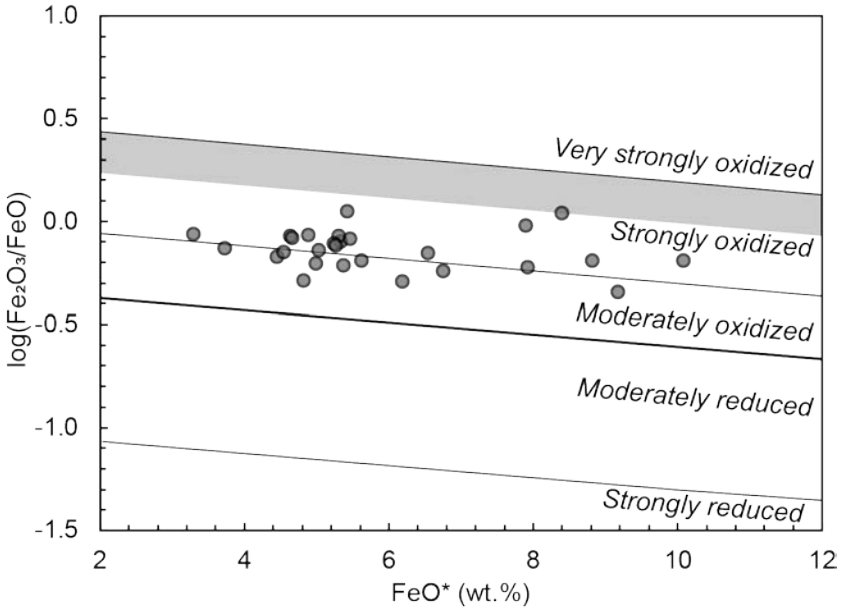

Figure 3-9 Redox classification of TIC samples (without TIC aplites which have FeO* <2 wt.%) according to the scheme developed for igneous rocks by Blevin (2004). FeO* is total Fe in the sample as FeO. Also shown is the area (grey field) corresponding to igneous rock suites from the northern New England Orogen associated with porphyry Cu-Au mineralisation.

Crystallisation and fractionation driven by plagioclase and clinopyroxene began within the compositional range of gabbroic to dioritic composition and lead to decreasing CaO and Al_2O_3 concentrations in the residual liquids. Fractionation of plagioclase resulted in continuously decreasing Eu/Eu* from ~1.0 to 0.58, as observed from the quartz diorite to the most evolved granodiorite (Figure 3-5). This is consistent with the measured An contents of plagioclase (Figure 3-6A), decreasing from An_{70-60} in gabbro to An_{50-40} in quartz diorite, and An_{40-20} in more evolved monzodiorite and granodiorite. Oscillatory, and in some cases reverse, zonation in analysed plagioclase grains suggests periodic injections of more mafic magmas into the system. The largest range in An compositions is recorded in sample TIC-

03 (An_{60-20}) which, together with the reported occurrence of quartz diorite xenoliths within more evolved rocks (Beams, 1994, unpubl.) indicates either some degree of mixing within the magmatic system, or convection within the magma chamber. The fractionation model is also supported by the measured – but limited – pyroxene data, recording a significant change in orthopyroxene composition from high-magnesian enstatite in gabbro (Mg# 72 - 69) to diorite (Mg# 58 – 49), which is also reflected in the decreasing MgO bulk rock compositions (see Fig. 3-4).

Furthermore, a general change in rock-forming mineral assemblages from two – pyroxene gabbro and diorite towards cpx-hbl-bt bearing mafic granodiorite varieties, and lastly a hydrous hbl-bt felsic granodiorite suggests that the TIC magma evolved from relatively dry, water-undersaturated, towards more hydrous compositions with fractionation. This change in mineralogy is also reflected in increasing La/Yb (13.7 – 19.9) and decreasing Dy/Yb ratios (2.55 – 1.55) with progressing magma differentiation (see electronic appendix 3-II); trends typically ascribed to rocks that have undergone amphibole fractionation (e.g. Davidson et al., 2007).

3.6.2 Apatite petrography and textures

Apatite geochemistry has great potential to track the inventories and evolution of volatiles in magmatic/hydrothermal systems, and has been successfully applied to a variety of geotectonic settings at the abyssal and hypabyssal levels (e.g. Piccoli and Candela, 2002; Zhang et al., 2012; Scott et al., 2015; Webster and Piccoli, 2015 and references therein; Wang et al., 2016; Chelle-Michou and Chiaradia, 2017; Richards et al., 2017; Zhu et al., 2018). However, to accurately link apatite evolution to the magma it crystallised from, it is crucial to constrain the timing of apatite crystallisation relative to the major mineral assemblages in the investigated samples (e.g. Piccoli and Candela, 2002). Therefore, I provide a more detailed description of the relationships and textures of TIC apatite (Figure 3-10), thereby establishing the relative timing at which apatite crystallised relative to the major rock forming minerals.

Based on petrographic observations, apatite occurs as an early magmatic phase, as shown by its sub- to euhedral, equant to subequant habit, intergrown with, or fully enclosed by, early magmatic phases (e.g. pyroxene and Fe-Ti oxides) (e.g. Figure 3-10A, D, G, J, K). These textures suggest most TIC apatite formed as part of the magmatic mineral assemblage (e.g. Webster and Piccoli, 2015). Petrographic observations also show the presence of minor interstitial apatite in some samples (e.g. Figure 3-10D-F, J), and small acicular apatite grains (commonly <50 μm) are found in many of the more evolved rocks. Interstitial growth is normally attributed to late magmatic crystallisation, whereas highly-acicular crystal habits are generally interpreted to result from crystallisation far from equilibrium, or hydrothermal/deuteric conditions (e.g. Webster and Piccoli, 2015). The relative timing of crystallisation of interstitial apatite in TIC diorite is difficult to determine since it appears to occur in equilibrium with both early plagioclase and augite, but also shows ‘clean’ grain boundaries towards late interstitial amphibole, biotite and quartz. Euhedral apatite inclusions abundantly occur within Fe-Ti oxides and to a lesser extent in amphibole and/or biotite in samples up to ~65 wt.% bulk rock SiO_2, suggesting that the early apatite crystallised at higher temperatures (Figure 3-10A-J). In contrast, apatite in the most felsic granodiorites (Figure 3-10L, sample TIC17-07) is only rarely associated with magnetite and more commonly found as sub- to euhedral grains enclosed by amphibole and, occasionally, biotite. Overall, the presence of more than one apatite morphology in TIC rocks suggests a complex crystallisation and cooling history.

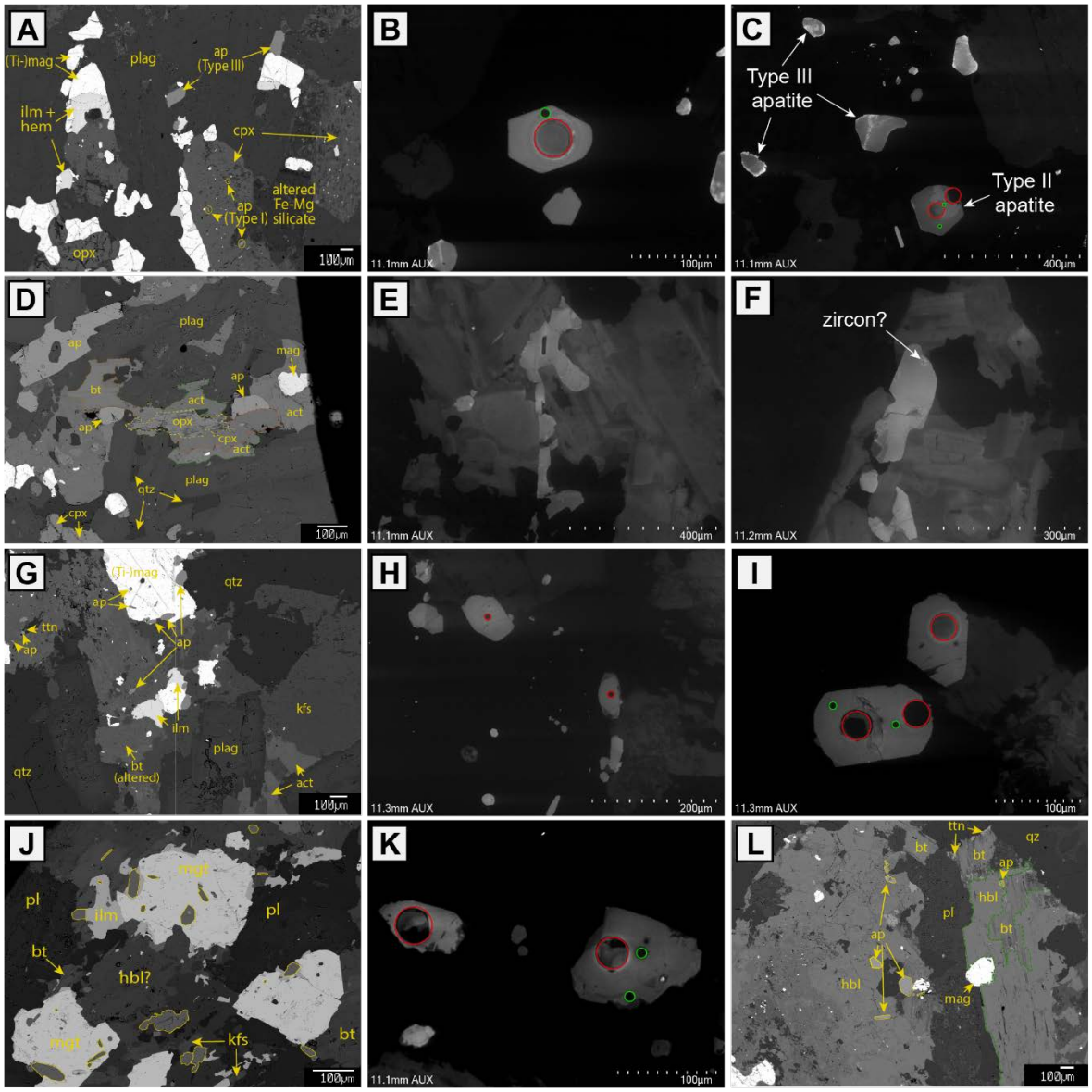

Figure 3-10 Backscatter electron (BSE) and cathodoluminescence (CL) images showing typical apatite relationships and textures in TIC rocks. Analytical spots are marked where applicable (green = electron microprobe; red = LA-ICP-MS). (A) – (C) TIC gabbro (sample TKR-38); (D) – (F) Dominantly interstitial apatite in quartz diorite (sample TKR-43); (G) – (I) Examples from quartz monzodiorite (sample TIC17-03), note the variable habits and sizes in (H); (J) and (K) Multiple varieties of apatite (yellow outline) in granodiorite sample TKR-06 (J) and minimal zonation in some grains (K). (L) Predominantly euhedral apatite (yellow outline) in equilibrium with amphibole in the most evolved felsic granodiorite sample TIC17-07. Also note the absence of ilmenite compared to sample TKR-06 (J).

Backscattered electron and CL imaging of TIC apatite reveals occasional core-rim zonation in some grains, and such zonation patterns are typically attributed to variation in the contents of trace elements, such as the REE and Mn (Waychunas, 2002). Some TIC apatites exhibit grain porosity that may be indicative of grain dissolution. However, CL imaging of the Type III apatites in TIC gabbro are distinct in that they have anhedral to rounded forms with a cloudy interior and a CL bright rim zone (Figure 3-10C).

This apatite generation is also distinctively Cl and Sr rich (Figure 3-8), so this apatite is interpreted to be of hydrothermal origin and likely formed due to alteration (e.g. via dissolution-reprecipitation; e.g. Harlov, 2015) of Type I and II apatites by Cl-rich hydrothermal fluids.

In summary, all TIC rocks contain magmatic apatite which, based on textural evidence formed near equilibrium early in the crystallisation sequence, but also apatite that evidently grew at later stages, far from equilibrium or show textures that support substantial hydrothermal replacement (in particular Type III apatite found in TIC gabbro).

3.6.3 Element substitution in apatite

Based on the absence of significant amounts of other potential REE-bearing minerals, and the relatively high REE contents of TIC apatite (Figure 3-8B), I assume that apatite is the principal REE host within the TIC. REEs are commonly incorporated into or removed from apatite by the coupled substitution reactions (Pan and Fleet, 2002; Hughes and Rakovan, 2015):

$$REE^{3+} + Na^{+} = 2\ Ca^{2+} \quad (1)$$

and

$$REE^{3+} + Si^{4+} = P^{5+} + Ca^{2+} \quad (2)$$

Both substitution mechanisms likely play a role in REE incorporation into the TIC apatites, although these correlations are highly variable. Overall, Na, Si and REE + Y contents of apatite generally increase with host rock evolution (e.g. increasing bulk SiO_2 content, not shown). In TIC gabbro Sr^{2+} is an important substitute, and Sr correlates positively with Ca^{2+} (not shown).

The predominant incorporation of sulfur into the apatite crystal structure as S^{6+} has long been suggested to occur by replacing P^{5+}, and charge-balance substitutions involving Na^{+}, Si^{4+}, and $(REE + Y)^{3+}$ cations (Rouse and Dunn, 1982; Liu and Comodi, 1993; Tepper and Kuehner, 1999, Parat et al., 2002). However, µ-XANES measurements by Konecke et al. (2017) have demonstrated that apatite can also incorporate some minor amounts of S^{4+} and S^{2-}, but their influence on overall charge balance might be negligible. Possible substitution reactions for apatite involving S^{6+} are:

$$S^{6+} + Na^{+} \Leftrightarrow P^{5+} + Ca^{2+} \text{ (Liu and Comodi, 1993),} \quad (3)$$

$$S^{6+} + Si^{4+} \Leftrightarrow 2P^{5+} \text{ (Rouse and Dunn, 1982),} \quad (4)$$

$$S^{6+} + Na^{+} + Si^{4+} + REE^{3+} \Leftrightarrow 2P^{5+} + 2Ca^{2+} \text{ (Tepper and Kuehner, 1999)} \quad (5)$$

$$Si^{4+} + 2Na^{+} + 2S^{6+} + 4REE^{3+} \Leftrightarrow 4P^{5+} + 5Ca^{2+} \text{ (Parat et al., 2002),} \quad (6)$$

As illustrated in Figure 3-11, for the mafic to intermediate samples, sulfur and sodium contents are too low to have any significant impact on the overall charge and other elements may exert a more important control (e.g. REE + Y $(REY)^{3+}$, Sr^{2+}, Mn^{2+}, or Fe^{2+}). The observed pattern in Figure 3-11D (Eq. 4) is the only equation which shows a general correlation over the range of all samples, where decreasing phosphorus correlates with increasing sulfur and silica. However, considering the generally low amounts of Na and S in TIC apatite, Si and in particular REE + Y (REY) seem to dominantly control the overall charge balance. Evidently, further work is required to resolve substitution mechanisms accounting for all processes at play during progressive magma differentiation.

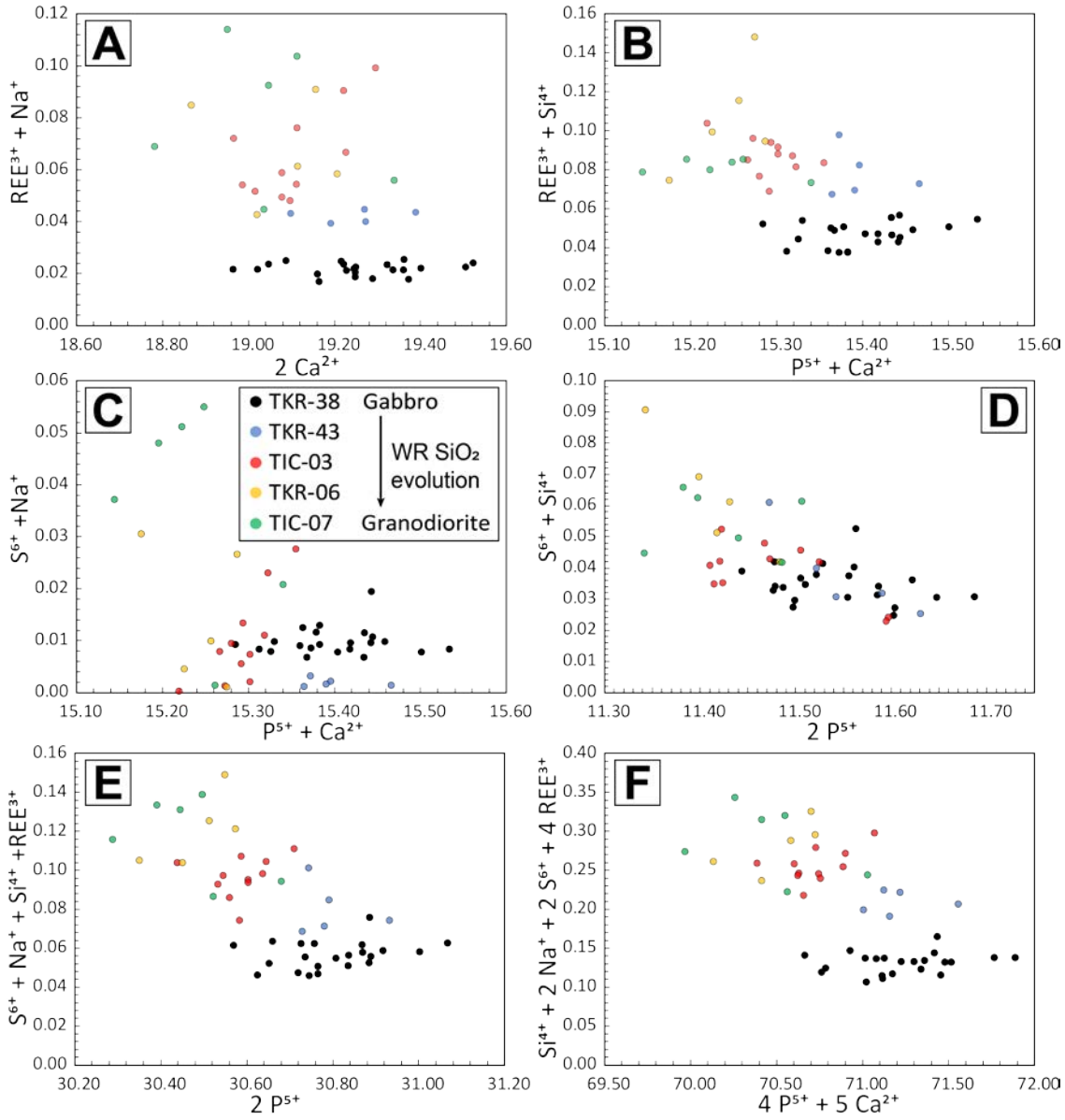

Figure 3-11 Possible substitution mechanisms (A-F = Eq. 1–6) in order of appearance within the text for TIC apatites involving sulfur (see text for references and reactions).

3.6.4 Apatite volatile content and distribution

Given the presence of magmatic apatite across the range of rocks of the TIC, apatite can be used as a monitor of magmatic volatile contents during magma evolution. Here, I focus on apatites that are interpreted to be magmatic; hydrothermal apatite (e.g., Type III apatite) will be addressed in relation to hydrothermal processes in a later section below.

Zhu and Sverjensky (1991) recognised that the general proportions of F, Cl, OH (and CO_3) within magmatic apatite depend on three principal factor; (1) the melt and/or fluid composition; (2) the presence of other F- and Cl- bearing minerals (e.g. biotite, amphibole, muscovite, or scapolite); and (3) the P-T conditions at the time of apatite precipitation. In addition, modification of primary apatite composition via diffusion and hydrothermal alteration ("apatite metasomatism", e.g. Harlov, 2015, and references therein) also needs to be considered. In particular, chlorine is a fast diffusing element in apatite (Brenan, 1993), and magmatic T of ~800 °C, will likely obliterate and homogenize any initial chlorine zonation within weeks or years (Boyce and Hervig, 2008), unless crystallising apatite is either subject to rapid cooling and/or isolated from gradient in chemical activity of Cl-F-OH.

The study of the volatile inventory of TIC magmatic apatite reveals a general trend from Cl-rich Type I apatite in TIC gabbro to near end-member fluorapatite (where molar X_F > 0.8) in most evolved granodiorite (Figure 3-8). The predominance of fluorapatite component is a common observation in most igneous rocks and is shared by TIC apatite (e.g. Piccoli and Candela, 2002; Marks et al., 2012; Webster and Piccoli, 2015, and references therein). Chlorine-rich Type I early apatite in TIC gabbro (here with ~2 wt.% Cl) may be the 'normal' apatite composition to be expected to crystallize from oxidised, mafic arc magmas. Significantly more Cl-rich magmatic apatite (>3.5 wt.%), comparable to Type III apatite from TIC gabbro has been reported from layered intrusions where they are most commonly considered to have either crystallised from Cl-rich fluids or are the product of metasomatism (e.g. McCubbin et al., 2011; Webster and Piccoli, 2015).

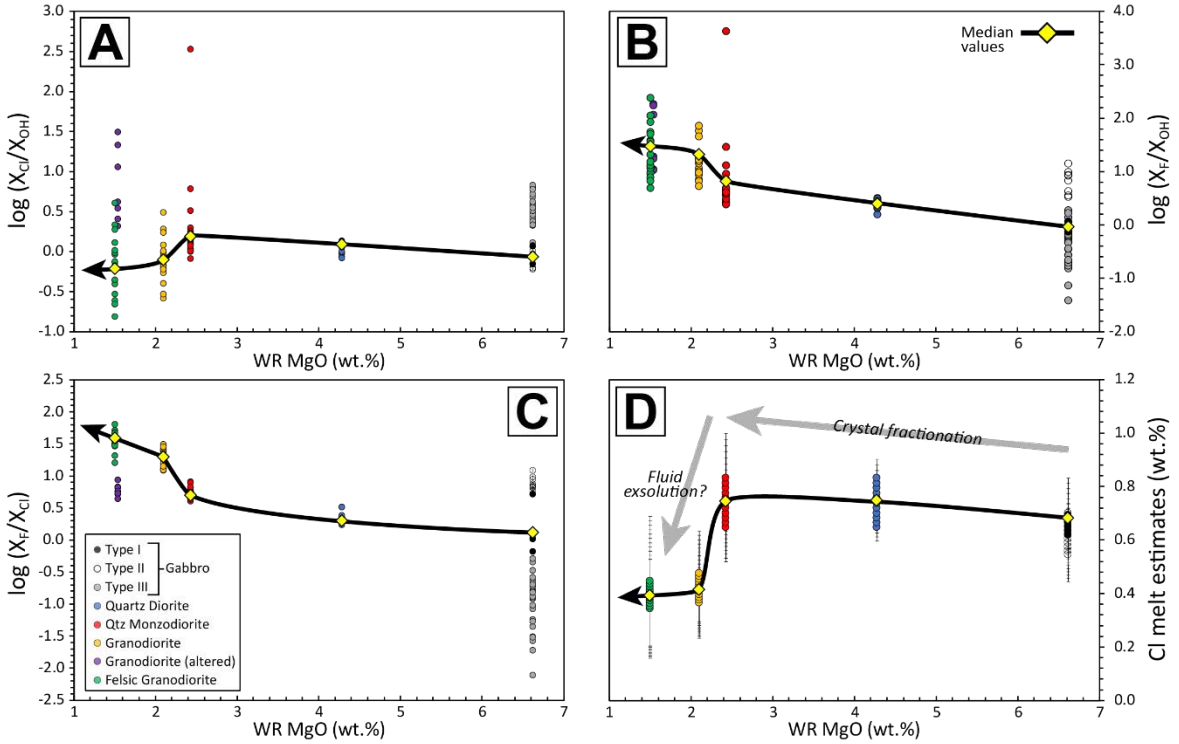

Figure 3-12 (A) – (C) Volatile systematics of TIC apatite as a function of magma evolution (whole rock MgO). Logarithmic ratios are used for illustrative purposes with X_{Cl}, X_F, and X_{OH} as molar proportions of TIC apatite. Yellow diamonds represent median values and curves are fitted by eye to highlight apparent trends. (D) Chlorine melt estimates from TIC apatite (see text for detailed explanation); error bars are given as 1 sigma.

The general behaviour of Cl and F in TIC apatite (for illustration purposes expressed as $\log(X_{Cl}/X_{OH})$, $\log(X_F/X_{OH})$, and $\log(X_F/X_{Cl})$, where X_A = molar fraction of volatile A) following TIC magma evolution is illustrated in Figure 3-12A-C. Figure 3-12A-B show that both Cl and F contents slightly increase from gabbro to quartz monzodiorite, but systematically diverge at around ~2.5 – 2 wt.% whole rock MgO (equivalent to ~62 - 65 wt.% SiO_2) into decreasing Cl and increasing F with further magma evolution.

An increase in F/Cl ratios in magmatic apatite is commonly inferred to relate to either decreasing temperature, (e.g. through a magmatic fractionation series), devolatilisation, or a combination of both (e.g. Piccoli and Candela, 2002). For the TIC, the observed volatile trends support a model based on close system fractional crystallisation from a fluid-undersaturated magma up to magma compositions of ~ 62 - 65 wt.% SiO_2. The decrease in Cl ($\log(X_{Cl}/X_{OH})$) at higher SiO_2 is inconsistent with closed system fractionation, and hence requires an additional process, which I suggest is fluid saturation and release of a volatile-rich fluid phase. Such a fluid phase would be expected to preferentially partition Cl and H_2O relative to F (Webster et al., 2009), and hence can explain the F enrichment and Cl depletion trend in apatite at the high SiO_2 rocks (Figure 3-12B).

Such a process has been previously suggested by Zhang et al. (2012) who studied the evolution of F and Cl using apatite, biotite and amphibole in the mafic Liujiawa pluton, China. The authors estimated constant Cl melt compositions over the major crystallisation interval, but recorded a significant decrease at near solidus temperatures (≤650 °C) as a result from fluid exsolution, whereas estimated melt F remained nearly constant over the entire interval and F was not lost to a fluid phase. Fluid loss (and/or degassing) of a magma will generally drive apatite compositions towards the F-rich apex (X_F > 0.8) of the F-Cl-OH ternary diagram and Cl-OH loss during degassing of silicate melts should develop apatite compositions on a path towards binary F-Cl or F-OH compositions before reaching endmember F-apatite (e.g. McCubbin et al., 2011). Both these observations are made for the evolution of TIC apatite (Figure 3-8), in particular for rocks crystallising close to or after presumed volatile exsolution (e.g. samples TKR-06 and TIC17-07) and support the interpretation that fluid exsolution occurred at around ~65 wt.% SiO_2.

3.6.5 Chlorine and fluorine concentration of the melt – Estimates from apatite

Chlorine concentrations of the melt can be estimated from measured chlorine compositions of apatite, assuming that apatite and melt were in equilibrium at the time of apatite crystallisation (e.g. Piccoli and Candela, 2002). Here, I utilize the recently calibrated thermodynamic apatite/melt chlorine partitioning model of Li and Hermann (2017) using the experimental partition coefficients from Webster et al. (2009) obtained at 200 MPa and ~900 °C. I argue that this temperature (and pressure) range is reasonable for TIC rocks, based on our observation that the majority of TIC apatite crystallised early within respective rocks, as indicated by their association with early magmatic phases such as pyroxene and Fe-Ti oxides.

In general, apatite/melt exchange equilibria are strongly temperature dependent and therefore the knowledge of the temperature at which apatite crystalised is important when considering magmatic volatile concentrations (e.g. Piccoli and Candela, 2002). The formulas and detailed reasoning behind our temperature choices are provided in Appendix 3-V, and I computed the Cl melt concentrations at temperature ranges of 950 – 850 °C for gabbro, 900 – 800 °C for quartz diorite and quartz monzodiorite, and 850 – 750 °C for the granodiorites, which are reasonable approximations based on the present mineral assemblages.

Our results (Figure 3-12D) indicate that melt Cl contents increase from TIC gabbro (median Cl_{melt} = ~0.69 ± 0.11) to quartz monzodiorite (median Cl_{melt} = ~0.86 ± 0.15 wt.%) and then significantly drop in more felsic granodiorites to ~0.42 ± 0.15 wt.% (TKR-06) and 0.39 ± 0.22 wt.% (TIC17-07). In comparison, TIC F melt contents estimated using the formula of (Webster et al., 2009) increase from ~0.05 wt.% in TIC gabbro (on the basis of F measured in Type I apatite) to ~0.27 wt.% in evolved granodiorites and follow the same trend as observed for F apatite composition shown in Figure 3-12C. These melt Cl and F contents fall well within the general range of halogen abundances measured in glasses and silicate melt inclusions in mafic to intermediate arc magmas of 0.01 – 0.85 wt.% Cl, and 0.01 – 0.5 wt.% F (Aiuppa et al., 2009 and references therein).

Interestingly, the observed drop in estimated Cl_{melt} coincides with changes in the bulk-rock geochemistry (e.g. “flare-up” of F composition, shift from e.g. increasing Ba and Zr to decreasing trends) at the inflection point at about ~65 wt.% bulk rock SiO_2 (see Figure 3-4). Since the calculation method depends on the input of temperature, the values presented here represent approximations, and I place little emphasis on small variations in calculations in Cl_{melt} between samples. Nevertheless, the overall observed TIC Cl and F trends remain, irrespective of uncertainties in crystallisation temperatures. Our observations are consistent with experimental studies which found Cl to generally partition in favour of fluid(s) > apatite > felsic melt, whereas F partitions in the order apatite > melt at conditions of 50-200 MPa and 900 °C (Mathez and Webster, 205; Webster et al., 2009; Doherty et al., 2014), and support our interpretation of the volatile evolution of the TIC in which apatite records a decrease in Cl and increase in F in a system controlled by fractional crystallisation to the likely point of fluid-saturation and fluid exsolution/degassing.

3.6.6 Sulfur concentrations in melt

Apatite from the TIC systematically show very low sulfur concentrations (<0.1 wt.% SO_3), with only apatite from the most evolved sample TIC17-07 having higher concentrations (~0.1 – 0.25 wt.% SO_3). The low S concentrations could either derive from: (i) low magmatic sulfur contents in the source region/coexisting melt or; (ii) fO_2 conditions at which the dominant sulfur species is S^{2-} (Jugo et al., 2010; Baker and Moretti, 2011), which cannot (or only to very limited amounts) enter the crystal structure of apatite (e.g. Parat et al., 2011; Konecke et al., 2017).

Partitioning for S between apatite and melt is expected to be strongly temperature dependent (Peng et al. (1997), with S concentrations in apatite tending to be lower compared to coexisting melt at higher temperatures (Carroll and Rutherford, 1987; Luhr, 1990; Webster and Botcharnikov, 2011). As shown by Figure 3-8F, most sulfur analyses are below the limit of detection and there is no existing clear trend from mafic to more mafic granodiorite varieties. However, there also is a clear measurable increase from the granodiorite sample TKR-06 towards the felsic, and most evolved granodiorite sample TIC17-07 (at presumably lower melt temperature). Following the above considerations, the overall increase might be expected from apatite crystallising from a 'cooler' magma from intermediate towards more felsic rock compositions.

Despite the issues with low measured sulfur concentrations, I used the empirically calibrated non-Henrian partitioning relationship for sulfur between apatite/melt of Parat et al. (2011), derived from a set of natural and experimental apatite/melt partitioning data for andesitic to rhyolitic melts:

$$S_{apatite}\ (wt.\%) = 0.0629 \times \ln S_{melt}\ (wt.\%) + 0.4513 \qquad (7)$$

This largely results in estimated TIC melt sulfur concentrations of <30 ppm, which is well below expected S contents of arc basalts of >300 ppm (Wallace, 2005). Only apatite from sample TIC17-07 returned a large scatter in calculated S_{melt} ~8 – 350 ppm (average ~100 ppm). In any case, these concentrations lie well within the limits of the Eq (7), which is constrained to <0.1 wt.% S_{melt}.

However, assuming that almost all sulfur measured in apatite is present as S^{6+}, our results should only represent a minimum estimate for the melt S content, since at upper crustal pressure and fO_2 ranging between NNO +1 and NNO +2, reduced sulfur will also be present in the melt (Jugo et al., 2010; Baker and Moretti, 2011; Matjuschkin et al., 2016).

The possibility that S has been lost to early sulfide saturation in the TIC suite – in which case Cu and other metals would expected to be depleted due to precipitation of sulfide - may be an additional reason for the low overall S contents in melt and apatite. If this is the case, I expect sulfide saturation to have occurred prior to the crystallisation of TIC gabbro, as there are no early sulfides in any of our samples; indeed sulfide was only reported in miarolitic cavities in late aplites (Blevin and Morrison, 1997). Very early sulfide segregation from the magmatic system would be expected to deplete the melt of Cu and other chalcophile elements, and would also be consistent with whole rock Cu contents within the TIC suite of between 20 – 50 ppm, which falls to the lower end of Cu contents (50 – 90 ppm) of primitive to intermediate arc magmas (Lee et al., 2012).

The slight, but measurable increase in apatite S contents in granodiorite, in particular sample TIC17-07 (Figure 3-8F), indicates relative changes in melt fO_2 at the time of crystallisation, resulting in the presence of more oxidised S. This change, however, is expected to be relatively subtle, as fO_2 indicators based on Fe_2O_3/FeO (Figure 3-9) do not show a significant change across the range of our TIC samples. A change in melt oxidation could have occurred through loss of S species (such as H_2S) and H_2 driven by degassing or diffusion (e.g. Christie and Carmichael, 1986) or exsolution of Cl-bearing aqueous volatiles, which has been suggested to drive magmatic oxidation by mobilising Fe^{2+} from the melt, and thereby increasing fO_2 conditions (Bell and Simon, 2011). Consequently, a combination of hydrogen-based self-oxidation processes, complemented by exsolution of a Cl-rich volatile phase may explain the progressively increasing appearance of relatively more oxidised S in apatite (and the melt), and might explain why apatite from samples that crystallised earlier than TIC granodiorite, presumably prior to exsolution of a Cl-rich phase and lower magmatic H_2O, have S contents systematically below the limit of detection.

3.6.7 Fluorine and chlorine distribution between apatite and biotite

Investigations on the direct partitioning of halogens between biotite and melt are limited (Icenhower and London, 1997), but quantitative calibration of halogen partitioning in the biotite-vapor space have been extensively investigated, and biotite has therefore long been utilised and incorporated into investigations on volatile evolution in magmas and magmatic-hydrothermal systems (e.g. Munoz, 1984; Zhu and Sverjensky, 1991, 1992; Icenhower and London, 1997; Coulson et al., 2001; Zhang et al., 2012; Bao et al., 2016). For the scope of this study, I qualitatively compare TIC apatite and biotite F and Cl contents on the basis of their F-Cl evolution as function of magma differentiation (Figure 3-13A-B), similar to the approach presented by e.g. Teiber et al. (2014).

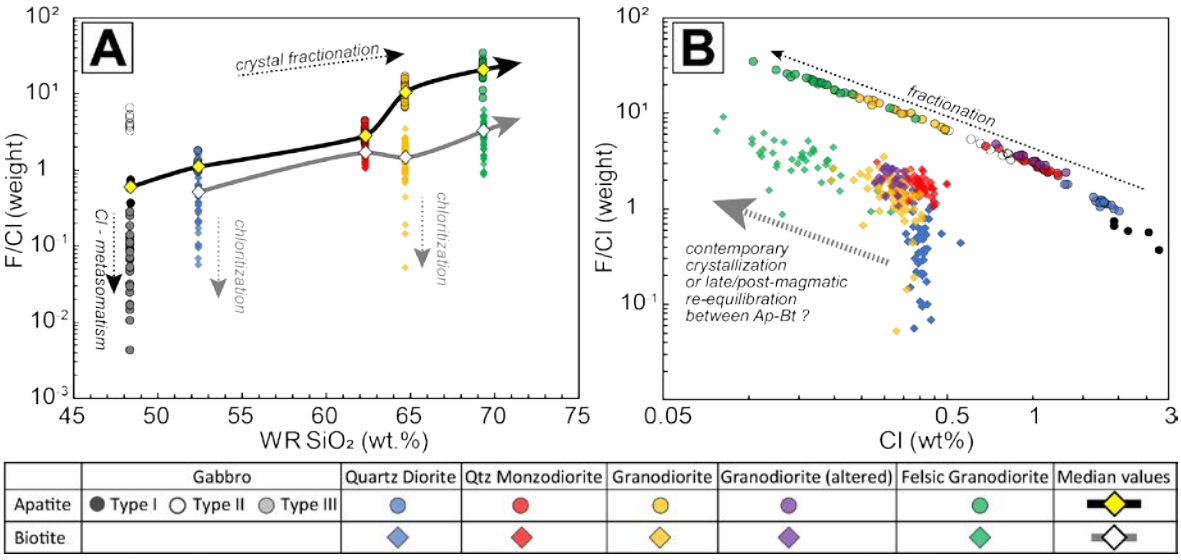

Figure 3-13 (A) and (B) Fluorine and chlorine distribution between apatite and biotite as a function of magma differentiation.

Biotite is absent in TIC gabbro, but is present as a late magmatic phase in the quartz diorite, monzodiorite and mafic granodiorite, and as a relatively early magmatic phase together with amphibole in the felsic granodiorite. F/Cl ratios are generally lower in biotite compared to apatite (Figure 3-12), but F/Cl trends of apatite and biotite characterised by decreasing Cl with relatively stable F contents are broadly parallel over the course of differentiation (Figures 3-7; 3-8; and 3-13). These observed trends of F and Cl between apatite and biotite are consistent with what is to be the expected halogen distribution between these two minerals, whereby apatite preferentially has higher F/Cl compared to coexisting biotite (e.g. Volfinger et al., 1985; Leger et al., 1996; Zhang et al., 2012; Teiber et al., 2014; 2015).

3.6.8 Implications for metallogeny

Halogens can control the speciation and solubilities of ore metals in magmatic vapours, aqueous fluids and hydrosaline brines, and can therefore have a significant impact on the ore-forming potential/fertility of a magmatic system (e.g. reviews in Aiuppa et al., 2009; Lecumberri-Sanchez et al., 2018). The behaviour of chlorine is of particular interest, since it is commonly available in abundance and known for its efficiency in complexing with ore metals making it an important transporting ligand in magmatic-hydrothermal systems. Although, the role of F may be less important compared to Cl in porphyry-epithermal environments, it is known to be an important metal-transporting ligand in mineralising fluids often associated with significant REE mineralisation (e.g. reviews in Aiuppa et al., 2009; Lecumberri-Sanchez et al., 2018). The significance of sulfur is without question, since it precipitates the transported metals as ore minerals in most magmatic-hydrothermal style deposits. However, this requires the abundant presence of S^{2-}, thus the behaviour of S is highly dependent on the oxidation state of the magma and hydrothermal fluid (e.g. Richards, 2015 and references therein).

Considering the above, the ability to track volatile evolution within magmatic suites, such as the TIC, is undoubtedly useful for understanding the spatial distribution of ore deposits within a province known to be fertile for porphyry-style Au-Cu mineralisation. The TIC itself can be considered barren of mineralisation (Beams, 1994; Blevin and Morrison, 1997), but economical grade porphyry-style Au deposits lie in close proximity to the TIC (e.g. Mount Leyshon, Mt. Wright, Figure 3-1B). These deposits are hosted by magmatic systems with very close genetic and temporal relationships to the TIC. The question remains if the TIC itself was capable of exsolving a metal-rich fluid that may have mineralised a potentially connected (but now eroded) volcanic system.

Based on our results, I suggest that exsolution of a Cl-rich fluid occurred at the transition from intermediate to more evolved felsic compositions. In addition, the presence of significantly Cl-enriched metasomatic apatite in TIC gabbro, and their occasional (but very minor) occurrence in the other investigated samples, indicates the interaction of a Cl-rich fluid at some stage after igneous formation of the TIC. The composition of this fluid would broadly be consistent with the fluid released during magmatic differentiation, although in this case the source of the altering fluid may be from a cogenetic crystallising body at depth, rather than the TIC itself.

The metal budget of the TIC could be considered relatively low with regards to Cu contents with few exceptions of ≥ 40 ppm. This alone however, is not a sufficient reason to be incapable of forming an ore deposit, since Cline and Bodnar (1991), Cline (1995), and most recently Chiaradia and Caricchi (2017) demonstrated that an average arc andesite containing 50 ppm Cu is capable to form an economical grade porphyry Cu deposit. The question at what potential becomes actual ore formation in arc magmas has been reviewed by Richards (2015) with regards to oxidation state, sulfur and Cu contents, and emphasizes the interplay of H_2O, S, and fO_2.

Considering these three factors for the TIC with regards to ore forming potential, I can derive three fairly simple conclusions for the ore forming potential of the TIC:

1. At the point of suggested fluid exsolution (~65 wt.% SiO_2) abundant magmatic H_2O must have been present (≥4 wt.%, Ridolfi et al., 2010) to stabilize hornblende and biotite, therefore the TIC magmas at this point should have had the capability of exsolving an aqueous fluid.
2. Sulfur contents measured from apatite are generally low, but measurably increase in rocks formed at the time or after the magma achieved fluid saturation (and exsolution of a fluid phase). This may be an indicator of a slight increase in the oxidation state of the melt, which serves to increase the abundance of S^{6+} that can enter the apatite crystal structure, (e.g. Konecke et al., 2017). Under moderately oxidising conditions it seems reasonable that S was abundantly present as S^{4+} and therefore may have degassed as SO_2. Although I cannot exclude the presence of S^{2-}, there is no evidence for sulfide precipitation within TIC rocks at this stage, but it remains speculation if low bulk-rock Cu concentrations were caused by early sulfide precipitation (and early removal of metals), or is a result of Cu complexing with Cl during the exsolution of a Cl-rich fluid phase.
3. The TIC broadly falls on the moderately to strongly oxidised boundary (Figure 3-9). In general, the TIC records relatively consistent fO_2 with progressive magmatic differentiation, but a slight shift in fO_2 may be indicated by the shift from magnetite-ilmenite to magnetite-only, presumably increasing magmatic H_2O contents, and as mentioned above, an increase in apatite S compositions. However, Figure 3-9 also shows that TIC

magmas are less oxidised compared to other Permocarboniferous granitoids of north Queensland directly associated with economic grade porphyry deposits, and therefore might not have been capable of retaining their ore metal budget.

In summary, the TIC shows petrogenetic evidence for increasing water contents, and thereby the ability to saturate in volatiles during magmatic differentiation and produce a Cl-rich fluid capable of carrying metals. However, it remains unclear if the TIC did form economic scale mineralisation. The magma appears to have not been oxidised enough across the course of differentiation A mineralisation-fertile system would be expected to show evidence of fluid loss (as shown here with Cl and F trends), but also have elevated S in apatite and elevated bulk rock Cu contents up to the point of volatile saturation, broadly indicating more oxidised magmas. Our results underline the great potential use of apatite halogen and S compositions to track magma fertility, but more information is needed on how these components are incorporated into apatite and interact with or are influenced by other element activities over a range of magma compositions and conditions (P, T, fO_2).

3.7 Conclusion

The results of this study help to understand halogen behaviour in intrusive arc plutons, and may be helpful in differentiating ore-unproductive from ore-productive intrusions. The key findings include:

- The TIC records a progressive sequence of gabbro to granodiorite and minor late-stage aplites, which formed by closed-system fractional crystallisation from a H_2O undersaturated, moderately oxidised parental melt with TIC gabbro composition, to relatively hydrous felsic granodiorite, where amphibole and biotite progressively replace pyroxene as the major Fe-Mg silicate phase.
- Apatite is present in all TIC samples, and there is clear textural and geochemical evidence that the majority of apatite crystallised early. However, the presence of three apatite types in TIC gabbro demonstrates complexity to apatite crystallisation within the TIC, including evidence that selective hydrothermal alteration of apatite (Type III) occurred within this rock.
- Chlorine and F melt compositions calculated from apatite halogen geochemistry record increasing Cl and F contents with progressive magma differentiation up to granodiorite composition (~65 wt.% SiO_2), thereafter Cl contents steeply decrease, whereas F contents minimally increase or remain the same. This change is interpreted to reflect exsolution of a Cl-rich volatile phase.
- Increasing S contents in apatite with progressive fractionation indicate a minor shift in the magmas fO_2 to more oxidising conditions at the time of apatite crystallisation in felsic granodiorite. The nature and cause of these changes in the case of the TIC is not fully understood, but may be connected to the exsolution of a Cl-rich volatile phase. Overall, the TIC was seemingly not oxidised enough to prevent early sulfide segregation prior to TIC gabbro crystallisation, thereby likely removing the bulk ore metal contents and stripping the TIC of its ore-productive potential.

3.8 References

Aiuppa, A., Baker, D. R., & Webster, J. D. (2009). Halogens in volcanic systems. Chemical Geology, 263(1), 1-18. doi:https://doi.org/10.1016/j.chemgeo.2008.10.005

Bain, J. H. C., & Draper, J. J. (1997). North Queensland Geology. Bulletin of the Australian Geological Survey Organisation, 240, 1 – 600

Baker, D. R., & Moretti, R. (2011). Modelling the solubility of sulfur in magmas: a 50-year old geochemical challenge. Reviews in Mineralogy and Geochemistry, 73(1), 167-213.

Bao, B., Webster, J. D., Zhang, D.-H., Goldoff, B. A., & Zhang, R.-Z. (2016). Compositions of biotite, amphibole, apatite and silicate melt inclusions from the Tongchang mine, Dexing porphyry deposit, SE China: Implications for the behavior of halogens in mineralised porphyry systems. Ore Geology Reviews, 79, 443-462. doi:https://doi.org/10.1016/j.oregeorev.2016.05.024

Beams, S. D. (1994). Geology and Petrography of the Permian Tuckers Igneous Complex, Ravenswood Block, North Queensland. Report (unpublished). AMIRA P425: Magmatic and hydrothermal evolution of intrusive related gold deposits, AMIRA, Melbourne, 130 pp.

Bell, A. S., & Simon, A. C. (2011). Experimental evidence for the alteration of the Fe3+/ΣFe of silicate melt caused by the degassing of chlorine-bearing aqueous volatiles. Geology, 39(5), 499-502. doi:10.1130/G31828.1

Belousova, E., Griffin, W., O'Reilly, S. Y., & Fisher, N. (2002). Apatite as an indicator mineral for mineral exploration: trace-element compositions and their relationship to host rock type. Journal of Geochemical Exploration, 76(1), 45-69.

Blevin, P. L., Chappell, B. W., & Allen, C. M. (1996). Intrusive metallogenic provinces in eastern Australia based on granite source and composition. Geological Society of America Special Papers, 315, 281-290. doi:10.1130/0-8137-2315-9.281

Blevin, P., & Morrison, G. (2001). A zoned magma chamber model for the production of Au–lithophile mineralisation in subvolcanic felsic igneous systems. Paper presented at the A hydrothermal Odyssey. Extended Conference Abstracts EGRU Contribution.

Blevin, P. L. (2004). Redox and compositional parameters for interpreting the granitoid metallogeny of eastern Australia: Implications for gold-rich ore systems. Resource Geology, 54(3), 241-252.

Bouzari, F., Hart, C. J., Bissig, T., & Barker, S. (2016). Hydrothermal alteration revealed by apatite luminescence and chemistry: a potential indicator mineral for exploring covered porphyry copper deposits. Economic Geology, 111(6), 1397-1410.

Boyce, J. W., & Hervig, R. L. (2008). Apatite as a monitor of late-stage magmatic processes at Volcán Irazú, Costa Rica. Contributions to Mineralogy and Petrology, 157(2), 135. doi:10.1007/s00410-008-0325-x

Brenan, J. (1993). Kinetics of fluorine, chlorine and hydroxyl exchange in fluorapatite. Chemical Geology, 110(1), 195-210. doi:https://doi.org/10.1016/0009-2541(93)90254-G

Brugge, E., Wilkinson, J. J., & Miles, A. (2017). Fingerprinting fertile porphyry magmas using apatite. Applied Earth Science, 126(2), 46-47. doi:10.1080/03717453.2017.1306236

Candela, P. A., & Holland, H. D. (1984). The partitioning of copper and molybdenum between silicate melts and aqueous fluids. Geochimica et Cosmochimica Acta, 48(2), 373-380.

Carroll, M. R., & Rutherford, M. J. (1987). The stability of igneous anhydrite: experimental results and implications for sulfur behavior in the 1982 El Chichon trachyandesite and other evolved magmas. Journal of Petrology, 28(5), 781-801.

Chambefort, I., Dilles, J. H., & Longo, A. A. (2013). Amphibole Geochemistry of the Yanacocha Volcanics, Peru: Evidence for Diverse Sources of Magmatic Volatiles Related to Gold Ores. Journal of Petrology, 54(5), 1017-1046. doi:10.1093/petrology/egt004

Champion, D. C., & Bultitude, R. J. (2013). Chapter 6 - Kennedy Igneous Association. In P. A. Jell (Ed.), Geology of Queensland (pp. 473-514): Geological Survey of Queensland, Brisbane.

Chelle-Michou, C., & Chiaradia, M. (2017). Amphibole and apatite insights into the evolution and mass balance of Cl and S in magmas associated with porphyry copper deposits. Contributions to Mineralogy and Petrology, 172(11), 105. doi:10.1007/s00410-017-1417-2

Chiaradia, M., & Caricchi, L. (2017). Stochastic modelling of deep magmatic controls on porphyry copper deposit endowment. Scientific Reports, 7, 44523.

Christie, D. M., Carmichael, I. S. E., & Langmuir, C. H. (1986). Oxidation states of mid-ocean ridge basalt glasses. Earth and Planetary Science Letters, 79(3), 397-411. doi:https://doi.org/10.1016/0012-821X(86)90195-0

Clark, D. A., & Lackie, M. A. (2003). Palaeomagnetism of the Early Permian Mount Leyshon Intrusive Complex and Tuckers Igneous Complex, North Queensland, Australia. Geophysical Journal International, 153(3), 523-547. doi:10.1046/j.1365-246X.2003.01907.x

Cline, J. S., & Bodnar, R. J. (1991). Can economic porphyry copper mineralisation be generated by a typical calc-alkaline melt? Journal of Geophysical Research: Solid Earth, 96(B5), 8113-8126.

Cline, J. S. (1995). Genesis of porphyry copper deposits: The behavior of water, chloride, and copper in crystallising melts. Arizona Geol. Soc. Dig., 20, 69-82.

Coulson, I. M., Dipple, G. M., & Raudsepp, M. (2001). Evolution of HF and HCl activity in magmatic volatiles of the gold-mineralised Emerald Lake pluton, Yukon Territory, Canada. Mineralium Deposita, 36(6), 594-606. doi:10.1007/s001260100191

Davidson, J., Turner, S., Handley, H., Macpherson, C., & Dosseto, A. (2007). Amphibole "sponge" in arc crust? Geology, 35(9), 787-790. doi:10.1130/g23637a.1

Deer, W. A., Howie, R. A., & Zussman, J. (2013). An introduction to the rock-forming minerals: Mineralogical Society. In: London.

Doherty, A. L., Webster, J. D., Goldoff, B. A., & Piccoli, P. M. (2014). Partitioning behavior of chlorine and fluorine in felsic melt–fluid(s)–apatite systems at 50 MPa and 850–950°C. Chemical Geology, 384, 94-111. doi:https://doi.org/10.1016/j.chemgeo.2014.06.023

Dolejš, D., & Zajacz, Z. (2018). Halogens in silicic magmas and their hydrothermal systems. In The Role of Halogens in Terrestrial and Extraterrestrial Geochemical Processes (pp. 431-543): Springer.

Duan, D.-F., & Jiang, S.-Y. (2018). Using apatite to discriminate synchronous ore-associated and barren granitoid rocks: A case study from the Edong metallogenic district, South China. Lithos, 310-311, 369-380. doi:https://doi.org/10.1016/j.lithos.2018.04.022

Fergusson, C. L., Henderson, R. A., Fanning, C. M., & Withnall, I. W. (2007a). Detrital zircon ages in Neoproterozoic to Ordovician siliciclastic rocks, northeastern Australia: implications for the tectonic history of the East Gondwana continental margin. Journal of the Geological Society, 164(1), 215.

Fergusson, C. L., Henderson, R. A., Withnall, I. W., Fanning, C. M., Phillips, D., & Lewthwaite, K. J. (2007b). Structural, metamorphic, and geochronological constraints on alternating compression and extension in the Early Paleozoic Gondwanan Pacific margin, northeastern Australia. Tectonics, 26(3). doi:10.1029/2006TC001979

Fergusson, C. L., & Henderson, R. A. (2013). Chapter 3 Thomson Orogen. In P. A. Jell (Ed.), Geology of Queensland (pp. 113 - 224). Brisbane: Geological Survey of Queensland.

Fricker, M. B., Kutscher, D., Aeschlimann, B., Frommer, J., Dietiker, R., Bettmer, J., & Günther, D. (2011). High spatial resolution trace element analysis by LA-ICP-MS using a novel ablation cell for multiple or large samples. International Journal of Mass Spectrometry, 307(1-3), 39-45.

Frost, B., & Lindsley, D. H. (1991). Occurrence of iron-titanium oxides in igneous rocks. Reviews in Mineralogy and Geochemistry, 25(1), 433-468.

Goldoff, B., Webster, J. D., & Harlov, D. E. (2012). Characterisation of fluor-chlorapatites by electron probe microanalysis with a focus on time-dependent intensity variation of halogens. American Mineralogist, 97(7), 1103-1115. doi:10.2138/am.2012.3812

Guillong, M., Meier, D. L., Allan, M. M., Heinrich, C. A., & Yardley, B. W. (2008). Appendix A6: SILLS: A MATLAB-based program for the reduction of laser ablation ICP-MS data of homogeneous materials and inclusions. Mineralogical Association of Canada Short Course, 40, 328-333.

Harlov, D. E., & Aranovich, L. (2018). The role of halogens in terrestrial and extraterrestrial geochemical processes: surface, crust, and mantle. In The Role of Halogens in Terrestrial and Extraterrestrial Geochemical Processes (pp. 1-19): Springer.

Harlov, D. E. (2015). Apatite: A Fingerprint for Metasomatic Processes. Elements, 11(3), 171-176. doi:10.2113/gselements.11.3.171

Harrison, T. M., & Watson, E. B. (1984). The behavior of apatite during crustal anatexis: equilibrium and kinetic considerations. Geochimica et Cosmochimica Acta, 48(7), 1467-1477.

Hughes, J. M., & Rakovan, J. F. (2015). Structurally Robust, Chemically Diverse: Apatite and Apatite Supergroup Minerals. Elements, 11(3), 165-170. doi:10.2113/gselements.11.3.165

Hutton, L. J., Rienks, I. P., Tenison-Woods, K. L., Hartley, J. S., & Crouch, S. B. S. (1994). Geology of the Ravenswood Batholith, north Queensland. Queensland Geological Record 1994/4, 124.

Icenhower, J. P., & London, D. (1997). Partitioning of fluorine and chlorine between biotite and granitic melt: experimental calibration at 200 MPa H2O. Contributions to Mineralogy and Petrology, 127(1), 17-29. doi:10.1007/s004100050262

Jugo, P. J., Wilke, M., & Botcharnikov, R. E. (2010). Sulfur K-edge XANES analysis of natural and synthetic basaltic glasses: Implications for S speciation and S content as function of oxygen fugacity. Geochimica et Cosmochimica Acta, 74(20), 5926-5938.

Konecke, B. A., Fiege, A., Simon, A. C., Parat, F., & Stechern, A. (2017). Co-variability of S6+, S4+, and S2− in apatite as a function of oxidation state: Implications for a new oxybarometer. American Mineralogist, 102(3), 548-557.

Kouzmanov, K., & Pokrovski, G. S. (2012). Hydrothermal controls on metal distribution in porphyry Cu (-Mo-Au) systems.

Kreuzer, O., Blenkinsop, T. G., Morrison, R., & Peters, S. (2007). Ore controls in the Charters Towers goldfield, NE Australia: Constraints from geological, geophysical and numerical analyses. Ore Geology Reviews, 32(1-2), 37-80.

Leake, B. E., Woolley, A. R., Arps, C. E., Birch, W. D., Gilbert, M. C., Grice, J. D., . . . Krivovichev, V. G. (1997). Report. Nomenclature of amphiboles: report of the subcommittee on amphiboles of the international mineralogical association commission on new minerals and mineral names. Mineralogical magazine, 61(2), 295-321.

Lecumberri-Sanchez, P., & Bodnar, R. J. (2018). Halogen geochemistry of ore deposits: contributions towards understanding sources and processes. In The Role of Halogens in Terrestrial and Extraterrestrial Geochemical Processes (pp. 261-305): Springer

Lee, C.-T. A., Luffi, P., Chin, E. J., Bouchet, R., Dasgupta, R., Morton, D. M., . . . Jin, D. (2012). Copper Systematics in Arc Magmas and Implications for Crust-Mantle Differentiation. Science, 336(6077), 64-68. doi:10.1126/science.1217313

Leger, A., Rebbert, C., & Webster, J. (1996). Cl-rich biotite and amphibole from Black Rock forest, Cornwall, New York. In: Mineralogical Society of America.

Lindsley, D. H. (1983). Pyroxene thermometry. American Mineralogist, 68(5-6), 477-493.

Liu, Y., & Comodi, P. (1993). Some aspects of the crystal-chemistry of apatites. Mineralogical magazine, 57(389), 709-720.

Locock, A. J. (2014). An Excel spreadsheet to classify chemical analyses of amphiboles following the IMA 2012 recommendations. Computers & Geosciences, 62, 1-11. doi:https://doi.org/10.1016/j.cageo.2013.09.011

Luhr, J. F. (1990). Experimental phase relations of water-and sulfur-saturated arc magmas and the 1982 eruptions of El Chichón volcano. Journal of Petrology, 31(5), 1071-1114.

Mackenzie, D. E., & Wellman, P. (1997). Kennedy Province. In J. H. C. Bain & J. J. Draper (Eds.), Bulletin of the Australian Geological Survey Organisation (Vol. 240, pp. 488 - 500).

Mao, M., Rukhlov, A. S., Rowins, S. M., Spence, J., & Coogan, L. A. (2016). Apatite Trace Element Compositions: A Robust New Tool for Mineral Exploration. Economic Geology, 111(5), 1187-1222. doi:10.2113/econgeo.111.5.1187

Marks, M. A. W., Wenzel, T., Whitehouse, M. J., Loose, M., Zack, T., Barth, M., . . . Markl, G. (2012). The volatile inventory (F, Cl, Br, S, C) of magmatic apatite: An integrated analytical approach. Chemical Geology, 291, 241-255. doi:https://doi.org/10.1016/j.chemgeo.2011.10.026

Mathez, E. A., & Webster, J. D. (2005). Partitioning behavior of chlorine and fluorine in the system apatite-silicate melt-fluid. Geochimica et Cosmochimica Acta, 69(5), 1275-1286. doi:https://doi.org/10.1016/j.gca.2004.08.035

Matjuschkin, V., Blundy, J. D., & Brooker, R. A. (2016). The effect of pressure on sulfur speciation in mid-to deep-crustal arc magmas and implications for the formation of porphyry copper deposits. Contributions to Mineralogy and Petrology, 171(7), 66.

McCubbin, F. M., Jolliff, B. L., Nekvasil, H., Carpenter, P. K., Zeigler, R. A., Steele, A., . . . Lindsley, D. H. (2011). Fluorine and chlorine abundances in lunar apatite: Implications for heterogeneous distributions of magmatic volatiles in the lunar interior. Geochimica et Cosmochimica Acta, 75(17), 5073-5093. doi:https://doi.org/10.1016/j.gca.2011.06.017

McCubbin, F. M., Vander Kaaden, K. E., Tartese, R., Boyce, J. W., Mikhail, S., Whitson, E. S., . . . Hauri, E. H. (2015). Experimental investigation of F, Cl, and OH partitioning between apatite and Fe-rich basaltic melt at 1.0–1.2 GPa and 950–1000 °C†. American Mineralogist, 100(8-9), 1790-1802. doi:10.2138/am-2015-5233

McDonough, W. F., & Sun, S. s. (1995). The composition of the Earth. Chemical Geology, 120(3), 223-253. doi:https://doi.org/10.1016/0009-2541(94)00140-4

Mi, J.-X., & Pan, Y. (2018). Halogen-rich minerals: crystal chemistry and geological significances. In The Role of Halogens in Terrestrial and Extraterrestrial Geochemical Processes (pp. 123-184): Springer.

Morimoto, N. (1988). Nomenclature of Pyroxenes. Mineralogy and Petrology, 39(1), 55-76. doi:10.1007/BF01226262

Morrison, G. W. (1988). Palaeozoic gold deposits of northeastern Queensland. In G. W. Morrison (Ed.), Epithermal and Porphyry Style Gold Deposits in North Queensland. Contribution of the Economic Geology Research Unit (Vol. 29, pp. 11-21). James Cook University.

Morrison, G. W., & Blevin, P. L. (2001). Magmatic and hydrothermal evolution and ore controls in the Mount Leyshon gold deposit. A hydrothermal Odyssey. Contribution of the Economic Geology Research Unit, 59, 146-147.

Munoz, J. L. (1984). F-OH and Cl-OH exchange in micas with applications to hydrothermal ore deposits. Reviews in Mineralogy and Geochemistry, 13(1), 469-493

Murgulov, V., O'Reilly, S. Y., Griffin, W. L., & Blevin, P. L. (2008). Magma sources and gold mineralisation in the Mount Leyshon and Tuckers Igneous Complexes, Queensland, Australia: U-Pb and Hf isotope evidence. Lithos, 101(3), 281-307. doi:https://doi.org/10.1016/j.lithos.2007.07.014

Pan, Y., & Fleet, M. E. (2002). Compositions of the apatite-group minerals: substitution mechanisms and controlling factors. Reviews in Mineralogy and Geochemistry, 48(1), 13-49.

Parat, F., Dungan, M. A., & Streck, M. J. (2002). Anhydrite, pyrrhotite, and sulfur-rich apatite: tracing the sulfur evolution of an Oligocene andesite (Eagle Mountain, CO, USA). Lithos, 64(3), 63-75. doi:https://doi.org/10.1016/S0024-4937(02)00155-X

Parat, F., Holtz, F., & Streck, M. J. (2011). Sulfur-bearing Magmatic Accessory Minerals. Reviews in Mineralogy and Geochemistry, 73(1), 285-314. doi:10.2138/rmg.2011.73.10

Paull, P. L., Hodkinson, I. P., Morrison, G. W., & Teale, G. S. (1990). Mount Leyshon gold deposit. Geology of the Mineral Deposits of Australia and Papua New Guinea, 14, 1471-1481.

Peccerillo, A., & Taylor, S. (1976). Geochemistry of Eocene calc-alkaline volcanic rocks from the Kastamonu area, northern Turkey. Contributions to Mineralogy and Petrology, 58(1), 63-81.

Peng, G., Luhr, J. F., & McGee, J. J. (1997). Factors controlling sulfur concentrations in volcanic apatite. American Mineralogist, 82(11-12), 1210-1224.

Perkins, C., & Kennedy, A. K. (1998). Permo-Carboniferous gold epoch of northeast Queensland. Australian Journal of Earth Sciences, 45(2), 185-200. doi:10.1080/08120099808728381

Piccoli, P., & Candela, P. (1994). Apatite in felsic rocks; a model for the estimation of initial halogen concentrations in the Bishop Tuff (Long Valley) and Tuolumne Intrusive Suite (Sierra Nevada Batholith) magmas. American Journal of Science, 294(1), 92-135.

Piccoli, P. M., & Candela, P. A. (2002). Apatite in Igneous Systems. Reviews in Mineralogy and Geochemistry, 48(1), 255-292. doi:10.2138/rmg.2002.48.6

Pokrovski, G. S., Kokh, M. A., Guillaume, D., Borisova, A. Y., Gisquet, P., Hazemann, J.-L., . . . Dubessy, J. (2015). Sulfur radical species form gold deposits on Earth. Proceedings of the National Academy of Sciences, 112(44), 13484-13489. doi:10.1073/pnas.1506378112

Pyle, D., & Mather, T. (2009). Halogens in igneous processes and their fluxes to the atmosphere and oceans from volcanic activity: a review. Chemical Geology, 263(1-4), 110-121.

Richards, J. P. (2015). The oxidation state, and sulfur and Cu contents of arc magmas: implications for metallogeny. Lithos, 233, 27-45. doi:https://doi.org/10.1016/j.lithos.2014.12.011

Richards, J. P., López, G. P., Zhu, J.-J., Creaser, R. A., Locock, A. J., & Mumin, A. H. (2017). Contrasting Tectonic Settings and Sulfur Contents of Magmas Associated with Cretaceous Porphyry Cu±Mo±Au and Intrusion-Related Iron Oxide Cu-Au Deposits in Northern Chile. Economic Geology, 112(2), 295-318.

Ridolfi, F., Renzulli, A., & Puerini, M. (2010). Stability and chemical equilibrium of amphibole in calc-alkaline magmas: an overview, new thermobarometric formulations and application to subduction-related volcanoes. Contributions to Mineralogy and Petrology, 160(1), 45-66. doi:10.1007/s00410-009-0465-7

Ridolfi, F., & Renzulli, A. (2012). Calcic amphiboles in calc-alkaline and alkaline magmas: thermobarometric and chemometric empirical equations valid up to 1,130°C and 2.2 GPa. Contributions to Mineralogy and Petrology, 163(5), 877-895. doi:10.1007/s00410-011-0704-6

Rieder, M., Cavazzini, G., D'yakonov, Y. S., Frank-Kamenetskii, V. A., Gottardi, G., Guggenheim, S., . . . Radoslovich, E. W. (1998). Nomenclature of the micas. Clays and clay minerals, 46(5), 586-595.

Rienks, I. P. (1997). Overview - late Paleozoic igneous rocks. In J. H. C. Bain & J. J. Draper (Eds.), Bulletin of the Australian Geological Survey Organisation (Vol. 240, pp. 184 - 186).

Rouse, R. C., & Dunn, P. J. (1982). A contribution to the crystal chemistry of ellestadite and the silicate sulfate apatites. American Mineralogist, 67(1-2), 90-96.

Scott, J. A. J., Humphreys, M. C. S., Mather, T. A., Pyle, D. M., & Stock, M. J. (2015). Insights into the behaviour of S, F, and Cl at Santiaguito Volcano, Guatemala, from apatite and glass. Lithos, 232, 375-394. doi:https://doi.org/10.1016/j.lithos.2015.07.004

Sha, L.-K., & Chappell, B. W. (1999). Apatite chemical composition, determined by electron microprobe and laser-ablation inductively coupled plasma mass spectrometry, as a probe into granite petrogenesis. Geochimica et Cosmochimica Acta, 63(22), 3861-3881.

Sillitoe, R. H. (2010). Porphyry copper systems. Economic Geology, 105(1), 3-41.

Spandler, C., Pettke, T., & Rubatto, D. (2011). Internal and External Fluid Sources for Eclogite-facies Veins in the Monviso Meta-ophiolite, Western Alps: Implications for Fluid Flow in Subduction Zones. Journal of Petrology, 52(6), 1207-1236. doi:10.1093/petrology/egr025

Stock, M. J., Humphreys, M. C. S., Smith, V., C., Johnson, R. D., Pyle, D. M., & EIMF. (2015). New constraints on electron-beam induced halogen migration in apatite†. American Mineralogist, 100(1), 281-293. doi:10.2138/am-2015-4949

Stormer, J., Pierson, M. L., & Tacker, R. C. (1993). Variation of F and Cl X-ray intensity due to anisotropic diffusion in apatite. American Mineralogist, 78, 641-648.

Tatsumi, Y., & Eggins, S. (1995). Subduction zone magmatism (Vol. 1): Wiley.

Tattitch, B. C., & Blundy, J. D. (2017). Cu-Mo partitioning between felsic melts and saline-aqueous fluids as a function of XNaCleq, fO2, and fS2. American Mineralogist, 102(10), 1987-2006.

Teiber, H., Marks, M. A. W., Wenzel, T., Siebel, W., Altherr, R., & Markl, G. (2014). The distribution of halogens (F, Cl, Br) in granitoid rocks. Chemical Geology, 374-375, 92-109. doi:https://doi.org/10.1016/j.chemgeo.2014.03.006

Teiber, H., Scharrer, M., Marks, M. A. W., Arzamastsev, A. A., Wenzel, T., & Markl, G. (2015). Equilibrium partitioning and subsequent re-distribution of halogens among apatite–biotite–amphibole assemblages from mantle-derived plutonic rocks: Complexities revealed. Lithos, 220-223, 221-237. doi:https://doi.org/10.1016/j.lithos.2015.02.015

Tepper, J. H., & Kuehner, S. M. (1999). Complex zoning in apatite from the Idaho batholith: A record of magma mixing and intracrystalline trace element diffusion. American Mineralogist, 84(4), 581-595.

Volfinger, M., Robert, J.-L., Vielzeuf, D., & Neiva, A. (1985). Structural control of the chlorine content of OH-bearing silicates (micas and amphiboles). Geochimica et Cosmochimica Acta, 49(1), 37-48.

Wallace, P. J. (2005). Volatiles in subduction zone magmas: concentrations and fluxes based on melt inclusion and volcanic gas data. Journal of Volcanology and Geothermal Research, 140(1-3), 217-240.

Wang, L.-X., Marks, M. A., Wenzel, T., & Markl, G. (2016). Halogen-bearing Minerals from the Tamazeght Complex (Morocco): Constraints On Halogen Distribution and Evolution in Alkaline To Peralkaline Magmatic Systems. The Canadian Mineralogist, 54(6), 1347-1368.

Waychunas, G. A. (2002). Apatite Luminescence. Reviews in Mineralogy and Geochemistry, 48(1), 701-742. doi:10.2138/rmg.2002.48.19

Webster, J. D., Tappen, C. M., & Mandeville, C. W. (2009a). Partitioning behavior of chlorine and fluorine in the system apatite–melt–fluid. II: Felsic silicate systems at 200MPa. Geochimica et Cosmochimica Acta, 73(3), 559-581. doi:https://doi.org/10.1016/j.gca.2008.10.034

Webster, J. D., & Botcharnikov, R. E. (2011). Distribution of sulfur between melt and fluid in SOHC-Cl-bearing magmatic systems at shallow crustal pressures and temperatures. Reviews in Mineralogy and Geochemistry, 73(1), 247-283.

Webster, J. D., & Piccoli, P. M. (2015). Magmatic Apatite: A Powerful, Yet Deceptive, Mineral. Elements, 11(3), 177-182. doi:10.2113/gselements.11.3.177

Webster, J. D., Baker, D. R., & Aiuppa, A. (2018). Halogens in mafic and intermediate-silica content magmas. In The Role of Halogens in Terrestrial and Extraterrestrial Geochemical Processes (pp. 307-430): Springer.

Withnall, I. W., & Hutton, L. J. (1997). Cape River Province. In J. H. C. Bain & J. J. Draper (Eds.), Bulletin of the Australian Geological Survey Organisation (Vol. 240, pp. 459 - 462).

Withnall, I. W., & Henderson, R. A. (2012). Accretion on the long-lived continental margin of northeastern Australia. Episodes-Newsmagazine of the International Union of Geological Sciences, 35(1), 166.

Zhang, C., Holtz, F., Ma, C., Wolff, P. E., & Li, X. (2012). Tracing the evolution and distribution of F and Cl in plutonic systems from volatile-bearing minerals: a case study from the Liujiawa pluton (Dabie orogen, China). Contributions to Mineralogy and Petrology, 164(5), 859-879. doi:10.1007/s00410-012-0778-9

Zhang, W., Lentz, D. R., Thorne, K. G., & McFarlane, C. (2016). Geochemical characteristics of biotite from felsic intrusive rocks around the Sisson Brook W–Mo–Cu deposit, west-central New Brunswick: An indicator of halogen and oxygen fugacity of magmatic systems. Ore Geology Reviews, 77, 82-96. doi:https://doi.org/10.1016/j.oregeorev.2016.02.004

Zhu, C., & Sverjensky, D. A. (1991). Partitioning of F-Cl-OH between minerals and hydrothermal fluids. Geochimica et Cosmochimica Acta, 55(7), 1837-1858. doi:https://doi.org/10.1016/0016-7037(91)90028-4

Zhu, C., & Sverjensky, D. A. (1992). F-Cl-OH partitioning between biotite and apatite. Geochimica et Cosmochimica Acta, 56(9), 3435-3467. doi:https://doi.org/10.1016/0016-7037(92)90390-5

Zhu, J.-J., Richards, J. P., Rees, C., Creaser, R., DuFrane, S. A., Locock, A., Petrus, J.A., and Lang, J. (2018). Elevated Magmatic Sulfur and Chlorine Contents in Ore-Forming Magmas at the Red Chris Porphyry Cu-Au Deposit, Northern British Columbia, Canada. Economic Geology, 113(5), 1047-1075.

Chapter 4

Concluding Summary

Based on the comparison of geochemical and petrographic data from an Early Permian volcanic suite of north-eastern Australia in Chapter 2, I assess cryptic fractionation processes involved in generating the volcanic rocks suites, and the use of geochemical proxies as indicators (fertile-barren distinction) for porphyry epithermal Cu-Au mineralisation. The general conclusions are that the generation of the "fertile" volcanic sequence associated with, and hosting, the high-sulfidation epithermal Au-Cu-Ag Mount Carlton deposit involved the fractionation of amphibole (±clinopyroxene) from a hydrous parental magma. In contrast, contemporary, unmineralised volcanic rocks of the same volcanic suite, formed by crystal fractionation from less hydrous parental magmas. Further, this work confirms earlier work of cited literature and also emphasizes that for volcanic rocks, that are almost ubiquitously altered to some extent within magmatic arc terranes, elements that tend to be insensitive to hydrothermal alteration (e.g. REE, V, Sc) can be used to proxy petrogenetic differences associated with the terms 'fertile' and 'barren' (e.g. hydrous melts vs. dry melts), provided sufficient sampling of volcanic sequences are used to assess fractionation trends and to account for volcanic-generated heterogeneities and complexities (e.g., volcanogenic mixing of rock-types).

The confirmation that fertile volcanic sequences in north-east Queensland record similar geochemistry and petrogenetic processes as known mineralising porphyry intrusions (as for example in the Andes), and can look beyond likely present hydrothermal alteration of these rocks, could now be used as a first order assessment tool to identify fertile terranes/successions where porphyry Cu-Au mineralisation may be buried and preserved beneath cogenetic volcanic successions. However, most effective exploration targeting can be achieved by using these geochemical proxies of magma fertility together with other geological/geophysical datasets to delineate crustal structures/trends that may focus mineralisation, and to recognize alteration systems that are implicitly linked with mineralisation.

Chapter 3 investigates the petrogenesis and apatite halogen systematics of the Early Permian Tuckers Igneous Complex (TIC), which is linked to Chapter 2 by geotectonic setting and relative time of formation (see Chapter 1). I initially investigate the petrogenesis of the TIC based on petrography and whole-rock and rock-forming mineral major and trace element chemistry. This is important with regards to the main subject of this study – Cl, F and S in apatite – as the study of apatite and petrogenetic implications heavily depend on its

relative timing of crystallisation and relationship towards the rock-forming minerals. Establishing these parameters, I use Cl and F apatite contents to estimate the magmas Cl and F composition at the time of apatite crystallisation and also discuss S systematics. I find that Cl and F in apatite (and melt) generally behave as expected from partitioning experiments in the system apatite – melt – fluid, recording initially increasing Cl and F compositions, which diverge at ~65 wt.% whole-rock SiO_2 into steeply decreasing Cl melt contents from ~0.8 to ~0.4 wt.% and increasing to relatively consistent F contents. This significant change is interpreted to relate to the exsolution of a Cl-rich volatile phase. Furthermore, measured apatite S contents, despite being relatively low and close to the limit of detection throughout the TIC, record a measurable increase in the most evolved felsic granodiorite, which crystallised presumably after the exsolution of a volatile phase. This may indicate temporary or local changes in the magmatic fO_2, as the apatite crystal structure is mainly capable of incorporating S in its oxidised form S^{6+}. The nature and cause of these changes in fO_2 within the TIC is not fully understood, but might partially be related to the exsolution of a Cl-rich volatile phase. However, the overall low S contents suggest that S was predominantly present as either S^{2-} or S^{4+}, and may therefore have degassed as $S^{4+}O_2$, as there is no evidence for sulfide precipitation at the given time of crystallisation. Alternatively, overall low Cu contents throughout the TIC lithologies may indicate that sulfide segregated early (i.e prior to crystallisation of TIC gabbro), thereby initially stripping the TIC of any ore-productive potential. My findings on halogen systematics based on TIC apatite may therefore offer an additional aid in identifying an arc magmas potential to exsolve a volatile phase and cause mineralisation (or be mineralised in its own regards).

My new results contribute to and extend existing magma fertility studies, and support the use of certain geochemical tools to aid mineral exploration, to track fractionation trends (magma evolution), and to pinpoint volatile exsolution late in the crystallisation sequence (e.g. using apatite chemistry). I also highlight the need for relatively oxidised magmas as it can prevent early sulfide saturation and metal loss.

In general, the Permocarboniferous arc system in north-eastern Queensland is well-known for hosting numerous previously (but little currently) mined, and/or known porphyry-epithermal style deposits and occurrences, and particularly the Early Permian marks a period of increased magmatic fertility. This time appears to represent a mature stage of the arc system with a well developed associated back-arc rifting zone. Many porphyry-epithermal

mineralised systems are located and arranged into belts or along lineaments, similar to e.g. the west coast of North and South America. Given the exploration potential, unravelling these details on a range of spatial scales (regional to prospect scale) promises to be an exciting subject for future research. Likewise, future studies of the extent and mineralisation potential of Cretaceous arc magmatism that has also affected the region (Corral et al., in prep.), also have great potential to aid mineral exploration and discovery in the region.